CAMILA YAMASHITA

Multi-caracterização de alginato de sódio ozonizado extraído de algas pardas para utilização na impressão 3D

Multi-characterization of ozonized sodium alginate extracted from brown algae for 3D printing

ASSIS

2024

CAMILA YAMASHITA

Multi-caracterização de alginato de sódio ozonizado extraído de algas pardas para utilização na impressão 3D

Tese apresentada à Universidade Estadual Paulista (UNESP), Faculdade de Ciências e Letras, Assis, para o para obtenção do título de Doutora em Biociências (Área de Concentração: Caracterização e Aplicação da Diversidade Biológica)

Orientadora: Ivanise Guilherme Branco

Bolsista: Coordenação de Aperfeiçoamento de Pessoal de Nível Superior - Brasil (CAPES) - Código de Financiamento 001

ASSIS

2024

Dados Internacionais de Catalogação na Publicação (CIP)
Maria Luiza Carpi Semeghini - CRB 8/8301

Y19m

Yamashita, Camila
Multi-caracterização de alginato de sódio ozonizado extraído de algas pardas para utilização na impressão 3D / Camila Yamashita. — Assis, 2024
113 f. : il.

Tese de Doutorado - Universidade Estadual Paulista (UNESP), Faculdade de Ciências e Letras, Assis
Orientadora: Profa. Dra. Ivanise Guilherme Branco

1. Ozônio. 2. Antocianinas. 3. Polissacarídeos. 4. Impressão tridimensional. 5. Biotecnologia vegetal. I. Título.

CDD 631.52

UNIVERSIDADE ESTADUAL PAULISTA

Câmpus de Assis

ATA DA DEFESA PÚBLICA DA TESE DE DOUTORADO DE CAMILA YAMASHITA, DISCENTE DO PROGRAMA DE PÓS-GRADUAÇÃO EM BIOCIÊNCIAS, DA FACULDADE DE CIÊNCIAS E LETRAS - CÂMPUS DE ASSIS.

Aos 29 dias do mês de fevereiro do ano de 2024, às 13:30 horas, no(a) Sala de Defesas da Pós-graduação e Sala Virtual: meet.google.com/afj-ymkj-qxt, realizou-se a defesa de TESE DE DOUTORADO de CAMILA YAMASHITA, intitulada **Multi-caracterização de alginato de sódio ozonizado extraído de algas pardas para utilização na impressão 3D**. A Comissão Examinadora foi constituida pelos seguintes membros: Profa. Dra. IVANISE GUILHERME BRANCO (Orientador(a) - Participação Presencial) do(a) UNESP/FCL - Assis/SP, Prof. Dr. CHARLES WINDSON ISIDORO HAMINIUK (Participação Virtual) do(a) UTFPR - Curitiba/PR, Profa. Dra. IZABEL CRISTINA FREITAS MORAES (Participação Virtual) do(a) USP - Pirassununga/SP, Profa. Dra. GRASIELE SCARAMAL MADRONA (Participação Virtual) do(a) UEM - Maringá/PR, Profa. Dra. MILENA MARTELLI TOSI (Participação Virtual) do(a) USP - Pirassununga/SP. Após a exposição pela doutoranda e arguição pelos membros da Comissão Examinadora que participaram do ato, de forma presencial e/ou virtual, a discente recebeu o conceito final: APROVADA. Nada mais havendo, foi lavrada a presente ata, que após lida e aprovada, foi assinada pelo(a) Presidente(a) da Comissão Examinadora.

Profa. Dra. IVANISE GUILHERME BRANCO

Ivanise G. Branco

AGRADECIMENTOS

O presente trabalho foi realizado com apoio da Coordenação de Aperfeiçoamento de Pessoal de Nível Superior - Brasil (CAPES) - Código de Financiamento 001.

This study was financed in part by the Coordenação de Aperfeiçoamento de Pessoal de Nível Superior - Brasil (CAPES) - Finance Code 001

À Fundação de Amparo à Pesquisa do Estado de São Paulo (FAPESP), processo nº 2022/05161-1.

Aos laboratórios parceiros:

Laboratório Tecnologia de Biopolímeros- FZEA/USP

Laboratório de Biotecnologia (Labiotec)- UTFPR/Curitiba

Laboratório de Biologia Aquática I e II (Labia)- UNESP/Assis

Laboratório de Engenharia e Química de alimentos- UNESP/Assis

Laboratório Multiusuário Labmult-LD- UTFPR/Londrina

Centro Multiusuário de Caracterização de Materiais (CMCM) – UTFPR/Curitiba

Laboratório de RMN – Departamento de Química- UFSCar

Laboratório Multiusuário no Departamento de Química Analítica- UNESP/Araraquara

RESUMO

O alginato de sódio (AS), notável por suas propriedades biocompatíveis e sustentáveis, destaca-se como um material versátil já empregado em diversas indústrias. Sua modificação estrutural pode aprimorar suas propriedades físicas e químicas. Assim, este estudo concentra-se na modificação desse polissacarídeo por meio da ozonização, técnica promissora e de baixo impacto ambiental, visando posterior utilização na encapsulação de biocompostos e na formulação de hidrogéis destinados à impressão 3D. Os resultados do capítulo 1 demonstraram que o processo de ozonização na solução de SA durante 10 min acarretou na redução de aproximadamente um terço do valor inicial de 102.30 ± 0.49 kDa do peso molecular viscosimétrico, despolimerizando eficientemente a cadeia polissacarídica, além de manter sua integridade estrutural, pureza e estabilidade térmica. Análises de cor indicaram índices semelhantes ao alginato comercial, sugerindo efeitos de branqueamento da ozonização. A solução ozonizada mostrou estabilidade mediante variação de pH, não apresentando variação significativa em relação ao potencial zeta (ZP), índice de polidispersividade e condutividade elétrica. Comparado ao alginato nativo, o ZP do polissacarídeo ozonizado apresentou-se mais carregado negativamente deslocando-se para valores que evitam aglomeração de partículas. A interação da solução de AS ozonizado com o extrato rico em antocianinas também foi objeto de investigação. Antocianinas, flavonoides presentes em frutas e vegetais, são pigmentos naturais com capacidade antioxidante e benefícios à saúde, apesar de serem suscetíveis à degradação. Assim, uma alternativa para aumentar sua estabilidade é a encapsulação em soluções poliméricas. Nesse contexto, no capítulo 2, antocianinas foram extraídas de amoras, e, por análise cromatográfica, destacou-se a presença proeminente de procianidina B2 e cianidina-3-O-glucosídeo. As características de cor das soluções compostas de AS e extrato rico em antocianinas apresentaram uma coordenada a* positiva dominante, indicando uma tonalidade avermelhada. Análises reológicas revelaram um comportamento não-newtoniano na presença do extrato rico em antocianinas, indicando um aumento na viscosidade aparente em comparação com as soluções de SA isoladas. Os espectros de ATR-MIR e ^{1}H-RMN sugeriram interações intramoleculares e a incorporação do extrato rico em antocianinas nas soluções de AS, corroborando os resultados reológicos. As soluções com AS ozonizado e extrato de antocianinas mostraram potencial na preservação e entrega eficaz desse composto bioativo. O emprego do AS ozonizado na impressão 3D demanda sua combinação com outros polímeros, visando alcançar as propriedades reológicas e mecânicas necessárias para essa tecnologia, resultando na formação de hidrogéis híbridos. Assim, no capítulo 3, a formulação de um hidrogel com ágar, outro polissacarídeo proveniente de algas, e

, juntamente com o alginato de sódio pré-reticulado foi caracterizada e empregada como tinta na tecnologia de impressão 3D. Inicialmente, essa formulação foi caracterizada reologicamente, indicando propriedades adequadas para impressão 3D, além de caracterizações físicas e de estrutura (ATR-MIR e MEV), que demonstraram interações entre os componentes da tinta de hidrogel. As condições de impressão (diâmetro da agulha, velocidade de impressão, largura e altura do filamento) foram otimizadas por meio de testes de printabilidade. Com os parâmetros otimizados (agulha de 21G, velocidade de impressão 5 mm/s e medidas do filamento de 1 mm), houve a impressão 3D de estruturas cubóides. Os testes de desvio de impressão demonstraram bons resultados para a formulação com o SA ozonizado, mantendo a estrutura estável por 24h. Além disso, os testes mecânicos revelaram um perfil de textura semelhante à formulação com AS comercial. A utilização do AS extraído de algas pardas ozonizado mostrou-se promissora para diferentes tipos de aplicação, com a maioria dos resultados comparáveis aos formulados com AS comercial. Em conclusão, os resultados encontrados para o AS ozonizado e suas possíveis aplicações são muito satisfatórios quando comparados com o AS comercial. Ele demonstrou ser versátil para encapsulação de componentes bioativos, além de sua exploração na tecnologia de impressão 3D, podendo ser utilizado em bioengenharia, farmacêuticos, nutracêuticos e na indústria alimentícia.

Palavras-chave: Ozônio. Antocianina. Polissacarídeo.

ABSTRACT

Sodium alginate (SA), notable for its biocompatible and sustainable properties, stands out as a versatile material widely employed in various industries. Structural modification through ozone treatment is explored to enhance its physical and chemical properties. This study focuses on ozonizing the polysaccharide, a promising and environmentally friendly technique, with the aim of subsequent utilization in the encapsulation of bioactive compounds and the formulation of hydrogels for 3D printing. The findings of chapter 1 showed that 10-minute ozone treatment of SA solution resulted in approximately one-third reduction of the initial viscosity-average molecular weight of 102.30 ± 0.49 kDa, efficiently depolymerizing the polysaccharide chain while maintaining its structural integrity, purity, and thermal stability. Color analysis indicated similar indices to commercial alginate, suggesting ozone-induced bleaching effects. The ozonized solution exhibited stability across pH variations, with no significant changes in zeta potential (ZP), polydispersity index, or electrical conductivity. Compared to native alginate, the ZP of ozonized polysaccharide showed a more negatively charged profile, avoiding particle agglomeration. The interaction of ozonized SA solution with anthocyanin-rich extract was also investigated. Anthocyanins, flavonoids present in fruits and vegetables, are natural pigments with antioxidant capacity and health benefits, albeit susceptible to degradation. Encapsulation in polymeric solutions emerges as an alternative to enhance stability. In this context, in chapter 2, anthocyanins were extracted from blackberries, and chromatographic analysis highlighted the prominent presence of procyanidin B2 and cyanidin-3-O-glucoside. The color characteristics of solutions composed of ozonized SA and anthocyanin extract displayed a dominant positive a* coordinate, indicating a reddish hue. Rheological analyses revealed non-Newtonian behavior in the presence of anthocyanin-rich extract, indicating increased apparent viscosity compared to isolated SA solutions. ATR-MIR and ^{1}H-NMR spectra suggested intramolecular interactions and the incorporation of anthocyanin-rich extract into SA solutions, corroborating rheological results. Ozonized SA and anthocyanin extract solutions showed potential in preserving and effectively delivering this bioactive compound. The use of ozonized SA in 3D printing requires its combination with other polymers to achieve the rheological and mechanical properties necessary for this technology, resulting in the formation of hybrid hydrogels. Thus, in chapter 3, a hydrogel formulation with agar, another polysaccharide from algae, and anthocyanin-rich extract, along with pre-crosslinked sodium alginate, was characterized and employed as ink in 3D printing technology. Initially, this formulation was rheologically characterized, indicating suitable properties

for 3D printing, along with physical and structural characterizations (ATR-MIR and SEM), demonstrating interactions between hydrogel ink components. Printability tests were conducted to optimize printing conditions (needle diameter, print speed, filament width, and height). With optimized parameters (21G needle, print speed 5 mm/s, and filament measurements of 1 mm), 3D printing of cuboid structures was achieved. Print deviation tests showed good results for the formulation with ozonized SA, maintaining stable structure for 24 hours. Additionally, mechanical tests revealed a texture profile similar to the formulation with commercial SA. The use of ozone-treated SA extracted from brown algae proved promising for various applications, with most results comparable to formulations with commercial SA. In conclusion, the findings for ozonized SA and its potential applications are highly satisfactory, highlighting its versatility for the encapsulation of bioactive components and exploration in 3D printing technology, applicable in bioengineering, pharmaceuticals, nutraceuticals, and the food industry.

Keywords: Ozone. Anthocyanin. Polysaccharide.

SUMÁRIO

1 INTRODUÇÃO GERAL

Os biopolímeros ou polímeros naturais têm despertado grande interesse devido a propriedades versáteis como biocompatibilidade, não-toxicidade e biodegradabilidade (Abbasian *et al*., 2019; Azimi *et al.* 2020). Polissacarídeos naturais como ágar, fucoidano, carragenana, alginato e seus derivados são exemplos de biopolímeros, os quais podem ser extraídos de algas marinhas (Salehi *et al*., 2019). As algas marinhas são extensivamente encontradas no oceano e costas marítimas, demonstrando uma oportunidade de exploração sustentável dessas áreas (Prabhu *et al*., 2020), incentivando o crescimento e desenvolvimento da economia azul de recursos ainda pouco explorados.

Sargassum é um gênero de macroalgas pardas abundantes na área costeira brasileira que apresenta um conjunto de polissacarídeos na composição de sua parede celular, dentre eles o ácido algínico (Fawzy; Gomaa, 2021; Leite *et al*., 2021). O alginato de sódio, um sal derivado do ácido algínico, tem sido extensivamente estudado por suas propriedades físico-químicas que garantem aplicabilidade em diferentes áreas industriais como na agricultura (Song *et al*., 2020), biorremediação (Mohammed *et al.*, 2022; Shi *et al.*, 2022), filmes para embalagens (Chen *et al.*, 2021), dispositivos vestíveis inteligentes (*smart wearable devices*) (Zhao *et al.*, 2022), agente estabilizante e espessante (Zhang *et al.*, 2023), impressão e bioimpressão 3D (Liu *et al.*, 2020; Cheng-Rong; Yung-Kai, 2022; Im *et al.*, 2022; Saravanou *et al.*, 2023), condução e liberação de medicamentos, nanopartículas ou compostos ativos (Im *et al.*, 2022; Ma *et al.*, 2023; Wang *et al*., 2023), entre outros.

O alginato de sódio é composto por resíduos de β-D-ácido manurônico (M) e α-L-ácido gulurônico (G) dispostos linearmente em blocos heteropoliméricos (MG), homopoliméricos (MM ou GG) unidos por ligação glicosídica 1-> 4 (Lee; Mooney, 2012) (Figura 1).

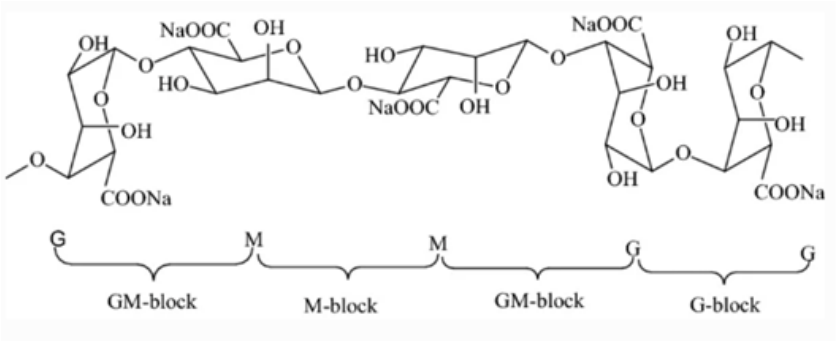

Figura 1 - Estrutura química do alginato com os blocos GG, MM e MG unidos por ligação glicosídica 1->4 (Sahoo; Biswal, 2021)

A modificação desse polissacarídeo pode potencializar algumas de suas propriedades, como diminuir a viscosidade e melhorar a solubilidade em água, trazendo mais benefícios em diversas áreas de aplicação, como na formulação de filmes e hidrogéis (Wang *et al.*, 2020). A aplicação do gás ozônio é considerada uma tecnologia inovadora para modificação de alginato. Além disso, é classificada como uma tecnologia verde, já que o ozônio se decompõe rapidamente em oxigênio, sem deixar resíduos nos alimentos ou meio ambiente (Pandiselvam *et al.*, 2019). Por ser um agente com alto potencial oxidativo, o gás ozônio é uma alternativa interessante aos processos de oxidação tradicionais utilizados na indústria de polissacarídeos. A modificação do alginato de sódio através do gás ozônio quebra as ligações glicosídicas do polímero, o que diminui sua massa molecular visosimétrica média e consequentemente, sua viscosidade, como constatado em estudos prévios (Yamashita *et al.*, 2021). De acordo com Vu *et al*. (2022), o alginato com menor massa molecular aumenta seu potencial reativo, o que pode ampliar sua capacidade de complexação com íons, por exemplo. Dessa forma, o polissacarídeo modificado terá uma maior capacidade de gelificação, já que as soluções de alginato de sódio podem formar géis quando o pH abaixo de seu pKa ou pela substituição de íons cátions de sódio nas resíduos de ácido gulurônico (Russo; Malinconico; Santagata, 2007; Abasalizadeh *et al*., 2020). Apesar de o alginato formar géis com cátions mono, di ou multivalentes (Hu *et al.*, 2021), o íon mais utilizado para complexação com alginato de sódio é o cálcio, com o modelo “caixa de ovo” estabelecido, em que há a ligação dos blocos G de polímeros adjacentes com o cátion (Grant *et al.*, 1973; Abasalizadeh *et al*., 2020), ilustrado na Figura 2. Essa capacidade de gelificação, juntamente com a complexação com íons, são propriedades essenciais exploradas na fabricação de hidrogéis.

Por definição, os hidrogéis são redes poliméricas hidrofílicas tridimensionais capazes de absorver e reter uma quantidade significante de água ou fluídos biológicos em sua estrutura, sem se

dissolver, características devido à reticulação de suas cadeias (Ahmed, 2015; Abasalizadeh *et al.*, 2020; Khattab; Kamel, 2022). Além disso, a disposição porosa de suas cadeias permite o carreamento de células, medicamentos, nanopartículas e/ou moléculas bioativas (Abasalizadeh *et al*., 2020; Im *et al.*, 2022; Corrales-Orovio *et al*., 2023; Ma *et al.*, 2023) .

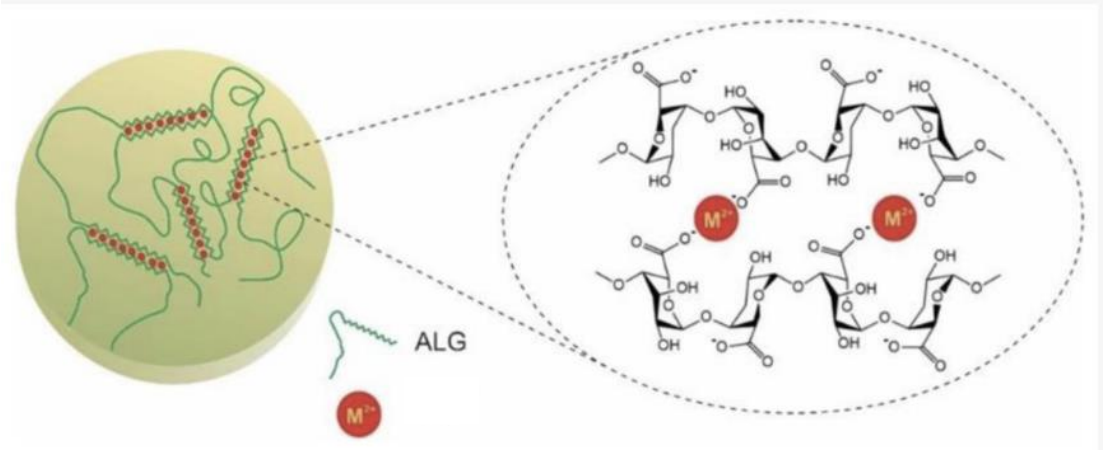

Figura 2 - Diagrama esquemático da reticulação do alginato de sódio por um cátion (M^{+2}) (Abasalizadeh *et al.*, 2020)

Dentre os inúmeros compostos ativos naturais, as antocianinas são flavonóides que se destacam por sua cor atrativa, não toxicidade, solubilidade em água e atividade antioxidante (Banach *et al.*, 2020; Liudvinaviciute *et al.*, 2020). Estudos já investigaram a incorporação das antocianinas em hidrogéis com alginato de sódio e obtiveram resultados significativos quanto sua complexação e aplicação, como por exemplo para liberação transdermal (Anghel *et al.*, 2021), curativo (Lotfinia *et al*., 2023) e monitoramento da qualidade de alimentos frescos (Dikmetas *et al.*, 2023). Hidrogéis também são amplamente utilizados na impressão 3D, tecnologia transformativa que contribuem com o desenvolvimento de diferentes setores, como engenharia tecidual e de alimentos (Fatimi *et al.*, 2022, Sharma *et al.*, 2023).

No entanto, dadas as suas limitações reológicas inerentes, o alginato de sódio é combinado com outros compostos, como proteínas, ou outros polímeros, sendo designados hidrogéis híbridos. O ágar é um material alimentar amplamente difundido que contém dois componentes chamados agarose e agaropectina (Saha; Bhattacharya, 2010). Esse biopolímero também pode ser extraído de algas marinhas e demonstrou sua capacidade de aumentar a viscosidade e melhorar propriedades mecânicas de tintas utilizadas na impressão 3D (Wang *et al*., 2021). Devido à sua

cor atrativa, as antocianinas surgem como substitutas promissoras aos corantes sintéticos utilizados nas indústrias alimentícia e cosmética (Arroyo-Maya; Mcclements, 2015). Estudos já demonstraram seu poder antioxidante, proporcionando diversos benefícios na prevenção de doenças (Yang *et al.*, 2022), o que amplia as vantagens de sua incorporação na tinta para impressão 3D. Além disso, quando adicionada em uma rede polimérica 3D, o processo de encapsulação pode contribuir para aumentar sua estabilidade (Sharif; Khoshnoudi-Nia; Jafari, 2020).

O presente estudo, desenvolvido no Laboratório de Engenharia de Processos (UNESP/Assis), teve como objetivo a multi-caracterização estrutural, física e química do alginato de sódio ozonizado obtido de algas pardas, explorando a modificação por meio da ozonização, uma tecnologia verde pouco explorada para esse propósito. Adicionalmente, a pesquisa se dedica à análise da encapsulação de extrato rico em antocianinas em soluções de alginato de sódio. O polissacarídeo ozonizado é também pré-reticulado, combinado com ágar e extrato enriquecido em antocianinas, visando a formulação de hidrogéis para aplicação na promissora tecnologia de impressão 3D. Portanto, este estudo objetiva não apenas expandir o conhecimento sobre o alginato de sódio modificado, mas também explorar novas fronteiras para aplicações potenciais e inovadoras como em curativos absorvíveis ou alimentos funcionais.

1. ESTRUTURA DA TESE

Essa tese foi dividida em 3 capítulos, com seus respectivos dados, resultados e discussões, para organizar melhor os temas abordados seguindo formatação e normas da revista Carbohydrate Polymers.

Capítulo 1 – **Extração e Modificação de Alginato de Sódio de Algas Pardas por Ozonização: Caracterização e Comportamento em Diferentes pHs** Esse capítulo descreve a extração do alginato de sódio de algas pardas do gênero *Sargassum* e sua modificação por aplicação do gás ozônio, como também realiza a caracterização de suas três formas (comercial, nativo, ozonizado) através das análises físicas, químicas e estruturais. Além disso, são mostrados os resultados do estudo da influência da alteração de pH nas propriedades físicas e químicas das soluções de alginato de sódio.

Capítulo 2 – **Encapsulação de extrato rico em antocianinas em diferentes soluções de alginato de sódio: nativo, ozonizado e comercial.** Esse capítulo apresenta o estudo da soluções compostas de alginato de sódio e extrato rico em antocianinas extraídas de amora,

comparando três tipos de alginato (alginato de sódio comercial, nativo e ozonizado). O estudo caracteriza as soluções através da avaliação do comportamento reológico, análise estrutural e microscópica.

Capítulo 3 – **Formulação e caracterização de hidrogéis pré-reticulados à base de alginato de sódio ozonizado e ágar contendo extrato rico em antocianinas aplicados à impressão 3D.** O capítulo aborda a caracterização reológica associada à printabilidade da formulação de hidrogel para impressão 3D composta por alginato de sódio ozonizado, ágar e extrato rico de antocianinas, comparado com a formulação utilizando alginato de sódio comercial. No capítulo também são realizadas análises estruturais e microscópicas das tintas, além de análises de printabilidade e da estrutura 3D.

2. OBJETIVOS

2.1. OBJETIVO GERAL

Caracterizar o alginato de sódio extraído de algas pardas, modificado por ozonização, e avaliar sua interação com extrato rico em antocianinas, explorando sua aplicabilidade na tecnologia de impressão 3D.

2.2. OBJETIVOS ESPECÍFICOS

- Extração de alginato de sódio de algas pardas (*Sargassum* spp.);
- Modificação da estrutura do alginato de sódio com gás ozônio;
- Investigação das propriedades físicas, químicas e estruturais do alginato de sódio modificado, comparado com o alginato de sódio nativo e comercial, mediante análises reológicas, colorimétricas e termogravimétricas, solubilidade, higroscopicidade, atividade de água, infravermelho por transformada de Fourier (ATR-MIR) e ressonância nuclear magnética de prótons (^{1}H RMN);
- Investigação do comportamento físico das soluções de alginato de sódio (comercial, nativo, ozonizado) em diferentes pHs através de análises reológicas, tamanho de partícula e potencial zeta.

- Extração, identificação e quantificação dos compostos do extrato rico em antocianinas de amora por cromatografia líquida;
- Investigação da encapsulação do extrato de antocianinas em soluções de alginato de sódio (comercial, nativo, ozonizado) através de caracterização física e química (caracterização reológica, ATR-MIR, ^{1}H RMN e microscopia eletrônica de varredura (MEV)).
- Formulação de hidrogéis pré-reticulados com íons cálcio à base de alginato de sódio (comercial e ozonizado), ágar e enriquecido com extrato rico em antocianinas de amora.
- Caracterização reológica oscilatória (varredura de taxa de cisalhamento, tensão de cisalhamento, frequência angular e rampa de temperatura) relacionada à printabilidade das tintas;
- Análise estrutural das tintas por meio de ATR-MIR para verificar as principais ligações entre os componentes da formulação;
- Análise microestrutural das tintas através de MEV;
- Otimização de variáveis de impressão (diâmetro da agulha de impressão, velocidade de impressão, largura e altura do filamento) através de testes de printabilidade (1D) das tintas;
- Impressão 3D com os parâmetros otimizados de estruturas cubóides e análise de textura e de estabilidade

CHAPTER 1: EXTRACTION AND MODIFICATION OF BROWN ALGAE-DERIVED SODIUM ALGINATE BY OZONIZATION: CHARACTERIZATION AND BEHAVIOR AT DIFFERENT PH LEVELS.

Abstract

Alginate, a biopolymer present in brown algae, offers diverse functionalities driven by its physicochemical properties, making it widely applicable in various industries. Ozone gas stands out as an innovative tool for modifying alginate, with potential benefits in enhancing some properties such as gel strength, hydrophobicity, and biodegradability. This study focuses on exploring the ozone-induced modifications in sodium alginate (SA) extracted from *Sargassum* spp., offering valuable insights into structural and physicochemical changes and potential industrial applications. The findings showed that ozone-treated SA kept its chemical integrity and thermal stability. Colorimetric analysis revealed similarities between the ozonized sample and commercial alginate, likely attributed to ozonation bleaching effect. Significant depolymerization of SA chains occurred after ozonation, leading to reduced average molecular weight (39.37 ± 1.91 kDa) and apparent viscosity. Rheological analysis demonstrated pH-dependent behavior, with commercial and ozonized samples (2% m/v at room temperature) exhibiting similar Newtonian characteristics. Polydispersity Index (PDI) analysis showed uniform molecular size distribution, and zeta potential decreased post-ozonation, properties that can be explored i.e. gel formation. These findings enhance our understanding of modified sodium alginate applications in industry, addressing a significant knowledge gap.

Keywords: Ozone gas; Low molecular weight polysaccharides; Depolymerization; Rheology

1. Introduction

Alginate is a natural polymer found in brown algae (Phaeophyceae) cell walls, among which *Sargassum* spp are considered as a potential renewable marine resource for many biotechnological applications (Fawzy & Gomaa, 2021; Fernando et al., 2022; Lu et al., 2022; Nogueira et al., 2022). Alginate is composed of two uronic acids: β-D-mannuronic acid (M) and α-L-guluronic acid (G), arranged either in heteropolymeric (MG) and/or homopolymeric (MM or GG) blocks joined via 1,4-glycosidic linking (Lee & Mooney, 2012). The composition and sequential structure may, however, vary according to seasonal, growth conditions, seaweed species which will reflect the functional properties of alginate, solubility, interaction with metal ions, gelling and viscosity (Bertagnolli et al., 2014; Benslima et al., 2021).

Besides these properties, alginate also presents attractive features such as nontoxicity, biodegradability and biocompatibility (Fernando et al., 2020) mainly reason for its wide range of applications, including tissue engineering (Saravanou et al., 2023; Serafin, Culebras & Collins, 2023), microencapsulation of nutraceuticals and drugs (Anghel et al., 2021; Ma et al., 2023), as well as in food applications as stabilizing, thickening, and gelling agents (Zhang et al., 2023), preparation of edible films (Chen et al., 2021), bioremediation (Mohammed et al., 2022; Shi et al., 2022) and inks for 3D printing (Cheng-Rong, Yung-Kai, 2022; Im et al., 2022; Saravanou et al., 2023).

Modification of alginate is used as a tool to enhance existing properties, for example to improve ionic gel strength by additional covalent crosslinking, increase hydrophobicity of the backbone, improve biodegradation (Pawar & Edgar, 2012; Reakasame & Boccaccini, 2018; Wang et al., 2023). The use of ozone gas is regarded as a cutting-edge technology for modifying alginate. It is considered a green technology because ozone quickly degrades into oxygen, leaving no residue in food or the environment (Pandiselvam et al., 2019). As an agent with a high oxidative potential, ozone gas is an interesting technology for performing polysaccharide oxidation processes.

In the present work, the modification of sodium alginate (SA) extracted from *Sargassum* spp. seaweed by ozonation has been studied in comparison with its native and commercial forms. Changes in alginate structure as well as in physicochemical properties were investigated. Because alginate exhibits pH-responsive properties (Afzal et al., 2018; Ramdhan et al., 2019), studies investigating the effect of alginate solution pH on its properties were also conducted to provide valuable information for its application. To the best of our knowledge, little has been known about the ozonation-induced changes in sodium alginate extracted from seaweeds. Therefore, this study

will provide new insights into the ozonation modification of sodium alginate for industrial applications.

2. Materials and Methods

2.1. Seaweed material

The brown seaweeds (*Sargassum* spp.) were collected from Ubatuba, São Paulo State, Brazil (23º28'00"S – 45º03'36"W) in October 2022, and transported in seawater at low temperature. The samples were washed with tap water and soaked in chlorinated water (25 ppm) for 30 min. The algal material was dried in a convection oven (Model 420-1D, Ethik Technology, Vargem Grande Paulista, Brazil) at 45 °C for 24 h, ground using a cutting mill and stored in airtight containers at room temperature prior to sodium alginate extraction.

2.2. Sodium Alginate Extraction Procedure

The milled algae (7 g) was treated twice with 99 % ethanol (EtOH 50 mL) with constant shaking for 3 h and dried overnight in an air circulation oven at 40 °C. The pretreated seaweed was supplemented with 20% citric acid (Anhydrous, Êxodo, Sumaré-SP, Brazil) (pH 1.5). Ultrasonic horn (OR-T-500, OMNI International™, 20 kHz frequency, and 400 W maximum power dissipation) was applied to the algal suspension at power of 160W for 9 min, using a probe with a 12.7 mm tip diameter. Ultrasonicated samples were washed with distilled water and then treated with 2% (w/v) sodium carbonate (Anhydrous, Impex, Diadema-SP, Brazil) (pH 10) under magnetic stirring for 90 min at 75.7 °C (Nogueira et al., 2022). The extract was filtered, and the supernatant precipitated with ethanol (99%) (2v). The extracted SA was dried at 45 °C for 24 h in a convection oven, named from now on native (N).

The SA yield (%) was calculated using Equation (1):

$$\text{Yield (\%)} = \frac{Dry\ wt.of\ SA\ (g)}{Dry\ wt.of\ seaweed\ (g)} \times 100 \qquad (1)$$

2.3. Ozonation of sodium alginate

The SA aqueous solution (1%, w/v) was modified though ozone gas application. The solution was placed in a 500 mL glass container (diameter 7 cm × height 20 cm) which was half-filled by the ozonation reaction. The ozone gas was obtained by the conversion of oxygen (O_2) to ozone (O_3) in an ozone generator (Model GOBSUS, OzonioBras, Araçatuba, Brazil). The ozone was bubbled continuously into the SA solution through a fine bubble diffuser on the inner bottom of the glass container. The SA solution was treated with a feed gas flow of 1L/min and kept under magnetic stirring for 10 min at 25 °C. The feed gas flow (O_2) was controlled by a pressure regulator and the solution temperature was maintained using a jacket connected to a thermostatic bath. After ozone treatment, samples were concentrated in a rotary evaporator (60 °C), precipitated in ethanol 99% (2v), and dried at 45 °C for 24 h in a convection oven. Therefore, following the ozonation process, the sample will be referred to as ozonized (O) sodium alginate. For comparison purposes, commercial alginate (Sigma-Aldrich, A1112) was employed in all analyses.

2.4. Characterization of sodium alginates

2.4.1. Rheological analyses

2.4.1.1. Determination of viscosity-average molecular weight (Mv)

The Mv was obtained through capillary-viscosimetric measurement using a Cannon Fenske viscometer (size 100). Solutions at different concentrations (0.1-0.5 g/dL) were prepared with 0.1 M NaCl (Impex, Diadema, SP, Brazil) at 25 °C and the flow time of each SA solution was recorded. The Mv values of alginates were calculated using the Mark-Houwink equation (Eq. 2), which correlates the Mv of the polysaccharide and the intrinsic viscosity [η] which was determined by extrapolating reduced specific viscosity against the concentration curve to zero (Sellimi et al., 2015).

$$[\eta] = K (Mv)^{\alpha} \quad (2)$$

where [η] is the intrinsic viscosity (dL/g), Mv is the viscosity-average molecular weight (kDa); K and α are dependent constants of the biopolymer, solvent and temperature (K= 0.023 dL/g and α = 0.984) (Clementi, Mancini, & Moresi, 1998).

2.4.1.2. Flow curves

Rheological analyses of SA solutions (2%, w/v) and in different pHs were performed using an AR2000 rotational rheometer (TA Instruments, New Castle, DE, USA) with a double concentric cylinder geometry (external radius 17.5 mm, internal radius 16.0 mm; internal radius 15.3 mm, height 56 mm, gap 2000 (μm)) at 25 °C. Shear stress was determined at shear rates in the range of 0.01 to 300 s^{-1}.

Table 1 - Rheological model fitting

Model	Equation	
Newtonian	$\tau = \mu * \gamma$	(3)
Ostwald-de-Waele (Power Law)	$\tau = K * \gamma^n$	(4)

where μ is the viscosity, τ is the shear stress (Pa), τ_0 is the yield stress (Pa), Υ is the shear rate (s^{-1}), K is consistency index ($Pa.s^n$), n is the flow behavior index (dimensionless).

2.4.2. Thermogravimetric analysis

Thermogravimetric analysis (TGA) and Differential Scanning Calorimetry (DSC) was performed using a NETZSCH TGA/DSC1 (STA 449 F3 Jupiter). Alginate samples (10 mg) were studied in a nitrogen atmosphere and scanned at a gas flow of 80 mL/min and temperature range of 25–800 °C with a ramp of 20 K/min.

2.4.3. Solubility

Determination of alginates' solubility was evaluated based on the method described by the gravimetric method, according to Eastman and Moore (1984), with minor modifications by Xu et al. (2022). The sample (0.2 g) was dispersed in 20 mL of distilled water and stirred at room temperature for 30 min. The suspension was then transferred to a tube and centrifuged at 3000 g for 5 min. The upper aqueous phase was transferred to a pre-weighed Petri dish, dried in a convection oven at 105 °C and the dried weight of the soluble solid was calculated gravimetrically (Eq. 5).

$$\text{Solubility (\%)} = \frac{\text{Dried supernatant weight}}{\text{Initial sample weight}} \times 100 \qquad (5)$$

2.4.4. Hygroscopicity

The methodology of Cai and Corke (2000) was employed, with slight modifications, to ascertain the hygroscopicity of alginates. For one week, sample (0.25 g) was conditioned in a desiccator containing saturated NaCl solution, which imparts a relative humidity of 75% at 25 °C. The results were expressed as the weight of the hygroscopic moisture per g of dry solid after 7 days of storage (Eq. 6).

$$\text{Hygroscopicity (\%)} = \frac{\text{Mf}-\text{Mo}}{\text{Mo}} \quad (6)$$

where M_f is the final mass after 7 days and M_o is the initial mass.

2.4.5. Water activity (aw) and Colorimetric parameters

For these analyses, solutions of both native and ozonized SA were subjected to freeze-drying to ensure the uniformity of measurements. The a_w was measured in an Aqualab CX-2 (Decagon, Pullman, USA) hygrometer at 25 °C. The color of the freeze-dried alginates was measured using a HunterLab colorimeter (MiniScan XE, HunterLab, Reston, USA). Indicators lightness index L* (0-100, black-white), a* (green-red) and b* (yellow-blue) were obtained. Before measuring, the colorimeter was standardized with black and white calibration tiles provided with the instrument. The total color difference (ΔE) was calculated through the followed Equation 7 (Xu et al., 2020):

$$\Delta E = \sqrt{(L_0^* - L^*)^2 + (a_0^* - a^*)^2 + (b_0^* - b^*)^2} \quad (7)$$

where L_0*, a_0* and b_0* are the color values of the commercial sodium alginate.

2.4.6. Attenuated total reflectance-mid-infrared (ATR-MIR) spectroscopy

A Fourier transform infrared spectrometer (Perkin Elmer, Spectrum One, Waltham, MA, USA), equipped with Spectrum Universal Attenuated Total Reflectance (ATR) accessory, was used to investigate the functional groups present in the commercial, native and ozonized SA samples in the mid-infrared region (MIR). Spectra were recorded in the range of 4000–650 cm^{-1} by acquiring 32 scans with 4 cm^{-1} resolution.

2.4.7. Proton nuclear magnetic resonance spectroscopy (1H NMR)

The ^{1}H NMR spectra were acquired employing an NMR spectrometer (Bruker AVANCE III, Karlsruhe, BW, Germany) with an operational temperature of 80°C and a frequency of 400 MHz. The three types of SA (commercial, ozonized and native) were dissolved in deuterium oxide (D_2O), with TSP-d4 (sodium salt of trimethylsilylpropionic acid) serving as the internal reference. Chemical shifts of the anomeric proton signals, block structure, and M/G ratio were determined following the methodology outlined by Jensen, Larsen & Engelsen (2015). The data collected were subsequently analyzed using TopSpin software version 4.3.0.

2.5. Characterization of the alginates at different pH values

The pH of (2% w/v) solutions of sodium alginate (SA), including commercial, native, and ozonized, was adjusted to different pH levels (3, 5, 7, 9) using NaOH (0.5 M) and HCl (1 M) solutions at 25 °C. In addition to the rheological behavior, as previously mentioned, the solutions were characterized through Particle Size, Polydispersity Index (PDI), zeta potential, and Conductivity assessments were performed by dynamic light scattering (DLS) technique (Litesizer 500, Anton Paar) at 25 °C. The samples were diluted (1:10) with Milli-Q water and subjected to analysis.

2.6. Statistical Analysis

All experiments were carried out at least in duplicates (n = 2), and the results were expressed as the mean values ± standard deviation. Significant differences were determined by one-way analysis of variance (ANOVA) followed by a post-hoc Tukey's test with a significance level of $p < 0.05$. The adjustment of rheological models, plotting of FTIR spectra, and statistical analyses were conducted using OriginPro 2018 software (OriginLab Corporation, MA, USA).

3. Results and Discussion

3.1. Alginate Yield

Alginate extraction yield from seaweed *Sargassum* spp. was 46.45 ± 2.38 %. Different ranges of yields can be observed in the literature due to the influence of variations on both the alginate extraction methodology employed and the seasonal fluctuations of the algae, as highlighted by Belattmania et al. (2022). The yield obtained in this study surpassed those achieved through the conventional extraction process (9.0-30.0%) using the same seaweed genus, which relies on hydrochloric acid without ultrasound assistance (Rahelivao et al., 2013; Bertagnolli et al., 2014; Sellimi et al., 2015; Mohammed et al., 2018). In their optimized experimental conditions, Fawzy & Gomaa (2021) achieved approximately 29% yield of SA from *Sargassum* by using citric acid as the acidic treatment for extraction. Remarkably, this value aligns closely with the highest yield reported in studies employing hydrochloric acid. These findings suggest that citric acid could potentially offer superior efficacy in SA extraction while mitigating adverse environmental impacts. Furthermore, it is noteworthy that the authors employed a shaking incubator during the extraction process, suggesting that the utilization of an ultrasonic horn may enhance alginate extraction. This can also be further supported by the yield of 15% using an ultrasonic bath and lemon juice as a substitute for hydrochloric acid (Flórez-Fernández, Domínguez, & Torres, 2019). In their investigation, Nogueira et al. (2022) successfully achieved a remarkably similar yield value (45.79%) by optimizing the alkaline treatment, although the conventional acidic treatment. Consequently, the methodology employed in this study presents an excellent alternative for SA extraction, effectively reducing the time required for the procedure.

3.2. Physicochemical and Rheological analyses

Table 2 presents the physicochemical analysis of SA. Notably, the water activity (a_w), solubility, and hygroscopicity of both native and ozonized SA exhibited no significant differences. Commercial samples exhibit half the a_w value of native and ozonized samples, indicating reduced water availability for microbial metabolic activity and growth. Nevertheless, all samples exhibited a a_w within a range below the threshold considered favorable for microbial growth. Typically, bacteria require a minimum a_w value of 0.91, while fungi necessitate at least 0.6 for optimal growth conditions (Allen Jr, 2018). Water activity is connected with hygroscopicity property which is the tendency of materials to take up water vapor from the atmosphere (Newman, Reutzel-Edens &

Zografi, 2008). Thus, the same tendency was observed for hygroscopicity values, wherein the commercial sample exhibited the lowest value, while both the native and ozonized samples demonstrated higher values, with no statistically significant differences observed.

Solubility assessments revealed that the samples exhibited relatively high solubility levels, with the commercial sample displaying slightly higher solubility compared to the native and ozonized SA, which no statistically significant difference between them (Table 2). However, the hypothesis that alginate modification would increase its solubility was not substantiated. This outcome aligns with the observations made by Mao et al. (2012), who also found no significant disparity in solubility among alginates with molecular weights ranging from 100 to 30 kDa. Moreover, it is worth noting that the solubility of SA can be influenced by the extraction procedure, as highlighted by Sugiono et al. (2018). Their work suggested that an elevated pH during extraction led to greater solubility of alginate, and further, that the solubility rate of alginates exhibited a logarithmic proportionality to both the duration and alkali concentration utilized in the extraction process. These insights underscore the multifaceted nature of alginate solubility, which can be significantly impacted by extraction parameters.

An important finding emerges when considering the viscosity-average molecular weight (Mv) values. It becomes evident that the ozonized samples suffered depolymerization, with their Mv values decreasing to approximately one-third compared to those of the native SA. This phenomenon highlights a substantial alteration in the polymer chain structure caused by ozonation, resulting in a Mv similar to the low-viscosity commercial SA. Compared to the existing literature, even the native sample exhibited a relatively low Mv, once algae belonging to the same genus found along the Madagascar seacoast presented a Mv of 451 kDa (Rahelivao et al., 2013). Besides climate conditions during growth or harvesting (Bertagnolli et al.,2014; Belattmania et al., 2022), this disparity in Mv can be attributed to the utilization of an ultrasonic probe during the extraction process, which effectively disrupts polymer chains (Dodero, Vicini & Castellano, 2020). Medium-viscosity commercial alginate experienced notable degradation through thermal treatment, resulting in a reduction of Mv from 200 kDa to 75 kDa after 4.5 h (Kelishomi et al., 2016) as well as through oxidative degradation conducted for 1 h at 20°C, with a drop in Mv from 350 kDa to approximately 100 kDa (Mao et al. 2012). In the present study, following 10 min of ozone exposure, the initial molecular weight of 102 kDa significantly decreased to 39 kDa (Table 2). These findings underscore the time-dependent nature of Mv reduction, as supported by prior research where molecular weights as low as 19 kDa were achieved (Yamashita et al., 2021). The results obtained from our ozone treatment experiment demonstrate its superior efficiency in Mv reduction. Moreover, the utilization of low molecular weight SA presents various possibilities, as

studies have demonstrated its enhanced bioactivity. Notably, it has shown promising outcomes in the effective protection of probiotics against the challenging conditions of digestion (Ramos et al., 2018). Additionally, its application extends to the field of tissue engineering in biomedicine, as highlighted in recent research (Wang, Chen & Zhang, 2021). Furthermore, SA has exhibited potential in promoting plant growth, as evidenced by studies focusing on plant-growth promotion (Abd El-Mohdy, 2017).

Table 2 - Physicochemical properties of sodium alginates samples

	a_w	Mv (kDa)	Solubility (%)	Hygroscopicity (gH_2O/g)
Commercial	$0.24^{a} \pm 0.004$	$46.39^{a} \pm 1.54$	$83.87^{a} \pm 0.50$	$0.18^{a} \pm 0.005$
Native	$0.57^{b} \pm 0.006$	$102.30^{b} \pm 0.49$	$79.65^{b} \pm 1.31$	$0.22^{b} \pm 0.002$
Ozonized	$0.58^{b} \pm 0.006$	$39.37^{c} \pm 1.91$	$79.66^{b} \pm 0.88$	$0.23^{b} \pm 0.003$

Different letters in the column indicate significant differences ($p \leq 0.05$). Data are the mean ± SD ($n = 3$).

The flow curves of 2% (w/v) SA solutions at 25 °C in various pH levels are presented in Fig. 1 and the fitting of the data to rheological models is summarized in Table 3. The rheological characteristics of both commercial and ozonized samples exhibited great similarity. At pH levels 5, 7, and 9, they closely resembled Newtonian fluids with shear stress directly proportional to the shear rate (Fig. 1) and flow behavior index (n) value approximately 1 (R^2 exceeding 0.99). In contrast, these samples at pH 3 and the native SA in all pH levels, indicating non-Newtonian fluids with shear-thinning behavior (R^2 above 0.99). In general, both the commercial and ozonized samples exhibited comparable rheological behavior due to their low viscosity. Nevertheless, when considering the Newtonian model, it becomes evident that the viscosity of the commercial sample is greater than that of the ozonized sample. This finding is further substantiated by the data presented in Table 3, which shows a higher Mv for the commercial sample.

The rheological behavior is influenced by various factors, including the structural properties, molecular weight, concentration of the solution, extraction solvents and procedures (Yang, Chen & Fang, 2009; Hentati et al., 2020). The shear-thinning behavior observed in native SA aligns with previous literature findings in lower concentrations (1% w/v) (Nogueira et al., 2022), the same concentration (2% w/v) (Hentati et al., 2020) and higher concentrations (2.5% w/v) (El Atouani et al., 2016). The Newtonian-like behavior observed in commercial and ozonized SA is consistent with the behavior observed in the ultrasonic degradation of SA in saline solutions (Dodero, Vicini

& Castellano, 2020). Likewise, the same low-viscosity commercial SA exhibited a flow behavior index of 0.95, close to Newtonian index (Zimoch-Korzycka et al., 2021).

Concerning pH 3, it was expected their higher viscosity and distinct rheological behavior due to the acid-induced gelation of alginate. This comes from the fact that this pH level falls below the pKa values for SA acids, specifically 3.4 for mannuronic acid and 3.6 for guluronic acid (Haug, 1964). Consequently, the carboxylic acid units become less dissociated, resulting in a reduction in the degree of ionization within the alginate structure. This reduction leads to a decrease in the quantity of negatively charged groups (COO−) and a subsequent decrease in electrostatic repulsive interactions. Consequently, it allows the polymer chains to become protonated and form hydrogen bonds, allowing the formation of aggregates (Zhao et al., 2016), which could be noted by an increase in turbidity in these samples. As a result, these samples also exhibited a higher consistency index (K) and a lower "n" value, demonstrating their shear-thinning behavior. In general, it was observed higher viscosities for pH 3 solutions among the 4 studied pHs, indicating the sensitivity of rheological response to pH variations within the low pH range, likely reflecting intensified intermolecular interactions (Yang, Chen & Fang, 2009).

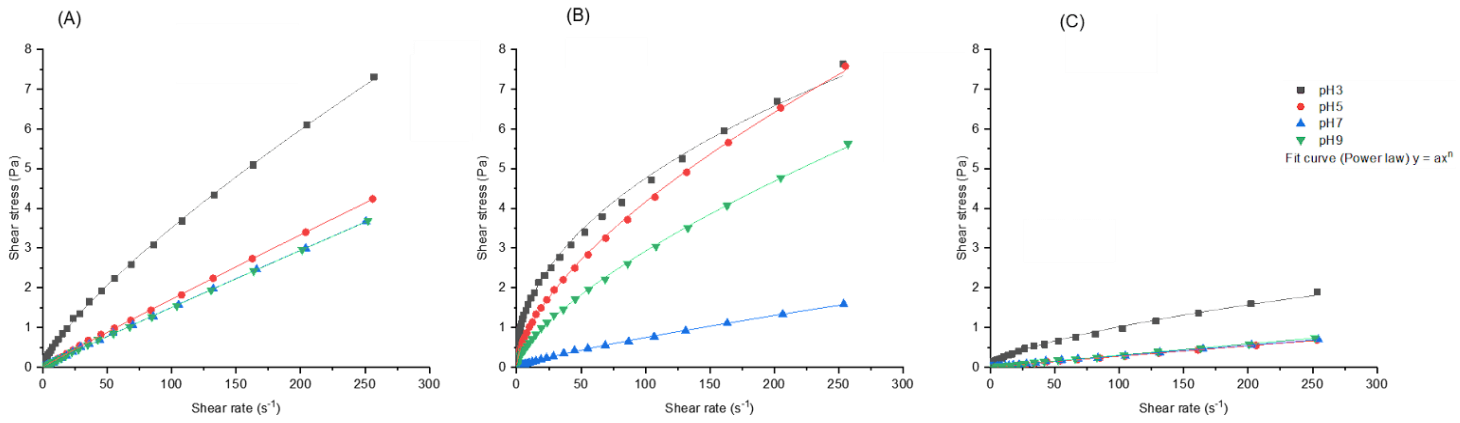

Fig. 1 – Flow curves of sodium alginate solutions at different pH levels with fit curves adjusted for the power law model. (A) - Commercial, (B) - Native, (C) - Ozonized

Table 3 - Rheological flow data of sodium alginate solutions (2% w/v) at various pH levels adjusted to Newtonian and Power Law models

Model	Parameters	Commercial				Native				Ozonized			
		pH3	pH5	pH7	pH9	pH3	pH5	pH7	pH9	pH3	pH5	pH7	pH9
Newtonian	μ	30	20	20	20	30	30	10	20	10	3	3	3
	R^2	0.98	0.99	0.99	0.99	0.90	0.96	0.99	0.97	0.96	0.99	0.99	0.99
Ostwald-de-Waele (Power Law)	n	0.77	0.96	0.96	0.97	0.47	0.62	0.80	0.68	0.62	0.96	0.93	0.96
	K	100	20	20	20	550	230	200	130	60	3	4	4
	R^2	0.99	0.99	0.99	0.99	0.99	0.99	0.99	0.99	0.99	0.99	0.99	0.99

where μ is the viscosity (mPa.s), τ is the shear stress (Pa), $\dot{\gamma}$ is the shear rate (s^{-1}), K is consistency index ($mPa.s^n$), n is the flow behavior index (dimensionless), R^2 is the coefficient of determination.

3.3. Colorimetric analysis

As already observed there is a color change of SA after its degradation, also named depolymerization. For example, the color of the SA solution changed from intense brown to yellow brown when the solution plasma process was applied to degrade it (Watthanaphanit & Saito, 2013). In addition, studies with ozone gas also observed the bleaching effect through SA solutions (Yamashita et al., 2021). In the present study, the colorimetric indices were used to characterize and compare commercial, native and ozonized SA (Fig. 2). Commercial sample exhibits the highest L* index, presumably due to the bleaching treatment it undergoes before being marketed. Following the commercial sample, the ozonized SA displays a slightly lower L* index, which may be due to the effects of the ozonation procedure. Conversely, a reversed trend was found for the a* index, where all samples are situated within the red color space. However, the b* index reveals a more pronounced yellow hue in the ozonized SA sample, while commercial and native did not show a significant difference. As we compared the native and ozonized samples with the commercially available SA, the degree of similarity was assessed using the total color difference (ΔE). As expected, the native sample (13.61 ± 1.37) exhibited a greater magnitude of difference compared to the ozonized sample (4.77 ± 0.49).

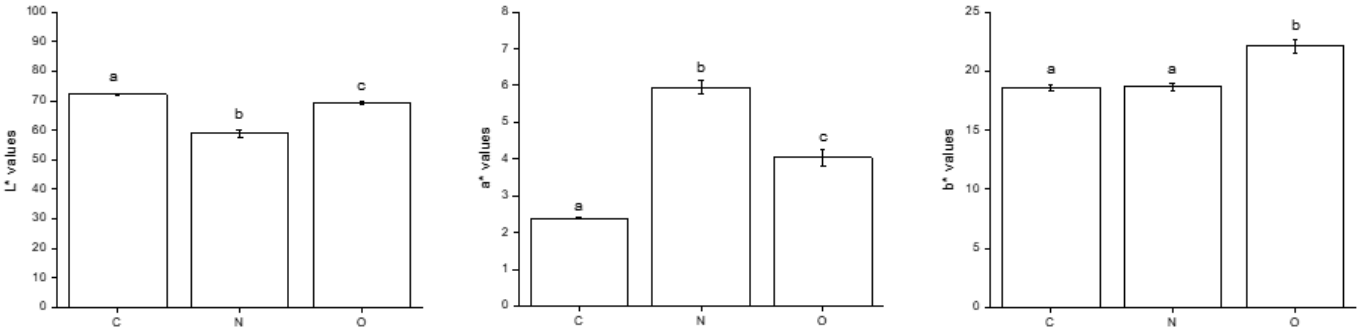

Fig. 2 - The color values of the C (commercial), N (native), O (ozonized) sodium alginates. Different letters above a column in the same group indicate significant differences ($p \leq 0.05$). Data are the mean ± SD (n = 3).

3.4. Thermogravimetric analysis

The TGA and DSC curves are displayed in Figs. 3 and 4. The mass of the samples change as the temperature rises during the test, and the thermal stability may be compared using both the final weight loss rate and the initial temperature, when decomposition begins (Liu et al., 2015). The thermal decomposition of the samples can be described in three consecutive steps. Firstly, a gradual weight loss of 10% for the commercial sample and 20% for both native and ozonized alginates was found until 225 °C, which is attributed to the evaporation of non-bonded water of the samples (Mallick et al., 2018). The lower water loss in commercial alginate may be due to the lower a_w in the sample (Table 2). The second weight loss step was observed within the temperature range of 225 °C to 275 °C, marked by a significant and sudden reduction in mass for the commercial SA. This observation suggests the decomposition of the salt component within the polymer network, specifically due to the dehydration of hydroxyl groups along the alginate backbone (Yan et al., 2016). The final weight loss step was identified within the temperature range of 275–800 °C, exhibiting a loss of approximately 20% across all three samples. This phenomenon can be attributed to the decomposition of the polymer network, leading to the generation of sodium carbonate and the subsequent formation of carbonized residues (Soares et al., 2004; Jain & Datta, 2016).

The TGA general profiles did not change markedly but it was noted that both native and ozonized SA samples demonstrate a slower rate of weight loss, resulting in significantly less mass reduction compared to the commercial sample. The total weight loss of commercial, native and ozonized

SA at 800 °C were 65%, 55%, 60% respectively. The ozonized and commercial samples exhibited reduced residual weight, which can be ascribed to the oxidation of hydroxyl groups within SA (Wang et al., 2022). This effect is significant since both samples exhibited a Newtonian-like behavior, and regardless of the method employed, commercial SA required the breakage of its polymer chains to achieve viscosity reduction. These findings can also be attributed to the viscosity-average molecular weight (Mv) since the native sample exhibits a higher value (Table 2).

From the DTG curves (Fig 3), it can be observed that a weight loss stage occurred at around 250 °C and was attributed to the thermal decomposition of the biopolymer, which was gradually cracked into CO, CO_2 and H_2O, resulting in a rapid decline in their weight (Liu et al., 2015). The temperatures corresponding to the maximum rates of the thermal decomposition weight loss of commercial SA was 245 °C and 250 °C for native and ozonized, respectively. The onset of thermal decomposition, marked by the inception of the dashed curve leading to the formation of a valley, revealed that the temperatures for commercial and ozonized were slightly lower than that for the native. A similar trend was observed in previous studies conducted by Mallick et al. (2018) and Wang et al. (2022). These studies established a connection between lower Mv polysaccharides and increased volatility, which could accelerate degradation. However, from our findings, the thermal stability of ozonized SA did not experience a significant decrease after structural cleavage through ozonation.

The DSC curves of alginates (Fig 4) shows an endothermic peak close to 250 °C followed by an exothermic peak at 300 °C. These phenomena were attributed to the polymer's decomposition, leading to the formation of carbonized residues, a correlation consistent with the findings from the TGA analysis. The dehydration process was not evident in the DSC curves, in contrast to what was observed in both the TGA graphs and the findings reported by Soares et al. (2004).

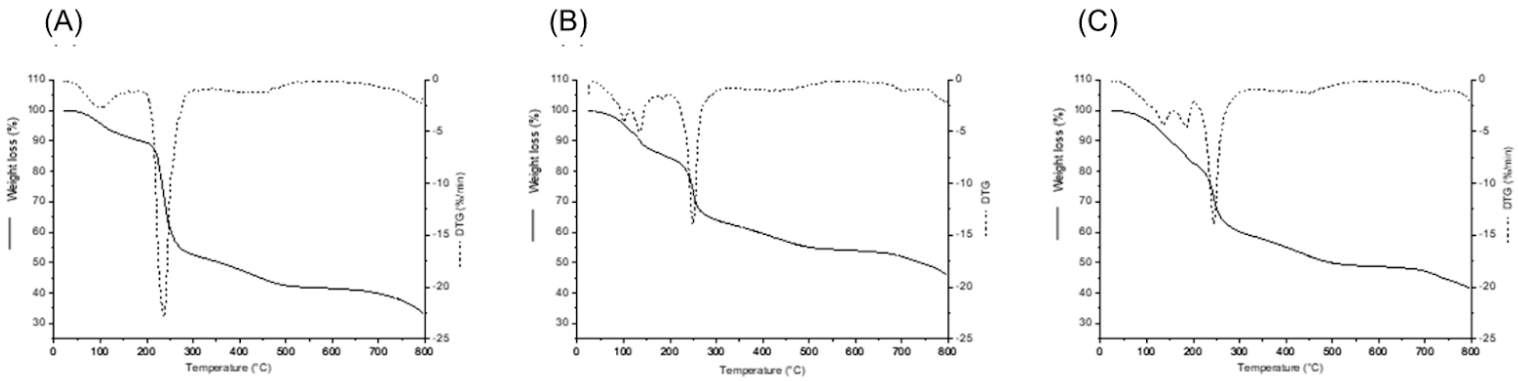

Fig. 3 - Thermogravimetric analysis of sodium alginates (A- Commercial, B – Native, C- Ozonized)

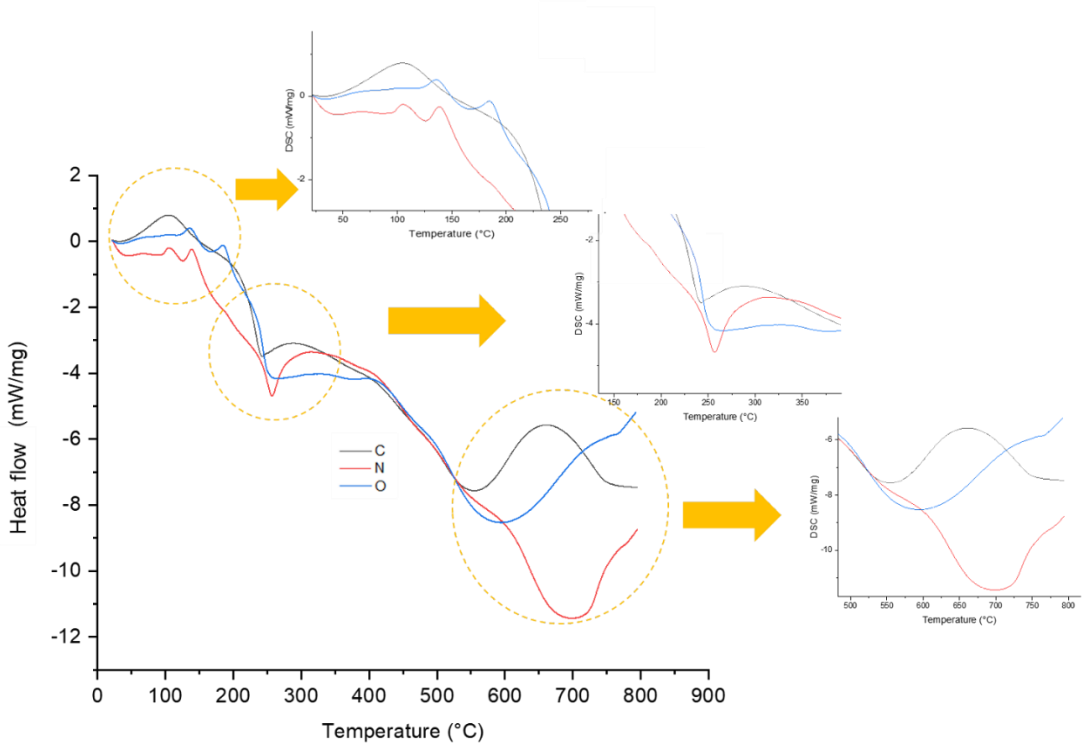

Fig. 4 - Differential scanning calorimetry (DSC) curves of commercial (C), native (N) and ozonized (O) sodium alginates

3.5. ATR-MIR spectroscopy

The MIR analysis (Fig. 5) shows the characteristic absorption bands of the SA with those previously reported (El Atouani et al., 2016; Yamashita et al., 2021; Yue et al., 2021; Wang et al., 2022) which are indicated by dotted lines. Spectra of alginates showed a broad peak around 3250 cm^{-1} and 2900 cm^{-1} corresponding to O-H and C-H stretching vibrations, respectively (Jain & Datta, 2016). These peaks at 4000–2000 cm^{-1} region are common to polysaccharides (El Atouani et al., 2016). The presence of bands at 1617 cm^{-1} and 1417 cm^{-1} are due, respectively, to asymmetric and symmetric stretching vibrations of the carboxylate group, indicating the presence of carboxyl groups (Kok & Wong, 2022). Distinctive band in the range of 1220–1260 cm^{-1} was attributed to the presence of sulfate ester groups (S = O) (Pereira, Gheda & Ribeiro-Claro, 2013). This is characteristic of sulfated polysaccharides. Only the native and ozonized samples exhibited this band, indicating the presence of these water-soluble compounds which were extracted with the alginate.

The peaks observed at 1090 cm^{-1} and 1030 cm^{-1} correspond to the stretching vibrations of the C–O group within the pyranose rings, with the latter attributed to the cyclic C–O bond found within the alginic acid ring (Jain & Datta, 2016). An observed reduction in the peak at 1090 cm^{-1} was noted in the low viscosity samples, both commercial and ozonized, when compared to the native sample. This decrease may be attributed to the cleavage of glycosidic bonds, as suggested by Mao et al. (2012). Furthermore, the band detected at 945.5 cm^{-1} is indicative of the C–O stretching vibration associated with guluronic acid, while the band at 810 cm^{-1} can be attributed to the characteristic signatures of mannuronic acid residues (Kok & Wong, 2022).

Nonetheless, the symmetric vibration associated with the aldehyde group, a possible product of ozonolysis reaction in alginate chain, at 1735 cm^{-1} (Wang et al., 2022), was absent in the ozone-treated sample. It is plausible that ozonation was insufficient to generate detectable levels of free aldehyde groups. Yue et al. (2021) produced low molecular weight SA by ozonation and did not find this peak either.

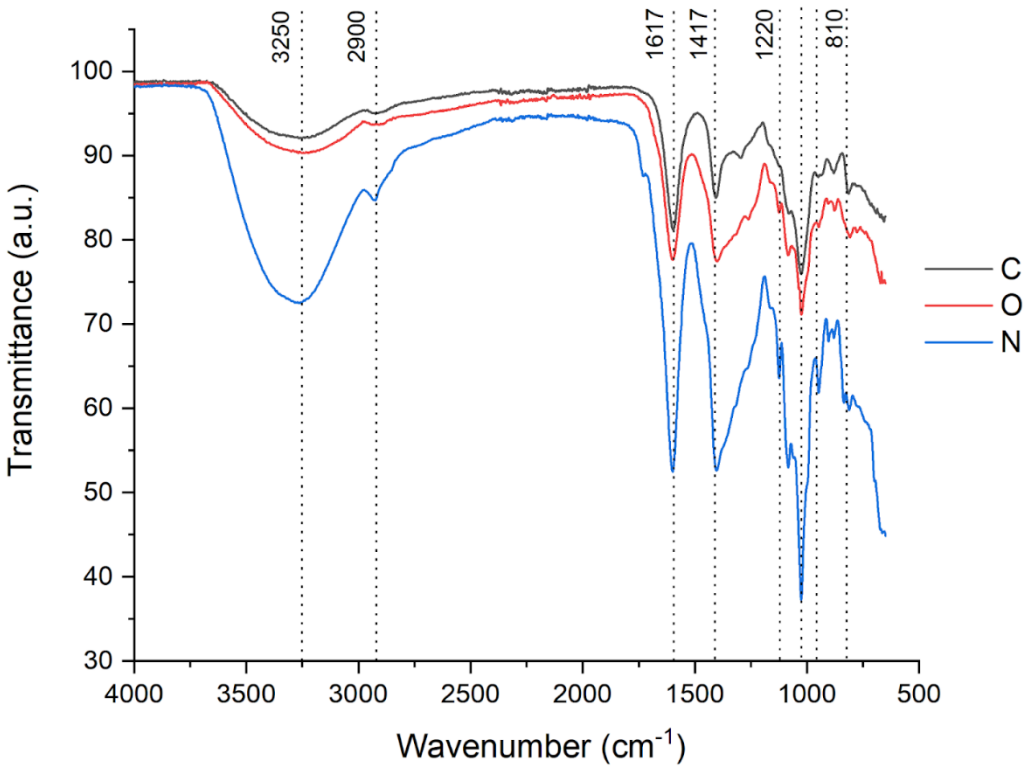

Fig. 5 - Attenuated Total Reflectance (ATR) Fourier-Transform Infrared (FTIR) in the mid-infrared region spectra of commercial (C), native (N) and ozone-treated (O) sodium alginates at 4000 −650 cm^{-1} region

No obvious differences were observed in the MIR spectra of ozone-treated and native SA in comparison with that of commercial, confirming the identity of the extracted sample as sodium alginate and indicating that main functional groups and chemical bonds still present after ozonation process.

3.6. ^{1}H NMR

The distribution sequence and composition of the two uronate residues in alginate samples were carried out ^{1}H NMR spectroscopy (Yuan & Macquarrie, 2015). Fig. 6 shows the NMR spectra of the SA extracted from the *Sargassum* spp., the ozone-treated and commercial samples with the peaks representing the H1 and H5 signals for mannuronic acid (M) and guluronic acid (G) residues. In accordance with literature data, the signal at approximately 5.0 ppm can be attributed to the H-1 of α-L-guluronic acid (G1), the minor peaks centred around 4.65 ppm arise from H-5 of G residues adjacent to mannuronic acid (M) residues (GM5), while the signals between 4.55 and 4.50 ppm were assigned to H-1 of β-D-mannuronic acid (M1) residues. The resonance at 4.40 ppm was attributed to H-5 of guluronic acid (G5) (Grasdalen, 1983).

The peak assignments in the spectra exhibit slight variations in the chemical shift, and these differences can be ascribed to the presence of trace of impurities in the extracted and ozone-treated alginates, as well as disparities in chemical composition and properties such as molecular weight (Mohammed et al., 2018). The chemical shifts of the signature protons for the native and ozonized alginates from *Sargassum* and commercial brand Sigma overlay suitably, confirming that the polysaccharide extracted was in fact alginate. In addition, these characteristics signals were also assigned on the basis of the data previously reported in the literature (Bertagnolli et al., 2014; Et Altouani et al., 2016; Mohammed et al., 2018; Wang et al., 2022; Wang et al., 2023).

The block structure and M/G ratio were calculated following the methodology outlined in the report by Jensen, Larsen, and Engelsen (2015). The M/G ratio (Table 4) of both extracted and ozonized SA lie within the range observed in the *Sargassum* genus, characterized by an enriched content of guluronic acid (Mohammed et al., 2018). In contrast, the commercial sample exhibited a high M/G ratio, indicating a prevalence of mannuronic residues. Furthermore, it can be inferred that ozonation induced depolymerization of the SA backbone, as also evidenced by a decrease in the M/G ratio from 0.76 (native) to 0.74 (ozonized), as observed by Rivero-Ramos et al. (2023) and Yamashita et al. (2021).

Although the similar rheological behavior as low-viscosity polysaccharides, it is crucial to note that the commercial and ozonized samples did not share similar chemical compositions. Therefore, given that the uronic acid sequence significantly influences the gelling capabilities of SA (Jensen, Larsen & Engelsen, 2015), it is plausible that they exhibit distinct gelling capacities. Alginates with M/G ratios exceeding one are well-suited for producing elastic gels applicable in the food,

cosmetic, or pharmaceutical industries, as M-blocks exhibit flexible and linear conformations (Murillo-Alvarez & Hernandez-Carmona, 2007). Nonetheless, gel formation occurs mainly as a result of the formation of enriched GG junction zones due to the cooperative binding of ions to G blocks (Draget & Taylor, 2011). Consequently, alginates characterized by a low M/G ratio yield hard and brittle gels (Penman & Sanderson, 1972).

Therefore, both native and ozonized sodium alginate (SA) are more likely to form strong gels since their M/G values show the possession of elevated guluronic acid content. Furthermore, the ozonation process proved effective in slightly modifying their chemical composition while ensuring satisfactory physicochemical properties for a broad spectrum of applications.

Table 4 - Uronic acid compositions and M/G ratio for sodium alginates samples

	F_G	F_M	F_{GG}	F_{MM}	F_{MG}	M/G
Native	0.57	0.43	0.27	0.14	0.29	0.75
Ozonized	0.58	0.42	0.28	0.11	0.31	0.72
Commercial	0.43	0.47	0.33	0.47	0.11	1.10

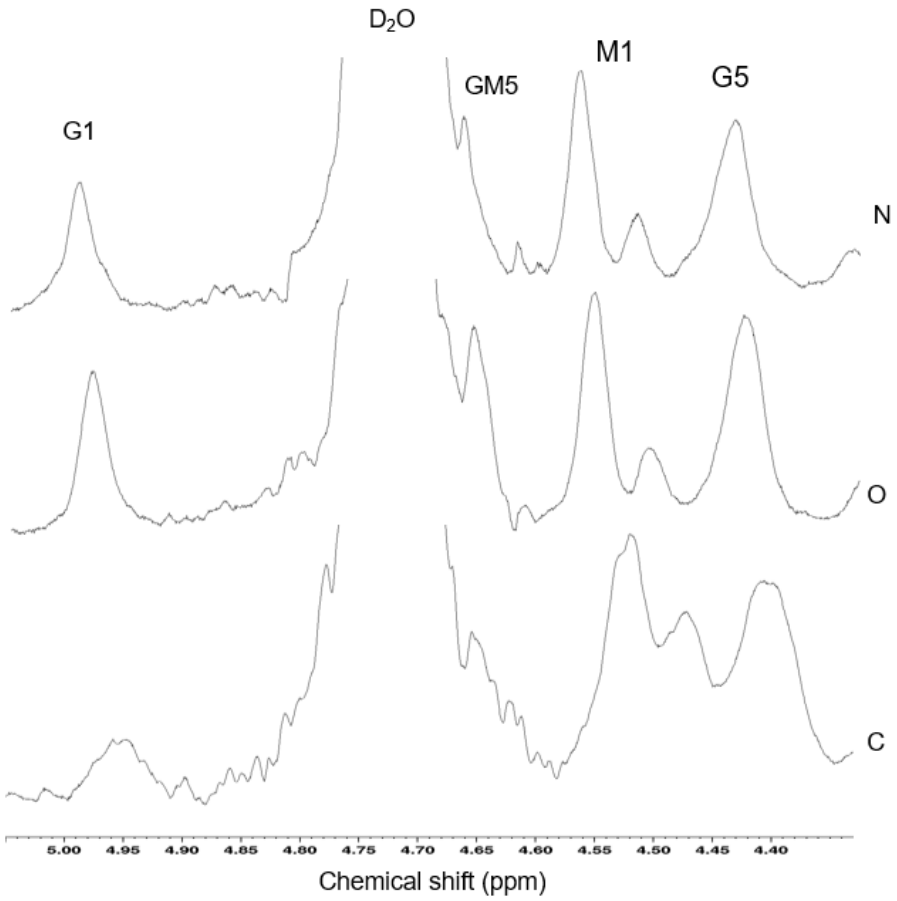

Fig. 6 - ^{1}H NMR spectrum of the sodium alginate from Sargassum spp. Native (N), ozonized (O) and commercial (C) sample.

3.7. Particle size, Polydispersity index (PDI), Zeta Potential (ZP) and Conductivity

The Hydrodynamic size, PDI, ZP, and conductivity were investigated across a range of pH levels for the commercial, native and ozonized SA. All alginates consistently exhibited the highest values of hydrodynamic size at pH 3 (Table 5), and were the only ones that demonstrated statistically significant differences within the pH range for commercial and native SA solutions. These results align with the rheological behavior (Table 3), where pH 3 exhibited a notably higher viscosity and a flow behavior index (n) that diverged further from Newtonian behavior, potentially attributed to a reduction in electrostatic repulsive interactions, resulting in increased chain entanglement, as previously discussed.

The PDI is a crucial parameter, offering insights into the width of droplet size distribution and the uniformity of SA solutions. A PDI value approaching zero is preferable, signifying a uniformly dispersed sample. Conversely, elevated PDI values, converging towards 1, denote a non-uniform distribution of globule sizes (Mirković et al., 2017). Analysis of the PDI (Table 5) reveals a similar and polydisperse droplet sizet distribution among all the alginates within the pH range. Statistical analysis did not reveal any significant trends or variations across the different pH levels. The recorded values are considered low, signifying a narrow mass distribution range, thus confirming the existence of a homogeneous alginate polymer (Hentati et al., 2018). The even distribution within the polymer structure may enhance its suitability for gel formation, ensuring the homogeneous creation of a robust network (Kuo & Ma, 2001).

Regarding zeta potential, its value should be lower than -30 mV or greater than +30 mv for an ample electrostatic repulsion, effectively preventing particle agglomeration (Guo et al., 2014). It is worth noting that acidic polysaccharides, such as SA, may encounter challenges in maintaining a stable system solely through electronic potential (Ghorbani et al., 2018). Table 5 and Fig. 7 show the zeta potential values of commercial, native, and ozonized SA at various pH levels. Across the pH range, samples exhibited zeta potential values below -20 mV, with the commercial and ozonized SA generally displaying the lowest values, except at pH 7, where native and ozonized presented similar results. These findings underscore the impact of the ozonation process, which tends to shift zeta potential values towards more negative ranges, comparing native and ozonized samples. This characteristic could contribute to the utilization of ozonized sodium alginate in the preparation of nanoparticles or (nano)emulsions, scenarios that demand particle repulsion. Additionally, this phenomenon is interconnected with the Mv (Table 3).

Conductivity is the inherent capability of a material to facilitate the flow of electric current (Ricaurte et al., 2018). Table 5 shows that solutions of SA at a pH of 3 exhibited significantly elevated conductivity values. This outcome underscores an enhanced degree of ionization within these solutions, indicative of a greater concentration of ions, thereby augmenting their conductivity. The conductivity of an aqueous solution is intrinsically linked to the concentration of ions where the presence of H^+ ions exerts a more pronounced influence than cations (Bonin et al., 2011).

Intriguingly, our data aligns with the hypothesis of free H^+ ions within the solution. At the onset, the initial pH of both native and ozone-treated samples approximates 10. Subsequently, the addition of HCl solution is incrementally increased to reach a pH of 3, resulting in a proportional elevation in the concentration of H^+ ions and, consequently, the measured conductivity values. In

the case of the commercial sample, which originally possesses an initial pH of approximately 5, it becomes evident that the introduction of HCl solution to lower the pH to 3 releases H^+ ions and increase in conductivity. Notably, the conductivity values further increase at pH levels of 7 and 9, where NaOH solution is introduced, thereby augmenting the concentration of OH^- ions.

Hence, it is noteworthy that ozone-treated SA exhibited a consistently stable response across the entire pH range under investigation. This stability is evident as the zeta potential, conductivity, and low PDI values showed no significant differences among the pH conditions studied. This attribute can be considered advantageous in the utilization of ozonized SA, which demonstrated stability in important parameters.

Table 5 - Hydrodynamic size (nm), polydispersity index (PDI), zeta potential (mV), and conductivity (mS/cm) of commercial, native and ozonized sodium alginates in different pHs

	Commercial				Native				Ozonized			
	pH 3	**pH 5**	**pH 7**	**pH 9**	**pH 3**	**pH 5**	**pH 7**	**pH 9**	**pH 3**	**pH 5**	**pH 7**	**pH 9**
Hydrodynamic size (µm)	$4.4^{a} \pm 0.8$	$1.9^{b} \pm 0.3$	$2.7^{b} \pm 0.8$	$1.8^{b} \pm 0.4$	$6.2^{c} \pm 0.1$	$0.7^{d} \pm 0.03$	$0.5^{d} \pm 0.07$	$1.2^{d} \pm 0.10$	$2.3^{e} \pm 0.2$	$1.3^{f} \pm 0.07$	$0.8^{g} \pm 0.05$	$1.2^{f} \pm 0.04$
PDI	$0.31^{a} \pm 0.02$	$0.26^{ab} \pm 0.03$	$0.25^{b} \pm 0.03$	$0.28^{ab} \pm 0.02$	$0.34^{c} \pm 0.03$	$0.29^{d} \pm 0.01$	$0.27^{d} \pm 0.01$	$0.29^{d} \pm 0.02$	$0.27^{e} \pm 0.05$	$0.29^{e} \pm 0.02$	$0.34^{e} \pm 0.02$	$0.30^{e} \pm 0.02$
Zeta Potential (mV)	$-37.5^{a} \pm 0.9$	$-32.5^{a} \pm 1.5$	$-24.3^{b} \pm 1.5$	$-37.3^{a} \pm 3.5$	$-31.7^{c} \pm 1.7$	$-25.6^{d} \pm 2.1$	$-30.6^{c} \pm 1.0$	$-20.2^{e} \pm 1.2$	$-34.2^{f} \pm 2.1$	$-33.2^{f} \pm 2.4$	$-30.1^{f} \pm 2.9$	$-35.2^{f} \pm 0.3$
Conductivity (mS/cm)	$0.9^{a} \pm 0.02$	$0.4^{b} \pm 0.01$	0.5 ± 0.0^{c}	$0.8^{d} \pm 0.02$	$1.1^{e} \pm 0.02$	$0.8^{f} \pm 0.01$	$0.8^{f} \pm 0.01$	$0.7^{g} \pm 0.01$	$0.8^{h} \pm 0.02$	$0.7^{i} \pm 0.02$	$0.65^{j} \pm 0.02$	$0.6^{j} \pm 0.01$

Statistical analysis was conducted on the various pH values within the same type of sodium alginate, with distinct letters denoting significant differences ($p \leq 0.05$). Data are the mean ± SD ($n = 3$).

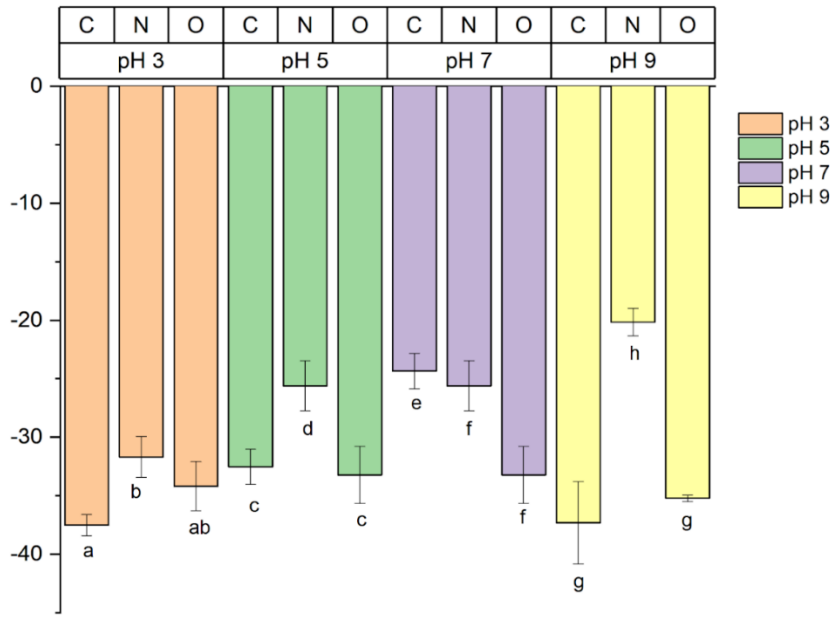

Fig. 7 - Zeta potential of commercial (C), native (N) and ozonized (O) sodium alginates in different pHs. Statistical analysis was performed among the different SA in the same pH value where distinct letters denoting significant differences ($p \leq 0.05$). Data are the mean ± SD ($n = 3$).

4. Conclusion

This study explored the potential of ozonation to modify sodium alginate, which was extracted with satisfactory yield using citric acid and ultrasound as a sustainable alternative. The structural analysis of SA after ozonation emphasized the integrity and high degree of purity of its chemical structure. Colorimetric analysis revealed similarities between the ozonized sample and commercial alginate, possibly due to the effects of ozonation. Significant depolymerization of the SA chains was observed after ozonation, resulting in a reduction in the average molecular weight of viscosity. Rheological analysis highlighted the influence of pH on rheological properties, with commercial and ozonized samples exhibiting similar Newtonian behavior. Even with depolymerization, ozonized alginate maintained its thermal stability. The Polydispersity Index (PDI) analysis indicated a uniform molecular size distribution among the alginates, and the zeta potential decreased after ozonation. These findings contribute significantly to the understanding of the industrial applications of modified sodium alginate, addressing a substantial knowledge gap. Moreover, they unveil new opportunities for diverse applications, driven by the properties elucidated in this study.

5. References

Abd El-Mohdy, H. L. (2017). Radiation-induced degradation of sodium alginate and its plant growth promotion effect. Arabian Journal of Chemistry, 10, S431-S438. https://doi.org/10.1016/j.arabjc.2012.10.003

Afzal, S., Maswal, M., & Dar, A. A. (2018). Rheological behavior of pH responsive composite hydrogels of chitosan and alginate: characterization and its use in encapsulation of citral. Colloids and Surfaces B: Biointerfaces, 169, 99-106. https://doi.org/10.1016/j.colsurfb.2018.05.002

Allen Jr, L. V. (2018). Quality Control: Water Activity Considerations for Beyond-use Dates. International Journal of Pharmaceutical Compounding, 22(4), 288-293.

Anghel, N., Dinu, M. V., Zaltariov, M., Pamfil, D., & Spiridon, I. (2021). New cellulose-collagen-alginate materials incorporated with quercetin, anthocyanins and lipoic acid. International Journal of Biological Macromolecules, 181, 30-40. https://doi.org/10.1016/j.ijbiomac.2021.03.120

Belattmania, Z., El Atouani, S., Bentiss, F., Jama, C., Falace, A., Chaouti, A., Reani, A., & Sabour, B. (2022). Seasonal patterns of growth, alginate content and block structure of the alien invader Sargassum muticum (Fucales, Ochrophyta) from the Atlantic coast of Morocco. Botanica Marina, 65(1), 69-78. https://doi.org/10.1515/bot-2021-0050

Benslima, A., Sellimi, S., Hamdi, M., Nasri, R., Jridi, M., Cot, D., Li, S., Nasri, M., & Zouari, N. (2021). The brown seaweed Cystoseira schiffneri as a source of sodium alginate: Chemical and structural characterization, and antioxidant activities. Food Bioscience, 40, 100873. https://doi.org/10.1016/j.fbio.2020.100873

Bertagnolli, C., Espindola, A. P. D., Kleinübing, S. J., Tasic, L., & da Silva, M. G. C. (2014). Sargassum filipendula alginate from Brazil: Seasonal influence and characteristics. Carbohydrate Polymers, 111, 619–623. https://doi.org/10.1016/j. carbpol.2014.05.024.

Bonin, J., Costentin, C., Louault, C., Robert, M., & Savéant, J. M. (2011). Water (in water) as an Intrinsically efficient proton acceptor in concerted proton electron transfers. *Journal of the American Chemical Society*, *133*(17), 6668-6674. https://doi.org/10.1021/ja110935c

Cai, Y. Z., & Corke, H. (2000). Production and properties of spray-dried Amaranthus Betacyanin pigments. Journal of Food Science, 65(6), 1248–1252. https://doi.org/10.1111/j.1365-2621.2000.tb10273.x

Chen, J., Wu, A., Yang, M., Ge, Y., Pristijono, P., Li, J., Jianrong, L., Xu, B., & Mi, H. (2021). Characterization of sodium alginate-based films incorporated with thymol for fresh-cut apple packaging. Food Control, 126, 108063. https://doi.org/10.1016/j.foodcont.2021.108063

Cheng-Rong, T. S. A. I., & Yung-Kai, L. I. N. (2022). Artificial steak: A 3D printable hydrogel composed of egg albumen, pea protein, gellan gum, sodium alginate and rice mill by-products. Future Foods, 5, 100121. https://doi.org/10.1016/j.fufo.2022.100121

Clementi, F., Mancini, M., & Moresi, M. (1998). Rheology of alginate from Azotobacter vinelandii in aqueous dispersions. Journal of food engineering, 36(1), 51-62. https://doi.org/10.1016/S0260-8774(98)00042-9

Dodero, A., Vicini, S., & Castellano, M. (2020). Depolymerization of sodium alginate in saline solutions via ultrasonic treatments: A rheological characterization. Food Hydrocolloids, 109, 106128. https://doi.org/10.1016/j.foodhyd.2020.106128

Draget, K. I., & Taylor, C. (2011). Chemical, physical and biological properties of alginates and their biomedical implications. Food hydrocolloids, 25(2), 251-256. https://doi.org/10.1016/j.foodhyd.2009.10.007

Eastman, J. E., & Moore, C. O. (1984). U.S. Patent No. 4,465,702. Washington, DC: U.S. Patent and Trademark Office.

El Atouani, S., Bentiss, F., Reani, A., Zrid, R., Belattmania, Z., Pereira, L., Mortadi, A., Cherjaoui, O. & Sabour, B. (2016). The invasive brown seaweed Sargassum muticum as new resource for alginate in Morocco: Spectroscopic and rheological characterization. Phycological Research, 64(3), 185-193. https://doi.org/10.1111/pre.12135

Fawzy, M. A., & Gomaa, M. (2021). Optimization of citric acid treatment for the sequential extraction of fucoidan and alginate from Sargassum latifolium and their potential antioxidant and Fe (III) chelation properties. Journal of Applied Phycology, 33, 2523-2535. https://doi.org/10.1007/s10811-021-02453-9

Fernando, I. P. S., Lee, W., Han, E. J., & Ahn, G. (2020). Alginate-based nanomaterials: Fabrication techniques, properties, and applications. Chemical Engineering Journal, 391, 123823. https://doi.org/10.1016/j.cej.2019.123823

Fernando, I. P. S., Kirindage, K. G. I. S., Jeon, H. N., Han, E. J., Jayasinghe, A. M. K., & Ahn, G. (2022). Preparation of microspheres by alginate purified from Sargassum horneri and study of pH-responsive behavior and drug release. International Journal of Biological Macromolecules, 202, 681-690. https://doi.org/10.1016/j.ijbiomac.2022.01.171

Flórez-Fernández, N., Domínguez, H., & Torres, M. D. (2019). A green approach for alginate extraction from Sargassum muticum brown seaweed using ultrasound-assisted technique. International journal of biological macromolecules, 124, 451-459. https://doi.org/10.1016/j.ijbiomac.2018.11.232

Ghorbani Gorji, E., Waheed, A., Ludwig, R., Toca-Herrera, J. L., Schleining, G., & Ghorbani Gorji, S. (2018). Complex coacervation of milk proteins with sodium alginate. Journal of agricultural and food chemistry, 66(12), 3210-3220.

Grasdalen, H. (1983). High-field, 1H-nmr spectroscopy of alginate: sequential structure and linkage conformations. Carbohydrate Research, 118, 255-260.

Guo, X., Zhao, W., Pang, X., Liao, X., Hu, X., & Wu, J. (2014). Emulsion stabilizing properties of pectins extracted by high hydrostatic pressure, high-speed shearing homogenization and traditional thermal methods: A comparative study. Food Hydrocolloids, 35, 217-225.

Haug, A. (1964). Composition and properties of alginates. In Thesis. Trondheim: Norwegian Institute of Technology.

Hentati, F., Delattre, C., Ursu, A. V., Desbrières, J., Le Cerf, D., Gardarin, C., Abdelkafi, S., Michaud, P., & Pierre, G. (2018). Structural characterization and antioxidant activity of water-soluble polysaccharides from the Tunisian brown seaweed Cystoseira compressa. Carbohydrate polymers, 198, 589-600. https://doi.org/10.1016/j.carbpol.2018.06.098

Hentati, F., Pierre, G., Ursu, A. V., Vial, C., Delattre, C., Abdelkafi, S., & Michaud, P. (2020). Rheological investigations of water-soluble polysaccharides from the Tunisian brown seaweed Cystoseira compressa. Food Hydrocolloids, 103, 105631. https://doi.org/10.1016/j.foodhyd.2019.105631

Im, S., Choe, G., Seok, J. M., Yeo, S. J., Lee, J. H., Kim, W. D., Lee, J. Y., & Park, S. A. (2022). An osteogenic bioink composed of alginate, cellulose nanofibrils, and polydopamine nanoparticles for 3D bioprinting and bone tissue engineering. International Journal of Biological Macromolecules, 205, 520-529. https://doi.org/10.1016/j.ijbiomac.2022.02.012

Jain, S., & Datta, M. (2016). Montmorillonite-alginate microspheres as a delivery vehicle for oral extended release of venlafaxine hydrochloride. Journal of Drug Delivery Science and Technology, 33, 149-156. https://doi.org/10.1016/j.jddst.2016.04.002

Jensen, H. M., Larsen, F. H., & Engelsen, S. B. (2015). Characterization of alginates by nuclear magnetic resonance (NMR) and vibrational spectroscopy (IR, NIR, Raman) in combination with chemometrics. Natural Products From Marine Algae: Methods and Protocols, 347-363.

Kelishomi, Z. H., Goliaei, B., Mahdavi, H., Nikoofar, A., Rahimi, M., Moosavi-Movahedi, A. A., Mamashli, F & Bigdeli, B. (2016). Antioxidant activity of low molecular weight alginate produced by thermal treatment. Food chemistry, 196, 897-902. https://doi.org/10.1016/j.foodchem.2015.09.091

Kok, J. M. L., & Wong, C. L. (2022). In vitro properties of methanol extract and sodium alginate of Sargassum polycystum C. Agardh brown seaweed collected from Malaysia. Tropical Life Sciences Research, 33(1), 55. 10.21315/tlsr2022.33.1.4

Kuo, C. K., & Ma, P. X. (2001). Ionically crosslinked alginate hydrogels as scaffolds for tissue engineering: Part 1. Structure, gelation rate and mechanical properties. Biomaterials, 22(6), 511-521. https://doi.org/10.1016/S0142-9612(00)00201-5

Lee, K. Y., & Mooney, D. J. (2012). Alginate: properties and biomedical applications. Progress in polymer science, 37(1), 106-126. https://doi.org/10.1016/j.progpolymsci.2011.06.003

Liu, Y., Zhao, J. C., Zhang, C. J., Guo, Y., Cui, L., Zhu, P., & Wang, D. Y. (2015). Bio-based nickel alginate and copper alginate films with excellent flame retardancy: preparation, flammability and thermal degradation behavior. RSC advances, 5(79), 64125-64137. https://doi.org/10.1039/C5RA11048C

Liu, J., Yang, S., Li, X., Yan, Q., Reaney, M. J., & Jiang, Z. (2019). Alginate oligosaccharides: Production, biological activities, and potential applications. Comprehensive Reviews in Food Science and Food Safety, 18(6), 1859-1881. https://doi.org/10.1111/1541-4337.12494

Lu, X., Qin, L., Guo, M., Geng, J., Dong, S., Wang, K., Xu, H., Qu, C., Miao, J., & Liu, M. (2022). A novel alginate from Sargassum seaweed promotes diabetic wound healing by regulating oxidative stress and angiogenesis. Carbohydrate Polymers, 289, 119437. https://doi.org/10.1016/j.carbpol.2022.119437

Ma, H., Zhao, J., Liu, Y., Liu, L., Yu, J., & Fan, Y. (2023). Controlled delivery of aspirin from nanocellulose-sodium alginate interpenetrating network hydrogels. Industrial Crops and Products, 192, 116081. https://doi.org/10.1016/j.indcrop.2022.116081

Mallick, D., Poddar, M. K., Mahanta, P., & Moholkar, V. S. (2018). Discernment of synergism in pyrolysis of biomass blends using thermogravimetric analysis. Bioresource technology, 261, 294-305. https://doi.org/10.1016/j.biortech.2018.04.011

Mao, S., Zhang, T., Sun, W., & Ren, X. (2012). The depolymerization of sodium alginate by oxidative degradation. Pharmaceutical development and technology, 17(6), 763-769. https://doi.org/10.3109/10837450.2011.583927

Mirković, D., Ibrić, S., Balanč, B., Knez, Ž., & Bugarski, B. (2017). Evaluation of the impact of critical quality attributes and critical process parameters on quality and stability of parenteral nutrition nanoemulsions. Journal of Drug Delivery Science and Technology, 39, 341-347. https://doi.org/10.1016/j.jddst.2017.04.004

Mohammed, A., Bissoon, R., Bajnath, E., Mohammed, K., Lee, T., Bissram, M., John, N., Jalsa, N. K., Lee, K.Y., & Ward, K. (2018). Multistage extraction and purification of waste Sargassum natans to produce sodium alginate: An optimization approach. Carbohydrate polymers, 198, 109-118. https://doi.org/10.1016/j.carbpol.2018.06.067

Mohammed, C., Lalgee, L., Kistow, M., Jalsa, N., & Ward, K. (2022). On the binding affinity and thermodynamics of sodium alginate-heavy metal ion interactions for efficient adsorption. Carbohydrate Polymer Technologies and Applications, 3, 100203. https://doi.org/10.1016/j.carpta.2022.100203

Murillo-Álvarez, J. I., & Hernández-Carmona, G. (2007). Monomer composition and sequence of sodium alginate extracted at pilot plant scale from three commercially important seaweeds from Mexico. Journal of applied phycology, 19, 545-548. https://doi.org/10.1007/s10811-007-9168-5

Newman, A. W., Reutzel-Edens, S. M., & Zografi, G. (2008). Characterization of the “hygroscopic” properties of active pharmaceutical ingredients. Journal of pharmaceutical sciences, 97(3), 1047-1059. https://doi.org/10.1002/jps.21033

Nogueira, M. T., Chica, L. R., Yamashita, C., Nunes, N. S. S., Moraes, I. C. F., Branco, C. C. Z., & Branco, I. G. (2022). Optimal conditions for alkaline treatment of alginate extraction from the brown seaweed Sargassum cymosum C. Agardh by response surface methodology. Applied Food Research, 2(2), 100141. https://doi.org/10.1016/j.afres.2022.100141

Pandiselvam, R., Manikantan, M. R., Divya, V., Ashokkumar, C., Kaavya, R., Kothakota, A., & Ramesh, S. V. (2019). Ozone: An advanced oxidation technology for starch modification. Ozone: Science & Engineering, 41(6), 491-507. https://doi.org/10.1080/01919512.2019.1577128

Pawar, S. N., & Edgar, K. J. (2012). Alginate derivatization: A review of chemistry, properties and applications. Biomaterials, 33(11), 3279-3305. https://doi.org/10.1016/j.biomaterials.2012.01.007

Penman, A., & Sanderson, G. R. (1972). A method for the determination of uronic acid sequence in alginates. Carbohydrate Research, 25(2), 273-282. https://doi.org/10.1016/S0008-6215(00)81637-7

Pereira, L., Gheda, S. F., & Ribeiro-Claro, P. J. (2013). Analysis by vibrational spectroscopy of seaweed polysaccharides with potential use in food, pharmaceutical, and cosmetic industries. International Journal of Carbohydrate Chemistry. http://dx.doi.org/10.1155/2013/537202

Rahelivao, M. P., Andriamanantoanina, H., Heyraud, A., & Rinaudo, M. (2013). Structure and properties of three alginates from Madagascar seacoast algae. Food Hydrocolloids, 32(1), 143-146. https://doi.org/10.1016/j.foodhyd.2012.12.005

Ramdhan, T., Ching, S. H., Prakash, S., & Bhandari, B. (2019). Time dependent gelling properties of cuboid alginate gels made by external gelation method: Effects of alginate-CaCl2 solution ratios and pH. Food hydrocolloids, 90, 232-240. https://doi.org/10.1016/j.foodhyd.2018.12.022

Ramos, P. E., Silva, P., Alario, M. M., Pastrana, L. M., Teixeira, J. A., Cerqueira, M. A., & Vicente, A. A. (2018). Effect of alginate molecular weight and M/G ratio in beads properties foreseeing the protection of probiotics. Food Hydrocolloids, 77, 8-16. https://doi.org/10.1016/j.foodhyd.2017.08.031

Reakasame, S., & Boccaccini, A. R. (2018). Oxidized alginate-based hydrogels for tissue engineering applications: a review. Biomacromolecules, 19(1), 3-21. https://doi.org/10.1021/acs.biomac.7b01331

Ricaurte, L., Hernández-Carrión, M., Moyano-Molano, M., Clavijo-Romero, A., & Quintanilla-Carvajal, M. X. (2018). Physical, thermal and thermodynamical study of high oleic palm oil nanoemulsions. *Food chemistry*, *256*, 62-70. https://doi.org/10.1007/s12247-022-09619-z

Rivero-Ramos, P., Unthank, M. G., Sanz, T., Rodrigo, M. D., & Benlloch-Tinoco, M. (2023). Synergistic depolymerisation of alginate and chitosan by high hydrostatic pressure (HHP) and pulsed electric fields (PEF) treatment in the presence of H2O2. *Carbohydrate Polymers*, *316*, 120999. https://doi.org/10.1016/j.carbpol.2023.120999

Saravanou, S. F., Ioannidis, K., Dimopoulos, A., Paxinou, A., Kounelaki, F., Varsami, S. M., Tsitsilianis, C., Papantoniou, I., & Pasparakis, G. (2023). Dually crosslinked injectable alginate-based graft copolymer thermoresponsive hydrogels as 3D printing bioinks for cell spheroid growth and release. Carbohydrate Polymers, 312, 120790. https://doi.org/10.1016/j.carbpol.2023.120790

Sellimi, S., Younes, I., Ayed, H. B., Maalej, H., Montero, V., Rinaudo, M., et al. (2015). Structural, physicochemical and antioxidant properties of sodium alginate isolated from a Tunisian brown seaweed. International Journal of Biological Macromolecules, 72, 1358–1367. https://doi.org/10.1016/j.ijbiomac.2014.10.016

Serafin, A., Culebras, M., & Collins, M. N. (2023). Synthesis and evaluation of alginate, gelatin, and hyaluronic acid hybrid hydrogels for tissue engineering applications. International journal of biological macromolecules, 233, 123438. https://doi.org/10.1016/j.ijbiomac.2023.123438

Shi, T., Xie, Z., Zhu, Z., Shi, W., Liu, Y., & Liu, M. (2022). Highly efficient and selective adsorption of heavy metal ions by hydrazide-modified sodium alginate. Carbohydrate Polymers, 276, 118797. https://doi.org/10.1016/j.carbpol.2021.118797

Soares, J. D. P., Santos, J. E., Chierice, G. O., & Cavalheiro, E. T. G. (2004). Thermal behavior of alginic acid and its sodium salt. Eclética Química, 29, 57-64. https://doi.org/10.1590/S0100-46702004000200009

Sugiono, S., Masruri, M., Estiasih, T., & Widjanarko, S. B. (2018). Multiple-response optimization of the acidic pre-treatment of the brown alga Sargassum cristaefolium for the alginate extraction using twin screw extruder. Bioscience research, 15(2), 683-693.

Wang, M., Chen, L., & Zhang, Z. (2021). Potential applications of alginate oligosaccharides for biomedicine–A mini review. Carbohydrate Polymers, 271, 118408. https://doi.org/10.1016/j.carbpol.2021.118408

Wang, H., Chen, X., Wen, Y., Li, D., Sun, X., Liu, Z., Yan, H.; & Lin, Q. (2022). A study on the correlation between the oxidation degree of oxidized sodium alginate on its degradability and gelation. *Polymers*, *14*(9), 1679. https://doi.org/10.3390/ polym14091679

Wang, W., Liu, M., Shafiq, M., Li, H., Hashim, R., Mohamed, E. N., Hany, E. H., Morsi, Y., & Mo, X. (2023). Synthesis of oxidized sodium alginate and its electrospun bio-hybrids with zinc oxide nanoparticles to promote wound healing. International Journal of Biological Macromolecules, 232, 123480. https://doi.org/10.1016/j.ijbiomac.2023.123480

Watthanaphanit, A., & Saito, N. (2013). Effect of polymer concentration on the depolymerization of sodium alginate by the solution plasma process. Polymer degradation and stability, 98(5), 1072-1080. https://doi.org/10.1016/j.polymdegradstab.2013.01.011

Xing, M., Cao, Q., Wang, Y., Xiao, H., Zhao, J., Zhang, Q., & Song, S. (2020). Advances in research on the bioactivity of alginate oligosaccharides. Marine drugs, 18(3), 144.https://doi.org/10.3390/md18030144

Xu, Y., Xiao, Y., Lagnika, C., Li, D., Liu, C., Jiang, N., Song, J. & Zhang, M. (2020). A comparative evaluation of nutritional properties, antioxidant capacity and physical characteristics of cabbage (Brassica oleracea var. Capitate var L.) subjected to different drying methods. Food Chemistry, 309, 124935. https://doi.org/10.1016/j.foodchem.2019.06.002

Xu, W., Sun, H., Li, H., Li, Z., Zheng, S., Luo, D., Ning, L.; Wang, Y.; & Shah, B. R. (2022). Preparation and characterization of tea oil powder with high water solubility using Pickering emulsion template and vacuum freeze-drying. LWT, 160, 113330. https://doi.org/10.1016/j.lwt.2022.113330

Yamashita, C., Moraes, I. C. F., Ferreira, A. G., Branco, C. C. Z., & Branco, I. G. (2021). Multi-response optimization of alginate bleaching technology extracted from brown seaweeds by an eco-friendly agent. Carbohydrate Polymers, 251, 116992. https://doi.org/10.1016/j.carbpol.2020.116992

Yan, H.Q.; Chen, X.Q.; Li, J.C.; Feng, Y.H.; Shi, Z.F.; Wang, X.H.; Lin, Q. Synthesis of alginate derivative via the Ugi reaction and its characterization. Carbohydr. Polym. 2016, 136, 757–763. https://doi.org/10.1016/j.carbpol.2015.09.104

Yang, J., Chen, S., & Fang, Y. (2009). Viscosity study of interactions between sodium alginate and CTAB in dilute solutions at different pH values. Carbohydrate Polymers, 75(2), 333-337. https://doi.org/10.1016/j.carbpol.2008.07.037

Yuan, Y., & Macquarrie, D. J. (2015). Microwave assisted step-by-step process for the production of fucoidan, alginate sodium, sugars and biochar from Ascophyllum nodosum through a biorefinery concept. Bioresource technology, 198, 819-827. https://doi.org/10.1016/j.biortech.2015.09.090

Yue, W., Zhang, H. H., Yang, Z. N., & Xie, Y. (2021). Preparation of low-molecular-weight sodium alginate by ozonation. Carbohydrate Polymers, 251, 117104. https://doi.org/10.1016/j.carbpol.2020.117104

Zhang, H., Bian, X., Luo, S., Liu, C., & Hu, X. (2023). Effect of sodium alginate on the yogurt stability was dependent on the thickening effect and interaction between casein micelles and sodium alginate. International Journal of Biological Macromolecules, 235, 123887. https://doi.org/10.1016/j.ijbiomac.2023.123887

Zhao, Y., Shen, W., Chen, Z., & Wu, T. (2016). Freeze-thaw induced gelation of alginates. Carbohydrate Polymers, 148, 45-51. https://doi.org/10.1016/j.carbpol.2016.04.047

Zimoch-Korzycka, A., Kulig, D., Król-Kilińska, Ż., Żarowska, B., Bobak, Ł., & Jarmoluk, A. (2021). Biophysico-chemical properties of alginate oligomers obtained by acid and oxidation depolymerization. Polymers, 13(14), 2258. DOI: 10.3390/polym13142258

CHAPTER 2: ENCAPSULATION OF ANTHOCYANIN-RICH EXTRACT WITH DIFFERENT SODIUM ALGINATES: NATIVE, OZONIZED AND COMMERCIAL

Abstract

Anthocyanins, recognized for their health-promoting qualities and application as natural pigments, are, however, susceptible to degradation, necessitating approaches to enhance their stability. Biopolymer-based solutions are an alternative for interacting with and protecting these bioactive compounds. Ozonized alginate presents a potential candidate for complexing with anthocyanins due to its modified properties after ozonation. This study focuses on encapsulating and characterizing anthocyanin-rich blackberry extract in ozonized sodium alginate (SA) solutions derived from seaweeds, comparing them with native and commercial SA. Flow curves revealed a shear-thinning behavior in SA and anthocyanin-rich extract composite solutions, indicative of their incorporation and entanglement. Structural analyses (ATR-MIR and ^{1}H NMR) also provided insights into the interaction between the biopolymer and the extract, revealing new peaks and chemical shifts. Microscopic images displayed a porous network structure, indicating the formation of a complex between SA and anthocyanin-rich extract composite solutions. Additionally, the SA-encapsulated anthocyanin-rich extract solutions exhibited an attractive color. In conclusion, the complex comprising ozonized SA and anthocyanin-rich extract holds potential applications in diverse sectors, leveraging the low molecular weight of SA and the bioactive properties of anthocyanins, particularly in the food and medical industries.

Keywords: Sodium alginate; Depolymerization; Anthocyanin; Encapsulation

1. Introduction

Anthocyanins are a sub-class of secondary plant metabolites belonging to the group of flavonoids, which are abundant in a variety of fruits and vegetables (Choo, 2018). They are also known as natural water-soluble pigments expressing a wide array of red to blue colors depending on pH (Dangles & Fenger, 2018). However, anthocyanins are highly sensitive to chemical and biochemical degradation due to their unstable structure (Vidana, Lim, & Choo, 2022). As an instance, when subjected to sunlight exposure, the primary form of anthocyanins, anthocyanidins, undergoes a 30% degradation, which corresponds to the equivalent degradation observed when treated at 70°C for 30 min (Jiang & Zhang, 2023). Therefore, it is necessary to explore methods to improve anthocyanin stability.

Food polymers can preserve the stability of anthocyanins through the formation of molecular complexes in certain systems (Cortez et al., 2017). Given that anthocyanins are water-soluble pigments, they are typically anchored to hydrophilic polymers, most notably polysaccharides (Alizadeh-Sani et al., 2020). Biopolymer-based formulations are environmentally friendly, edible, cost-effective and easily modified, and therefore are ideal to be incorporated into food applications (Luo, Wang, & Zhang, 2020). Among biopolymers, alginates are linear anionic polysaccharides derived from brown seaweeds (Aguero et al., 2017). This water-soluble biopolymer is composed of monomeric units of (1 → 4)-linked α-D-mannuronate (M) and β-L-guluronate (G), arranged in M-blocks, G-blocks and alternating MG-blocks (Caetano, Almeida, & Gonçalves, 2016). Alginate has shown great binding affinities to anthocyanins (Liudvinaviciute et al., 2020; Dikmetas et al., 2023; Lotfinia et al., 2023), which are essential for the entrapment of anthocyanins into the blocks formed by the crosslinked polysaccharide.

Alginate could be further modified to improve its encapsulation properties. Oxidation can cause sodium alginate to degrade and reduce its molecular weight, resulting in lower viscosity and better rheological and reactivity properties (Reakasame & Boccaccini, 2018; Wei et al., 2023). Ozone gas is a high oxidative agent with a great potential for modifying alginate. Besides, it is considered a green technology because ozone quickly degrades into oxygen, leaving no residue in either food or the environment (Pandiselvam et al., 2019).

To the best of our knowledge, there is a lack of research exploring the encapsulation of anthocyanin-rich extract with ozonized sodium alginate, which has the potential to enhance pigment stabilization in various applications. Hence, the objective of this study is to examine the encapsulation of anthocyanin-rich extract using ozonized sodium alginate solution, and to

compare its rheological and physicochemical properties with those of the native and commercial counterparts.

2. Materials and Methods

2.1. Extraction of sodium alginate (SA) from seaweeds

The brown seaweeds (*Sargassum* spp.) were collected from Ubatuba-SP, Brazil (October 2022). The algal material were sanitized, dried for 24 h at 45°C in a convection oven (Model 420-1D, Ethik Technology, Vargem Grande Paulista, Brazil), ground with a cutting mill and stored in airtight containers at room temperature. The powder algae (7 g) was subjected to two rounds of treatment using 99% ethanol (EtOH 50 mL) with continuous agitation for 3 h, followed by overnight drying in an air circulation oven (Model 420-1D, EthikTechnology, Vargem Grande Paulista, Brazil) at 40 °C. Subsequently, the pre-treated seaweed was supplemented with a 20% citric acid solution (Anhydrous, Synth, Diadema-SP, Brazil) adjusted to a pH of 1.5. Algal suspension was ultrasonicated at power of 160 W for 9 min using a probe with a 12.7 mm tip diameter by an ultrasonic horn (OR-T-500, OMNI International™, 20 kHz frequency, and 400 W maximum power dissipation). Following ultrasonication, the samples were rinsed with distilled water and subsequently treated with 2% (m/v) sodium carbonate (Anhydrous, Impex, Diadema-SP, Brazil) at a pH of 10, under magnetic stirring, for 90 min at a temperature of 75.7 ºC (Nogueira et al. 2022). The resulting extract was filtered, the supernatant was precipitated using 99% ethanol (2v), and the extracted SA was dried at 45 °C for 24 h in a convection oven, hereafter referred to as native (N).

2.2. Ozonation of sodium alginate (SA) extracted from *Sargassum* spp.

The SA aqueous solution (1%, w/v) solution was placed in a 500 mL glass container (diameter 7 cm × height 20 cm) which was half-filled by the ozonation reaction. The ozone gas was obtained by the conversion of oxygen (O_2) to ozone (O_3) in an ozone generator (Model GOBSUS, OzonioBras, Araçatuba, Brazil). The SA solution was subjected to continuous bubbling of ozone via a bubble diffuser positioned at the inner base of the glass container. The treatment involved exposing the SA solution to a controlled feed gas flow of 1 L/min for 10 min at 25 °C. The feed

gas flow, consisting of O_2, was regulated using a pressure regulator, while the solution temperature was maintained by a jacket connected to a thermostatic bath. To ensure thorough and consistent exposure of the sample to ozone, the solution was subjected to magnetic stirring. After ozone treatment, samples were concentrated in a rotary evaporator (60 °C), precipitated in ethanol 99% (2v), and dried at 45 °C for 24 h in a convection oven. Consequently, post-ozonization, the sample will be denoted as ozonized sodium alginate (O). For comparison purposes, low-viscosity commercial alginate (Sigma-Aldrich, A1112) was utilized in all analyses.

2.3. Anthocyanin-rich extract

Frozen blackberry (DeMarchi, Pelotas-RS, Brazil) *Rubus* spp. was stored in a freezing chamber at −10 °C and thawed in a refrigerator (7–8 °C) for 24 h. Water was added at a 1:3 fruit-to-water (w/v) ratio, and the mixture shaken mechanically at room temperature in the dark for 8 h. The extract was then filtered through a sieve and concentrated using a rotary evaporator at 60 °C, until 1/3 of the initial volume remained (Souza, Thomazini, Balieiro, & Fávaro-Trindade, 2015). The concentrated extract was freeze-dried and stored in dark glass recipients.

The identification and quantification of bioactive compounds of the extract was performed by HPLC-DAD/UV-vis. The bioactive compounds of blackberry extract were identified and quantified by high-performance liquid chromatography coupled with diode array detection (HPLC-DAD, Prominence Model, Shimadzu). A Hypersil BDS column (C18, 250 × 6 mm) at 35ºC was used to separate the compounds. The sample (111 mg) was dissolved in methanol under stirring for 10 min and centrifuged. The supernatant (0.5 mL) was mixed with methanol (0.25 mL) and acetonitrile (0.25 mL) and filtered through a 0.22 µm pore filter. Subsequently, 10 µL of the sample was injected. The mobile phase comprised solvent A (0.1 % phosphoric acid, v/v) and solvent B (acetonitrile). The following gradient was applied: 2% B (0–30 min), 8% B (30–50 min), 30% B (50-52 min), and 2% B (52–62 min), followed by washing and reconditioning of the column. The flow rate was 1.0 $mL \cdot min^{-1}$, and the runs were monitored at different wavelengths for phenolic acids and the flavonoids as detailed in Table 2. Quantification was performed using calibration curves of standards.

2.4. Production of sodium alginates solutions doped with anthocyanin-rich extract

Aqueous solutions of three distinct alginates (ozonized, native, and commercial) were prepared at a concentration of 2% (w/v) using distilled water, and the pH was meticulously adjusted to 4.9 ± 0.1 with HCl (1 M) solution. To each SA solution was added anthocyanin powder until a final concentration of 100 mg/mL, with continuous magnetic stirring overnight.

2.4.1. Colorimetric analysis

The color of anthocyanin-rich extract-SA solutions was quantified using a colorimeter (CR-5, Konica Minolta, Ramsey, New Jersey, USA) in accordance with the CIELAB (L*, a*, b*) color space. Key color attributes, including lightness (L*), chromatic coordinates a* (+a = red; −a = green), and b* (+b = yellow; −b = blue), as well as additional metrics such as Chroma (C*) and hue angle (h), were assessed. The samples were diluted at a 1:1 ratio with distilled water due to low lightness measurements. The overall color variation (ΔE) among the commercial compared with native and ozonized samples was computed using the Equation 1.

$$\text{Total color difference } (\Delta E) = \sqrt{(L - L_0)^2 + (a - a_0)^2 + (b - b_0)^2}. \quad (1)$$

where L_o, a_o, and b_o are the color parameters of commercial sample and L, a, and b are the color parameters of the native and ozonized samples.

2.4.2. Rheological measurements

Steady-state shear measurements for the SA and anthocyanin-rich extract composite solutions were conducted in a rheometer (TA Instruments AR2000, New Castle, DE, USA) using a double concentric cylinder (external radius 17.5 mm, internal radius 16.0 mm; internal radius 15.3 mm, height 56 mm, gap 2000 (μm)) at 25 °C. Shear stress was determined at shear rates in the range of 0.01 to 300 s^{-1}. The experimental data were adjusted according to the rheological models of Table 1 and the fitting quality was assessed by statistical parameters (coefficient of determination (R^2), the residual sum of squares (RSS) and the Chi-square (χ^2).

Table 1 . Mathematical models for fluid flow and their equations.

Model	Equation	
Ostwald-de-Waele (Power Law)	$\tau = K \times \Upsilon^n$	(1)
Hershel-Bulkley	$\tau = \tau_0 + K \times \Upsilon^n$	(2)
Cross	$\eta = \eta_\infty + \frac{\eta_0 - \eta_\infty}{1+(\alpha \times \Upsilon)^m}$	(3)

where τ is the shear stress (Pa), Υ is the shear rate (s^{-1}), K is consistency index ($Pa.s^n$), n is the flow behavior index (dimensionless), τ_0 is the yield stress (Pa), η is the viscosity, η_0 is the zero shear viscosity, $\eta\infty$ viscosity at infinite shear rates, α is a time constant with the dimensions of time, *m* is a dimensionless rate constant.

2.4.3. Attenuated total reflectance-mid-infrared (ATR-MIR) spectroscopy

The functional groups and bonds of alginates with anthocyanin-rich extract were characterized with MIR spectroscopy (Perkin Elmer, Spectrum One, Waltham, MA, USA), equipped with Spectrum Universal Attenuated Total Reflectance (ATR) accessory. The samples were freeze-dried and analysis was carried out in the range of 4000 cm^{-1} to 650 cm^{-1} at a scan rate of 32 scans with a 4 cm^{-1} spectral resolution. For comparison purposes, analyses were also performed in the SA without the anthocyanin extract.

2.4.4. Proton nuclear magnetic resonance spectroscopy (^{1}H NMR)

The ^{1}H NMR spectra were recorded on a Bruker Avance III NMR spectrometer (Karlsruhe, BW, Germany) operating at a frequency of 400 MHz and 80° C. The freeze-dried samples of pure SA (ozonized, native and commercial) and with anthocyanin-rich extract were dissolved in deuterium oxide (D_2O), with TSP-d4 (sodium salt of trimethylsilylpropionic acid) serving as the internal reference. The chemical shifts of the anomeric proton signals, block structure, and M/G ratio were determined using the methodology outlined by Jensen, Larsen, and Engelsen (2015). Subsequently, the collected data were analyzed using TopSpin software version 4.3.0.

2.4.5. Morphological properties

The morphological properties of freeze-dried SA (ozonized, native and commercial) and anthocyanin-rich extract composite solutions were carried out using a scanning electron microscope (Zeiss, model EVO MA 15). The powdered samples were coated with gold after attaching with the tape stubs. The samples were analyzed under 20 kV energy with 100, 1000 and 5000× magnification.

2.5. Statistical analysis

Data values are displayed as the mean ± standard deviation based on at least three independent experiments. One-way analysis of variance (ANOVA) was used for comparison among the groups with a post-hoc pairwise Tukey's test. Values of $p < 0.05$ were considered statistically significant. Statistical analysis and graph plotting were conducted using OriginPro 2018 software (OriginLab Corporation, MA, USA).

3. Results and Discussion

3.1. Anthocyanin-rich extract

SA (commercial, native, and ozonized) solutions (2% w/v) were used to study the formation of complexes with anthocyanins, a subgroup of flavonoids. The aqueous extract of commercially blackberry was chosen as a source of anthocyanins which is also known as a class of water-soluble pigments. The HPLC results (Fig. 1 and Table 2) revealed that 9 dominant components were present in the anthocyanin-rich extract and highlight the prevalence of procyanidin B2 and cyanidin-3-O-glucoside. These compounds are notably abundant in berries, with anthocyanins comprising aglycones (anthocyanidins) and their glycosides (Padmanabhan, Correa-Betanzo & Paliyath, 2016). Procyanidin B2 (Table 2) contains 4 benzene rings and 10 hydroxyl groups, and has several biological activities such as its probiotic effect on the intestinal microbiota preventing diet-induced obesity (Xing et al., 2019), wound healing (Fan et al., 2021), anti-oxidative stress (Zhuan et al., 2022) and inhibitory effect against cancers (Chen et al., 2023). Our results are in accordance with the literature which reported that the phenolics content in blackberry fruit varies between 114 and 1056 mg per 100 g of fresh weight, while the content of phenolic acids in

blackberries falls within the range of 7 to 64 mg per 100 g of FW (Padmanabhan, Correa-Betanzo & Paliyath, 2016).

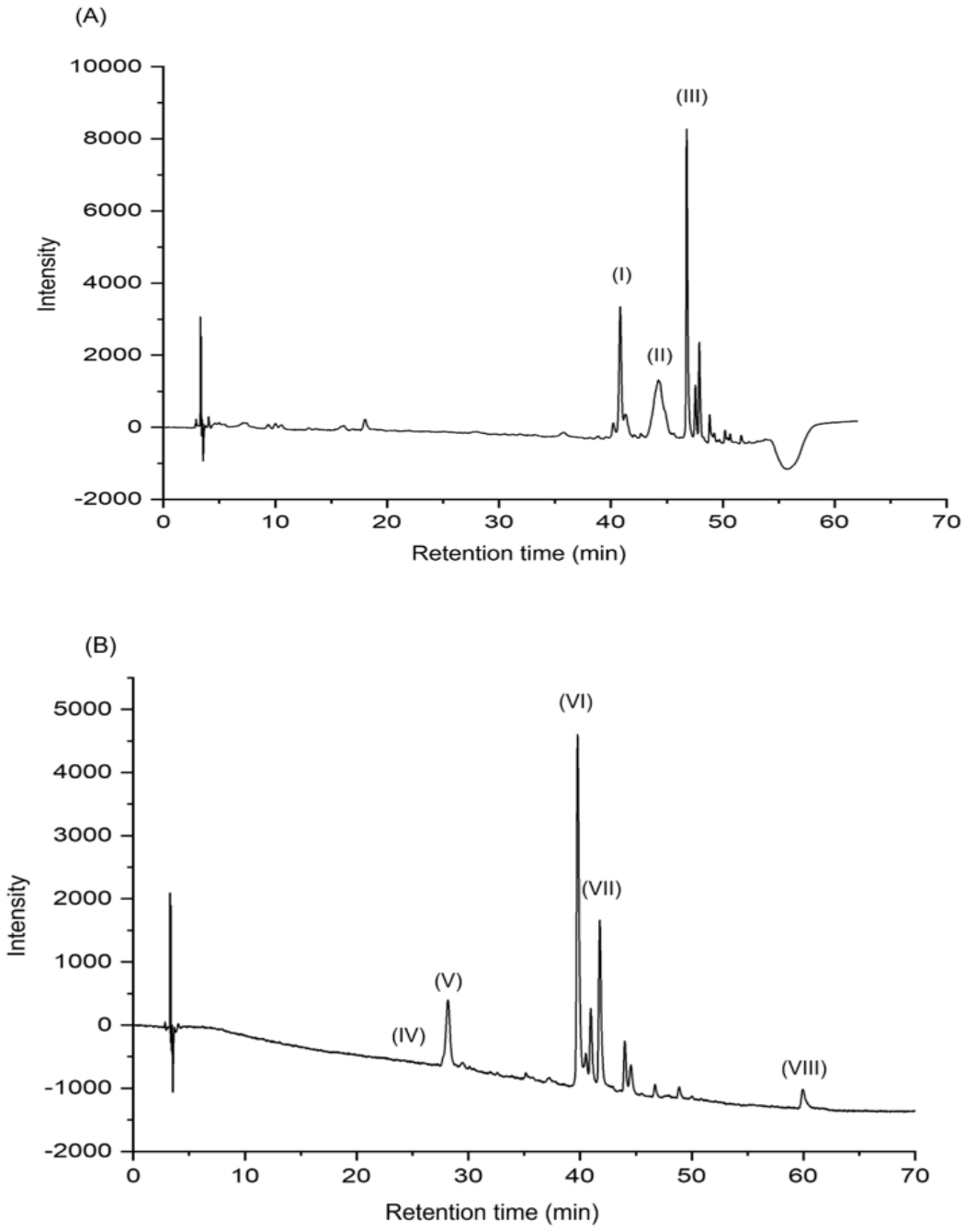

Fig. 1 - Chromatograms obtained for anthocyanin-rich extract from (A) phenolic acids at 300 nm and (B) flavonoids at 370 nm, where (I) corresponds to the retention time of syringic acid, (II) coumaric acid, (III) ferulic acid, (IV) catechin, (V) procyanidin B2 and cyanidin-3-O-glucoside, (VI) rutin, (VII) isoquercetin, and (VIII) quercetin.

Table 2 – Chemical composition (mg/100g) of freeze-dried anthocyanin extract from blackberry (*Rubus* spp)

Group of phenolic compounds	Compound	Retention time (min)	Wavelength (nm)	Concentration (mg/100g)
Phenolic acids	Coumaric acid	44.10	300	12.03
	Ferulic acid	46.53	320	34.81
	Syringic acid	39.42	276	47.27
Flavonoids	Catechin	24.96	280	3.95
	Quercetin	59.94	370	7.82
	Rutin	40.95	246	18.41
	Isoquercetin	41.75	280	37.88
	Cyanidin-3-O-glucoside	28.17	516	80.27
	Procyanidin B2	28.17	280	340.88

3.2. Color of SA and anthocyanin-rich extract composite solutions

The investigation of color attributes constitutes an important facet in the analysis of food ingredients. In addition to their already mentioned health-promoting attributes, anthocyanins possess an appealing color profile. Consequently, the investigation of color indices for the SA complexes was performed. A dominant positive a* value was observed across all formulations (Table 3). This outcome was predictable because the SA solutions maintained a pH of approximately 5 before the introduction of anthocyanins, a condition where there is the predominance of flavylium cation known to favor a reddish hue (Castañeda-Ovando et al., 2009). The b* values acquired were consistently positive (Table 3), indicative of a yellow coloration. Commercial samples showed a higher b* value, indicating a lighter coloration compared to the native and ozonized samples, which demonstrated a darker tendency towards blue hues. This observation is further substantiated by the luminosity (L) results (Table 3), where the commercial sample displayed the highest value. Consequently, the presence of anthocyanins resulted in a more pronounced and vibrant color in the commercial sample, as indicated by the elevated chroma value (Table 3), followed by the ozonized-SA composite. The hue angle is used as a color reference considering the reference 0° or 360° (red), 90° (yellow), 180° (green), and 270° (blue) (Kuck & Noreña, 2016). All samples exhibited values within the same quadrant (Table 3), indicating the prevalence of red hues and, thus, the dominance of anthocyanin pigmentation. The

hue angle for the commercial sample was the highest, indicative of a less intense color compared to the ozonized and native samples, which exhibited similar hue angle values. This discrepancy may be attributed to the potential lightening effect of the commercial sample, which could have resulted in the dilution of anthocyanin pigments, whereas the native and ozonized samples, with their inherent brownish undertones, could have accentuated the red hue. After analyzing each color index, it was expected that the ozonized sample would exhibit a smaller difference in comparison to the commercial sample, as indicated by the total color difference value (ΔE). However, it is noteworthy to emphasize that the ozonized variant presented the second-best performer after the commercial formulation, even exhibiting an inherent brownish coloration that did not seem to adversely affect the anthocyanin pigment.

Table 3 - Color Parameters (CIELab) of commercial, native, ozonized sodium alginates with the chroma, hue angle and total color change (ΔE).

	L	a	b	Chroma (C*)	Hue angle	ΔE
Commercial	$10.7^{a} \pm 0.05$	$33.0^{a} \pm 0.1$	$18.0^{a} \pm 0.1$	$37.6^{a} \pm 0.2$	$28.7^{a} \pm 0.1$	-
Native	$3.7^{b} \pm 0.05$	$20.6^{b} \pm 0.2$	$6.3^{b} \pm 0.1$	$21.6^{b} \pm 0.2$	$17.0^{b} \pm 0.3$	18.4
Ozonized	$4.4^{c} \pm 0.04$	$22.9^{c} \pm 0.2$	$7.4^{c} \pm 0.1$	$24.1^{c} \pm 0.2$	$17.9^{c} \pm 0.3$	15.9

Different letters above a column in the same group indicate significant differences ($p \leq 0.05$). Data are the mean ± SD ($n = 3$).

3.3. Flow behavior

The flow curves of 2% w/v SA, including commercial, native, and ozonized variants, with and without anthocyanin-rich extract are depicted in Fig. 2. Notably, the flow behavior exhibited substantial divergence between solutions with and without incorporation of the extract. While the solutions of SA displayed Newtonian-like characteristics, those containing anthocyanins showed non-Newtonian behavior. It could be clearly seen that the shear stress increased with the addition of anthocyanin-rich extract in the SA solutions. This rise could be due to the increase in the intramolecular interactions between SA molecules and the extract (Mogharbel et al., 2023), a possible result of the hydrogen-bonds formed between polyphenol molecules and SA (Zeng et al., 2021), specifically the -COOH group of SA and the -OH group of extract components (Liu, Su & Tan, 2012). Furthermore, the entrapment of the extract within the polymer network is enhanced, a phenomenon further amplified by the presence of solid solubles in the samples.

Rheological data were fitted to the different models (Table 1). Power law is generally used to fit flow curves for many polysaccharides, as sodium alginate, while HB is essentially a modified power law with yield stress component (Islam et al., 2004). On the other hand, Cross model fluids behave as power law fluids over a range of shear rates, also it includes regions of constant viscosity at a very low or zero shear rate (η_0) and at very high shear rates (η_∞) (Hauswirth et al., 2020). This model is based on the assumption that the pseudoplastic flow is related to the formation and rupture of structural linkages of the material (Afzal, Maswal & Dar, 2018). From the statistical parameters (Table 4), the three rheological models could be used to describe the flow behavior of SA + anthocyanin-rich extract (high R^2 and low RSS and $\chi^{2.}$). As observed in Table 3, all samples exhibited shear-thinning fluid behavior (n ‹ 1), with the native and ozonized SA doped with anthocyanin-rich extract exhibiting lower n values than the commercial SA complexes, i.e., more pseudoplastic behavior.

The values of n will be lower in case of stronger bonds due to increased noncovalent forces of attraction between nearby particles, which increases the lifetime of the temporary entanglement junctions (Islam et al., 2004). As expected, consistency index (K) was higher for native and ozonized SA complexes as well. The change in viscosity can be attributed to the entanglement–disentanglement process in response to shear rate, related to the number of links and interactions between its molecules (Bourbon et al., 2010). Regarding the Cross model parameters, both zero (η0) and infinite viscosities ($\eta\infty$) were elevated and comparable in the SA and anthocyanin-rich extract composite solutions formulated with native and ozonized, which can be attributed to the higher interactions between polymer chains as discussed above. The $\eta\infty$ among the samples did not show a very significant difference which suggests that the internal friction is similar to all the samples (Nik et al., 2005). The equilibrium time (α), marked by the end of zero-shear viscosity and the onset of shear thinning, is prolonged for the sample formulated with commercial SA. From a practical perspective, the Power law behavior over shear flow test would be the most suitable choice. This is primarily because the yield stress (τ_0), which represents the minimum stress required for the material to initiate flow (Barnes, 1999), is nearly negligible (less than 1) (Table 2). Consequently, this choice reduces the complexity of the components needed to describe the flow behavior.

The shear thinning behavior aligns with the findings of Feng et al. (2021), who mixed SA with dried rose petals rich in anthocyanins to create a printable 3D ink. Their study similarly documented an elevation in viscosity upon the addition of the rose petals. Nevertheless, it is noteworthy that both the native and ozonized samples exhibited remarkably similar behaviors. This suggests that, from

a rheological perspective, the modification of the SA derived from seaweeds did not yield discernible differences. Despite exhibiting similar rheological properties, when analyzed separately, commercial and ozonized samples demonstrated distinct outcomes when encapsulated with anthocyanin-extract. These variations may be attributed to differences in their chemical structures, thereby influencing their rheological behavior with the formulation of SA and anthocyanin-rich extract composite solutions.

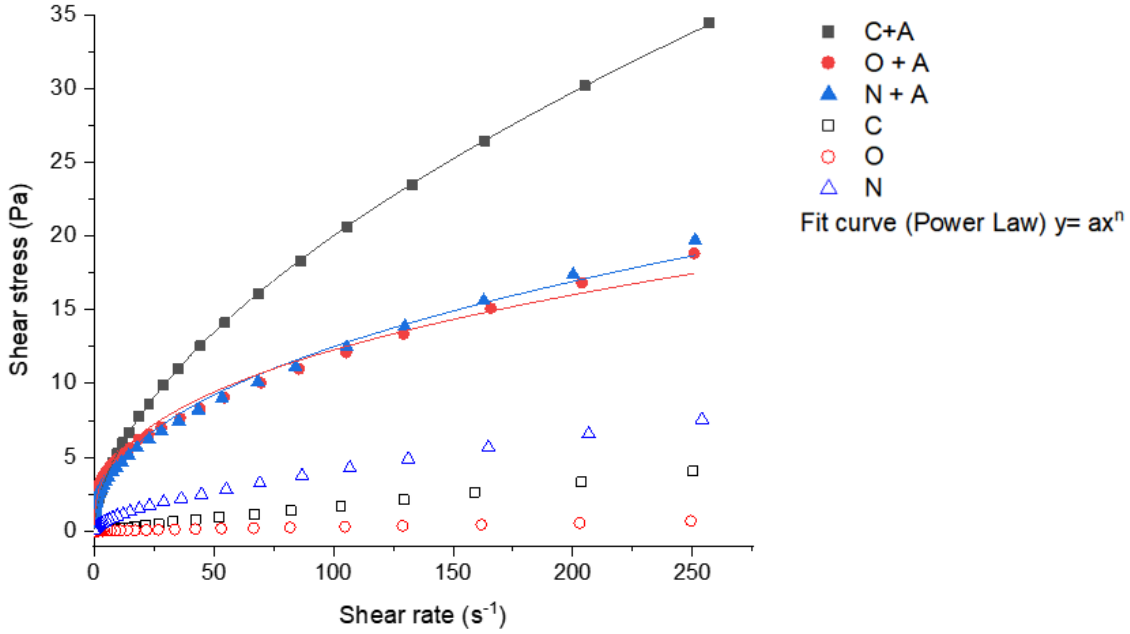

Fig. 2 - Flow curves of 2% w/v pure sodium alginates solutions (C- commercial, O- ozonized and N - native) and anthocyanin-rich extracted encapsulated in sodium alginate solutions (C +A - commercial + anthocyanin-rich extract; O + A - ozonized + anthocyanin-rich extract; N +A - native + anthocyanin-rich extract) with fit curves for the Power Law rheological model

Table 4 - Rheological model fitting and statistical parameters of SA incorporated with anthocyanin-rich extract

Model	Parameters	Commercial + anthocyanin extract	Native + anthocyanin extract	Ozonized + anthocyanin extract
Ostwald-de-Waele (Power Law)	n	0.57	0.44	0.38
	K (Pa.s^n)	1.44	1.66	2.10
	R^2	0.99	0.99	0.99
	RSS	0.20	6.54	8.05
	χ^2	0.005	0.15	0.18
Hershel-Bulkley	τ_0 (Pa)	0.10	0.68	0.74
	n	0.58	0.50	0.45
	K (Pa.s^n)	1.38	1.15	1.47
	R^2	0.99	0.99	0.99
	RSS	0.04	1.74	4.02
	χ^2	0.001	0.04	0.09
Cross	η_∞ (Pa.s)	0.16	0.20	0.20
	η_0 (Pa.s)	10401.73	92192.57	108781.89
	α (s)	1.23E^7	3.06E^6	5.01E^6
	m	0.55	0.72	0.71
	R^2	0.99	0.99	0.99
	RSS	0.19	3.67	5.23
	χ^2	0.005	0.087	0.12

where τ is the shear stress (Pa), Υ is the shear rate (s^{-1}), n is the flow behavior index (dimensionless), K is consistency index (Pa.s^n), τ_0 is the yield stress (Pa), $\eta\infty$ viscosity at infinite shear rates, η is the viscosity, η_0 is the zero shear viscosity, *α* is a time constant with the dimensions of time, *m* is a dimensionless rate constant, R^2 is the coefficient of determination, RSS is the residual sum of squares, χ^2 is the Chi-square.

It is crucial to highlight that the structural changes through ozonation did not induce different rheological properties of ozonized SA when compared with the native variant. However, the utilization of depolymerized ozonized SA can offer advantages for various applications. For instance, Li et al. (2023a) explored potential synergistic effects between alginate oligosaccharides and cyanidin-3-O-glucoside on gastrointestinal health- a promising application that may find relevance with ozonized SA. Li et al. (2023b) studied oxidized sodium alginate in a formulation with anthocyanins to fabricate films to monitor food freshness. It is noteworthy that the oxidative treatment via ozone gas has the potential to depolymerize the polysaccharide chain (Yamashita et al., 2021), thus offering promising possibilities for its application.

3.4. MIR-ATR spectroscopy

Infrared spectra analyses can provide information about the interactions involved in encapsulation of anthocyanin-rich extract in the SA solutions. The spectra of the separated ingredients, as well as the SA-encapsulated anthocyanin-rich extract solutions are shown in Fig. 3. The spectrum of pure SA showed vibrational bands at 3300 cm^{-1}, attributed to the hydroxyl group. However, in the SA solutions containing the extract, the intensity is higher indicating the occurrence of strong intermolecular hydrogen-bonding interactions between them (Fan et al., 2022), with a more pronounced difference in the ozonized complex followed by the commercial sample. It can also be due to the incorporation of hydroxyl groups which may belong to phenolic groups (Santiago-Adame et al., 2015). Difference in intensity mainly for commercial and ozonized-complexes was also observed the bands centered at approximately 2900 cm^{-1} was attributed to the elongation of C-H bonds of pyranoid-ring carbons and 1080 cm^{-1} (C-O stretching) vibrations of C-O-C glycosidic bonds (Huang et al., 2017; Khajouei et al., 2018). Within the range of 1600 to 900 cm^{-1}, bands associated with phenolic compounds were evident. For instance, at approximately 1250 cm^{-1}, as depicted in the spectrum of the free extract, the presence of flavonoid tannins, specifically proanthocyanidins, was observed (Ping et al., 2012). Therefore, it can be seen the same band appearing in all SA and anthocyanin-rich extract composite formulations.

Moreover, alterations in the asymmetric and symmetric stretching vibrations of the carboxylate (COO) groups (Borazjani et al., 2017) were discernible, with changes in intensity at 1603 cm^{-1} and 1410 cm^{-1} observed in the SA solutions containing the extract structures, indicating the interaction between the compounds. These band changes can be attributed to the electrostatic interactions between the positively charged procyanidin/cyanidin and the negatively charged COO^- on SA (Zou et al., 2021).

More evidences that anthocyanins have been integrated into the SA polymeric matrix can be observed by alterations in the spectral region around the C=C stretching vibrations of aromatic rings and notable changes in the 750 cm^{-1} region, indicative of the presence of aromatic rings with ortho-substitution (Pereira, de Arruda & Stefani, 2015). Furthermore, the distinctive peak associated with the stretching vibration of the phenolic hydroxyl group, typically observed at approximately 3600 cm^{-1} for polyphenols, was notably absent in the MIR spectrum. This absence suggests the active involvement of the phenolic hydroxyl group of procyanidin in the complexation with SA (Ji et al., 2023). The changes in the intensity and wavenumber of the peaks indicate

interactions between SA groups and the anthocyanin flavylium cations (Castañeda-Ovando et al., 2009; Navikaite et al., 2016), also showed that the complexation kept the main structure of SA.

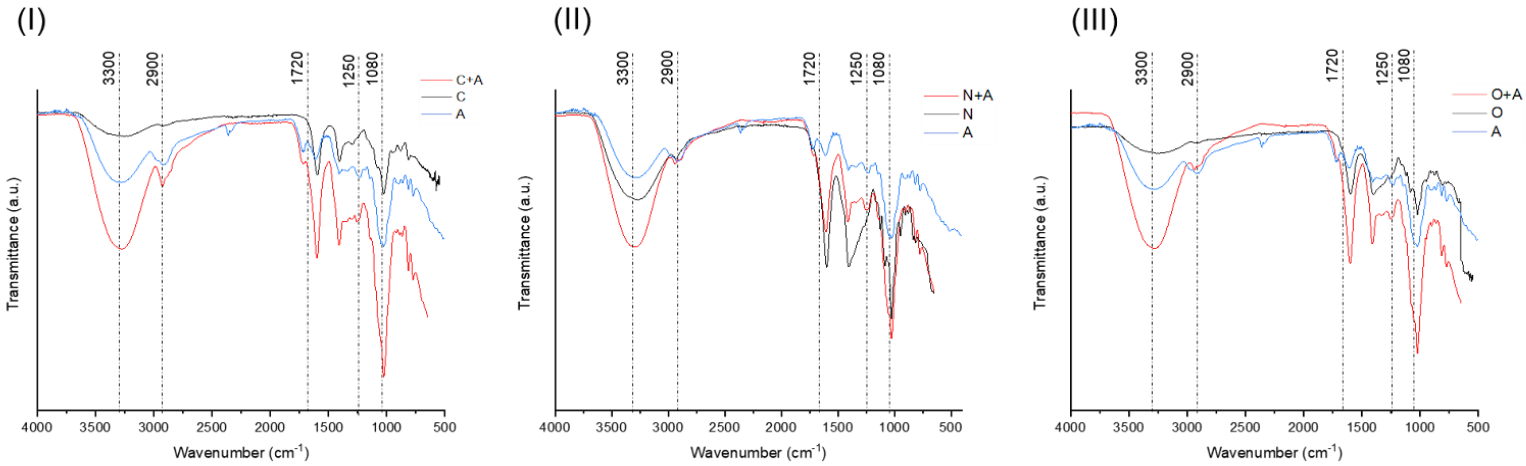

Fig. 3 - Fourier transform mid-infrared-attenuated total reflectance spectra of anthocyanin-rich (A) sodium alginates-encapsulated anthocyanin-rich extract solutions and their individual forms. (I) C- Commercial, C+A - Commercial and anthocyanin extract; (II) N- native, N+A - Native and anthocyanin extract; (III) O- Ozonized, O+A - Ozonized and anthocyanin extract.

3.5. ^{1}H NMR

^{1}H NMR analysis was conducted to explore the encapsulation and potential interaction between SA and the extract. In Fig. 4, two distinctive peaks are evident, allowing a comparison between the spectra of SA and the combination of SA with the anthocyanin-rich extract where the peak at 4.75 ppm, attributed to the solvent, was disregarded in the analysis. The spectra of SA without the extract reveals characteristic peaks corresponding to the two uronate residues in SA, assigned at 5.15, 4.5, and 4.4 ppm, representing H1-G (peak 1), H1-M + H5-GM (peak 2), and H5-GG (peak 3), respectively (Gomez, Rinaudo & Villar, 2007). Remarkably, in the spectra involving SA + the extract, cross-peaks are observed in the chemical shift for the anomeric glucose hydrogens at 4.5 and 5.2 ppm for α- and β-glucose, respectively (Pereira et al., 2005), while other signals of glucose, fructose, and sucrose (Pereira et al., 2005) in the 3.5-4.0 ppm range were incorporated. These findings indicate intermolecular interactions between SA and the anthocyanin-rich extract. Additionally, more peaks in the spectra with SA + extract were detected in the range of 3.5-4.5 ppm, which could be attributed to signals of H corresponding to the procyanidin structure (Goncalves, Mateus & De Freitas, 2011), a major component of the extract. Notably, both

ozonized and native samples, when incorporated with the anthocyanin-rich extract, induced a chemical shift downfield of peaks observed around 4.5 ppm in the spectra without the extract. Another notable signal is a singlet at 3.34 ppm, assignable to methoxyl groups (ferulic acid), also present in the anthocyanin-rich extract (Céspedes et al., 2010). In conclusion, the analysis provides insights into the binding and incorporation of the anthocyanin extract in the SA solution, with the formulations native and ozonized presenting more similar spectra.

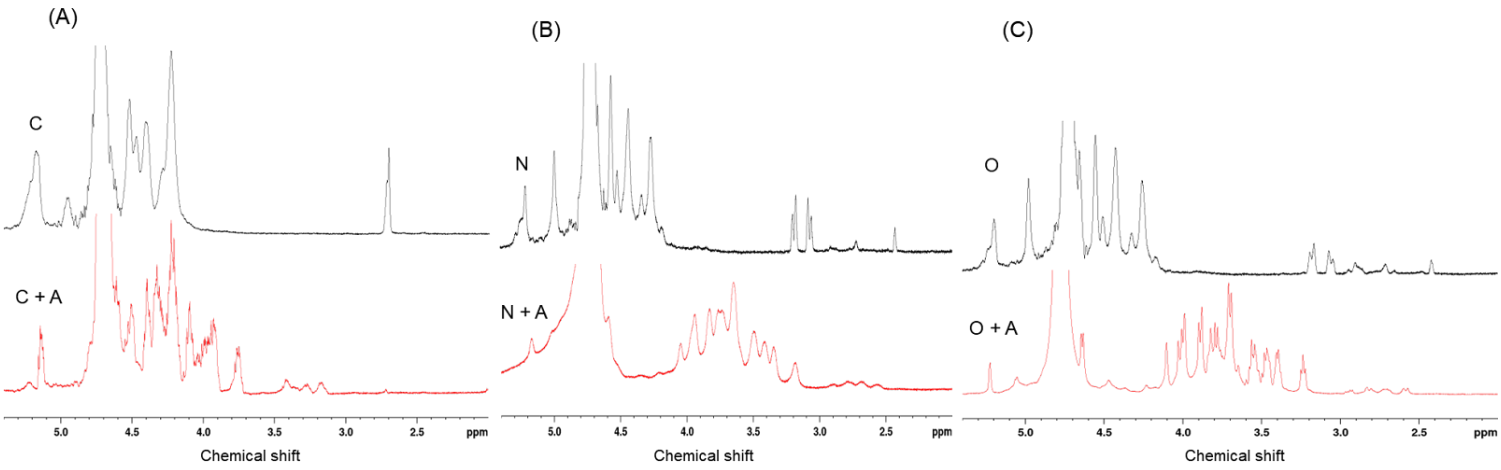

Fig. 4 - ^{1}H NMR spectrum of sodium alginate (SA_ and anthocyanin-rich extract composite solutions and pure SA dissolved in D2O at 80 °C. (A) C: commercial SA, C + A: commercial alginate and anthocyanin-rich extract, (B) N: native SA, N + A: native alginate and anthocyanin-rich extract, (C) O: ozonized SA, O + A: ozonized alginate and anthocyanin-rich extract.

3.6. Morphological observations

Scanning electron microscope (SEM) analysis was employed to investigate the morphology of anthocyanin-rich extract encapsulated in the SA solutions after freeze-drying. SEM observation (Fig. 5) revealed that the appearance of the samples show a porous network structure, indicating that the extract and the SA were connected by fiber-like bridges which collapsed when the water was removed by freeze-drying (Busic et al., 2018; Zou et al., 2021). In addition, the surface of the complex is rough, indicating that an ordered structure of SA was destroyed by the insertion of anthocyanin-rich extract which may be caused by interactions between them (Ji et al., 2023). The morphology and porosity observed in the freeze-dried samples closely resemble those reported in the study by Zou et al. (2021) involving cyanidin-3-O-glucoside and alginate. Smaller porous were observed in the SA and anthocyanin-rich extract composite solutions formulated with

commercial SA indicating an improvement in the interaction (Mao et al., 2023), which can enhance the stability of encapsulated bioactive molecules (Meng et al., 2021).

The SEM results show that the content of anthocyanin-rich extract was adequate once a high content would form aggregates (Zheng et al., 2022). All formulations showed irregular, disordered and dense pores, indicating an intensely unstable and easily destroyed structure (Chen & Zhang, 2019). Thus, that is why SA solutions have been associated with other components, such as proteins and other polysaccharides, to improve its stability, consequently its rheological and mechanical properties (Abasalizadeh et al., 2020; Wang et al., 2021; Serafin, Culebras, & Collins, 2023).

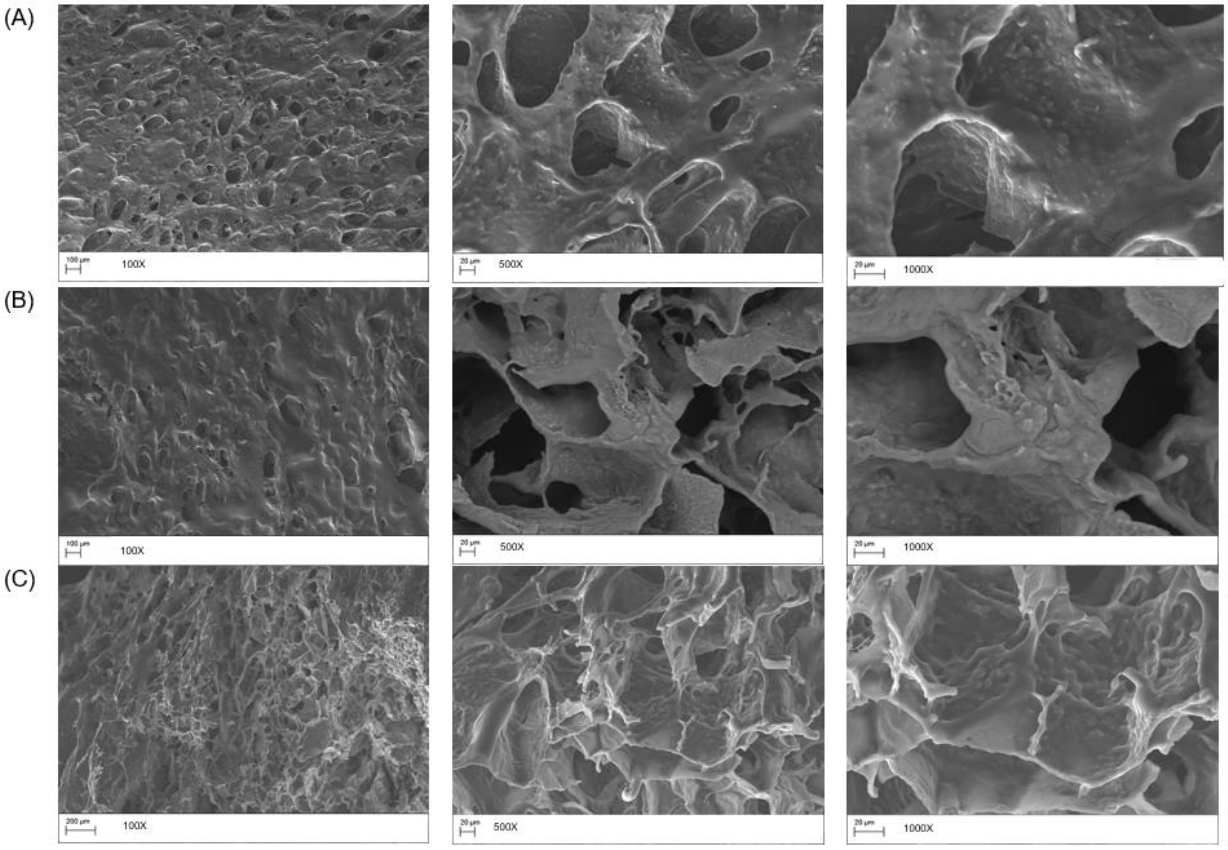

Fig. 5 - Photomicrographs as recorded by SEM. (A) Native, (B) Ozonized and (C) Commercial sodium alginates solutions with anthocyanin-rich extract.

4. Conclusion

This study focused on the formation of complexes between anthocyanins and three types of sodium alginate (commercial, native, ozonized). HPLC analysis revealed the presence of prominent anthocyanins, such as procyanidin B2 and cyanidin-3-O-glucoside, in the anthocyanin-rich blackberry extract. The color attributes of the complexes showed a dominant positive a* coordinate, indicating a reddish hue, with the commercial sample appearing lighter than the native and ozonized samples. Rheological analysis revealed non-Newtonian behavior in the presence of anthocyanins, accurately described by the Power law model. The FTIR and ^{1}H NMR analysis spectra indicated strong intermolecular interactions, particularly in the ozonized complex, and changes in the vibrational bands and chemical shifts, demonstrating complexation between anthocyanins and sodium alginate. These findings suggest the potential of ozonized sodium alginate in preserving and delivering anthocyanin pigments in various applications, with promising implications for food and pharmaceutical industries, also addressing the need for improved anthocyanin stability.

5. References

Abasalizadeh, F., Moghaddam, S. V., Alizadeh, E., Akbari, E., Kashani, E., Fazljou, S. M. B., Torbati, M., & Akbarzadeh, A. (2020). Alginate-based hydrogels as drug delivery vehicles in cancer treatment and their applications in wound dressing and 3D bioprinting. Journal of biological engineering, 14, 1-22. https://doi.org/10.1186/s13036-020-0227-7

Afzal, S., Maswal, M., & Dar, A. A. (2018). Rheological behavior of pH responsive composite hydrogels of chitosan and alginate: Characterization and its use in encapsulation of citral. *Colloids and Surfaces B: Biointerfaces*, *169*, 99-106. https://doi.org/10.1016/j.colsurfb.2018.05.002

Agüero, L., Zaldivar-Silva, D., Peña, L., & Dias, M. L. (2017). Alginate microparticles as oral colon drug delivery device: A review. *Carbohydrate polymers*, *168*, 32-43. https://doi.org/10.1016/j.carbpol.2017.03.033.

Alizadeh-Sani, M., Mohammadian, E., Rhim, J. W., & Jafari, S. M. (2020). pH-sensitive (halochromic) smart packaging films based on natural food colorants for the monitoring of food quality and safety. *Trends in Food Science & Technology*, *105*, 93-144.

Barnes, H. A. (1999). A brief history of the yield stress. *Applied Rheology*, *9*(6), 262-266. https://doi.org/10.1260/0266351991494722

Borazjani, N. J., Tabarsa, M., You, S., & Rezaei, M. (2017). Effects of extraction methods on molecular characteristics, antioxidant properties and immunomodulation of alginates from Sargassum angustifolium. *International journal of biological macromolecules*, *101*, 703-711. https://doi.org/10.1016/j.ijbiomac.2017.03.128

Bourbon, A. I., Pinheiro, A. C., Ribeiro, C., Miranda, C., Maia, J. M., Teixeira, J. A., & Vicente, A. A. (2010). Characterization of galactomannans extracted from seeds of Gleditsia triacanthos and Sophora japonica through shear and extensional rheology: Comparison with guar gum and locust bean gum. Food Hydrocolloids, 24(2-3), 184-192. https://doi.org/10.1016/j.foodhyd.2009.09.004

Bušić, A., Belščak-Cvitanović, A., Cebin, A. V., Karlović, S., Kovač, V., Špoljarić, I., Mršić, G., & Komes, D. (2018). Structuring new alginate network aimed for delivery of dandelion (Taraxacum officinale L.) polyphenols using ionic gelation and new filler materials. Food research international, 111, 244-255. https://doi.org/10.1016/j.foodres.2018.05.034

Caetano, L. A., Almeida, A. J., & Gonçalves, L. M. (2016). Effect of experimental parameters on alginate/chitosan microparticles for BCG encapsulation. *Marine drugs*, *14*(5), 90. https://doi.org/10.3390/md14050090

Castañeda-Ovando, A., de Lourdes Pacheco-Hernández, M., Páez-Hernández, M. E., Rodríguez, J. A., & Galán-Vidal, C. A. (2009). Chemical studies of anthocyanins: A review. *Food chemistry*, *113*(4), 859-871. https://doi.org/10.1016/j.foodchem.2008.09.001

Céspedes, C. L., Valdez-Morales, M., Avila, J. G., El-Hafidi, M., Alarcón, J., & Paredes-López, O. (2010). Phytochemical profile and the antioxidant activity of Chilean wild black-berry fruits,

Aristotelia chilensis (Mol) Stuntz (Elaeocarpaceae). Food Chemistry, 119(3), 886-895. https://doi.org/10.1016/j.foodchem.2009.07.045

Chen, K., & Zhang, H. (2019). Alginate/pectin aerogel microspheres for controlled release of proanthocyanidins. International Journal of Biological Macromolecules, 136, 936-943. https://doi.org/10.1016/j.ijbiomac.2019.06.138

Chen, J., Zhong, K., Jing, Y., Liu, S., Qin, S., Peng, F., Li, D., & Peng, C. (2023). Procyanidin B2: A promising multi-functional food-derived pigment for human diseases. *Food Chemistry*, *420*, 136101. https://doi.org/10.1016/j.foodchem.2023.136101

Choo, W. S. (2018). Fruit pigment changes during ripening. In *Encyclopedia of food chemistry* (pp. 117-123). Elsevier. https://doi.org/10.1016/B978-0-08-100596-5.21656-9

Cortez, R., Luna-Vital, D. A., Margulis, D., & Gonzalez de Mejia, E. (2017). Natural pigments: stabilization methods of anthocyanins for food applications. *Comprehensive Reviews in Food Science and Food Safety*, *16*(1), 180-198.

Dangles, O., & Fenger, J. A. (2018). The chemical reactivity of anthocyanins and its consequences in food science and nutrition. *Molecules*, *23*(8), 1970. https://doi.org/10.3390/molecules23081970

Dikmetas, D. N., Uysal, E., Karbancioglu-Guler, F., & Gurmen, S. (2023). Corrigendum to" The production of pH indicator Ca and Cu alginate cryogels containing anthocyanin obtained via red cabbage extraction for monitoring chicken fillet freshness"[Int. J. Biol. Macromol. 231C (2023) 123304]. *International journal of biological macromolecules*, *232*, 123579. doi: 10.1016/j.ijbiomac.2023.123579.

Fan, J., Liu, H., Wang, J., Zeng, J., Tan, Y., Wang, Y., Yu, X., Li, W., Wang, P., Yang, Z., & Dai, X. (2021). Procyanidin B2 improves endothelial progenitor cell function and promotes wound healing in diabetic mice via activating Nrf2. *Journal of cellular and molecular medicine*, *25*(2), 652-665.

Fan, Y., He, Q., Gan, C., Wen, Z., & Yi, J. (2022). Investigation of binding interaction between bovine α-lactalbumin and procyanidin B2 by spectroscopic methods and molecular docking. *Food Chemistry*, *384*, 132509.

Feng, C., Zhang, M., Bhandari, B., Wang, Y., & Wang, B. (2021). Improvement of 3D printing properties of rose-sodium alginate heterogeneous gel by adjusting rose material. *Journal of Food Process Engineering*, *44*(1), e13583. https://doi.org/10.1111/jfpe.13583

Gomez, C. G., Rinaudo, M., & Villar, M. A. (2007). Oxidation of sodium alginate and characterization of the oxidized derivatives. Carbohydrate Polymers, 67(3), 296-304. https://doi.org/10.1016/j.carbpol.2006.05.025

Goncalves, R., Mateus, N., & De Freitas, V. (2011). Influence of carbohydrates on the interaction of procyanidin B3 with trypsin. Journal of agricultural and food chemistry, 59(21), 11794-11802. https://doi.org/10.1021/jf203060s

Hauswirth, S. C., Bowers, C. A., Fowler, C. P., Schultz, P. B., Hauswirth, A. D., Weigand, T., & Miller, C. T. (2020). Modeling cross model non-Newtonian fluid flow in porous media. *Journal of Contaminant Hydrology*, *235*, 103708.

Huang, H., Grun, I. U., Ellersieck, M., & Clarke, A. D. (2017). Measurement of total sodium alginate in restructured fish products using fourier transform infrared spectroscopy. *EC Nutrition*, *11*(1), 33-45.

Islam, M. T., Rodriguez-Hornedo, N., Ciotti, S., & Ackermann, C. (2004). Rheological characterization of topical carbomer gels neutralized to different pH. *Pharmaceutical research*, *21*, 1192-1199. https://doi.org/10.1023/B:PHAM.0000033006.11619.07

Jensen, H. M., Larsen, F. H., & Engelsen, S. B. (2015). Characterization of alginates by nuclear magnetic resonance (NMR) and vibrational spectroscopy (IR, NIR, Raman) in combination with chemometrics. Natural Products From Marine Algae: Methods and Protocols, 347-363.

Ji, L., Fu, H., Wang, Y., Li, J., Yang, X., Gong, H., Meng, X., Jing, W., Dai, W., Li, Y., Lyu, B. & Yu, H. (2023). The complexes of soybean protein isolate and procyanidin B2 have synergistic hypolipidemic activity at the cellular level by activating the AMPKα pathway. *Food Chemistry*, *421*, 136181. https://doi.org/10.1016/j.foodchem.2023.136181

Jiang, M., & Zhang, Y. (2023). Biopolymer-based encapsulation of anthocyanins as reinforced natural colorants for food applications. *Journal of Agriculture and Food Research*, 100488. https://doi.org/10.1016/j.jafr.2022.100488

Khajouei, R. A., Keramat, J., Hamdami, N., Ursu, A. V., Delattre, C., Laroche, C., Gardarin, C., Lecerf, D.,Desbrieres, J., Djelveh, G. & Michaud, P. (2018). Extraction and characterization of an alginate from the Iranian brown seaweed Nizimuddinia zanardini. *International journal of biological macromolecules*, *118*, 1073-1081. https://doi.org/10.1016/j.ijbiomac.2018.06.154

Kuck, L. S., & Noreña, C. P. Z. (2016). Microencapsulation of grape (Vitis labrusca var. Bordo) skin phenolic extract using gum Arabic, polydextrose, and partially hydrolyzed guar gum as encapsulating agents. *Food chemistry*, *194*, 569-576. https://doi.org/10.1016/j.foodchem.2015.08.066

Li, J., Guo, Y., Ma, L., Liu, Y., Zou, C., Kuang, H., Han, B., Xiao, Y., & Wang, Y. (2023a). Synergistic effects of alginate oligosaccharide and cyanidin-3-O-glucoside on the amelioration of intestinal barrier function in mice. *Food Science and Human Wellness*, *12*(6), 2276-2285. https://doi.org/10.1016/j.fshw.2023.03.047

Li, L., Xia, L., Xiao, F., Xiao, Y., Liu, L., Jiang, S., & Wang, H. (2023b). Colorimetric active carboxymethyl chitosan/oxidized sodium alginate-Oxalis triangularis ssp. papilionacea anthocyanins film@ gelatin/zein-linalool membrane for milk freshness monitoring and preservation. Food Chemistry, 405, 134994. https://doi.org/10.1016/j.foodchem.2022.134994

Liu, M., Su, H., & Tan, T. (2012). Synthesis and properties of thermo-and pH-sensitive poly (N-isopropylacrylamide)/polyaspartic acid IPN hydrogels. Carbohydrate polymers, 87(4), 2425-2431. https://doi.org/10.1016/j.carbpol.2011.11.010

Liudvinaviciute, D., Rutkaite, R., Bendoraitiene, J., Klimaviciute, R., & Dagys, L. (2020). Formation and characteristics of alginate and anthocyanin complexes. *International Journal of Biological Macromolecules*, *164*, 726-734. https://doi.org/10.1016/j.ijbiomac.2020.07.157

Lotfinia, F., Norouzi, M. R., Ghasemi-Mobarakeh, L., & Naeimirad, M. (2023). Anthocyanin/Honey-Incorporated Alginate Hydrogel as a Bio-Based pH-Responsive/Antibacterial/Antioxidant Wound Dressing. *Journal of Functional Biomaterials*, *14*(2), 72. https://doi.org/10.3390/jfb14020072

Luo, Y., Wang, Q., & Zhang, Y. (2020). Biopolymer-based nanotechnology approaches to deliver bioactive compounds for food applications: a perspective on the past, present, and future. *Journal of Agricultural and Food Chemistry*, *68*(46), 12993-13000. https://doi.org/10.1021/acs.jafc.0c00277

Mao, S., Ren, Y., Chen, S., Liu, D., Ye, X., & Tian, J. (2023). Development and characterization of pH responsive sodium alginate hydrogel containing metal-phenolic network for anthocyanin delivery. Carbohydrate Polymers, 320, 121234. https://doi.org/10.1016/j.carbpol.2023.121234.

Meng, D., Zhang, L., Wang, Q., Zhang, Y., Sun, Y., Zhang, H., Wang, Z., Zhou, z., & Yang, R. (2021). Self-assembly of phycoerythrin with oligochitosan by electrostatic interaction for stabilization of phycoerythrin. Journal of Agricultural and Food Chemistry, 69(43), 12818-12827. https://doi.org/10.1021/acs.jafc.1c05205

Mogharbel, A. T., Ashour, G. R., Alkhamis, K., Al-bonayan, A. M., Abualnaja, M. M., Qurban, J., Katouah, H. A., & El-Metwaly, N. M. (2023). Preparation of Self-Healing Anthocyanidin-Containing Thermochromic Alginate Ink for Authentication Purposes. ACS Omega. https://doi.org/10.1021/acsomega.3c07874

Navikaite, V., Simanaviciute, D., Klimaviciute, R., Jakstas, V., & Ivanauskas, L. (2016). Interaction between κ-and ι-carrageenan and anthocyanins from *Vaccinium myrtillus*. *Carbohydrate Polymers*, *148*, 36-44. https://doi.org/10.1016/j.carbpol.2016.04.059

Nik, W. W., Ani, F. N., Masjuki, H. H., & Giap, S. E. (2005). Rheology of bio-edible oils according to several rheological models and its potential as hydraulic fluid. Industrial Crops and Products, 22(3), 249-255. https://doi.org/10.1016/j.indcrop.2005.01.005

Nogueira, M. T., Chica, L. R., Yamashita, C., Nunes, N. S. S., Moraes, I. C. F., Branco, C. C. Z., & Branco, I. G. (2022). Optimal conditions for alkaline treatment of alginate extraction from the brown seaweed Sargassum cymosum C. Agardh by response surface methodology. Applied Food Research, 2(2), 100141. https://doi.org/10.1016/j.afres.2022.100141

Padmanabhan, P., Correa-Betanzo, J., & Paliyath, G. (2016). Berries and Related Fruits, Encyclopedia of Food and Health, *Academic Press*, 364-371, https://doi.org/10.1016/B978-0-12-384947-2.00060-X.

Pandiselvam, R., Manikantan, M. R., Divya, V., Ashokkumar, C., Kaavya, R., Kothakota, A., & Ramesh, S. V. (2019). Ozone: An advanced oxidation technology for starch modification. *Ozone: Science & Engineering*, *41*(6), 491-507. https://doi.org/10.1080/01919512.2019.1577128

Pereira, G. E., Gaudillere, J. P., Van Leeuwen, C., Hilbert, G., Lavialle, O., Maucourt, M., Deborde, C.; Moing, A. & Rolin, D. (2005). 1H NMR and chemometrics to characterize mature

grape berries in four wine-growing areas in Bordeaux, France. Journal of agricultural and food chemistry, 53(16), 6382-6389. https://doi.org/10.1021/jf058058q

Pereira Jr, V. A., de Arruda, I. N. Q., & Stefani, R. (2015). Active chitosan/PVA films with anthocyanins from Brassica oleraceae (Red Cabbage) as Time–Temperature Indicators for application in intelligent food packaging. *Food Hydrocolloids*, *43*, 180-188. https://doi.org/10.1016/j.foodhyd.2014.05.014

Ping, L., Pizzi, A., Guo, Z. D., & Brosse, N. (2012). Condensed tannins from grape pomace: Characterization by FTIR and MALDI TOF and production of environment friendly wood adhesive. Industrial Crops and Products, 40, 13-20. https://doi.org/10.1016/j.indcrop.2012.02.039

Reakasame, S., & Boccaccini, A. R. (2018). Oxidized alginate-based hydrogels for tissue engineering applications: a review. *Biomacromolecules*, *19*(1), 3-21. https://doi.org/10.1021/acs.biomac.7b01331

Santiago-Adame, R., Medina-Torres, L., Gallegos-Infante, J. A., Calderas, F., González-Laredo, R. F., Rocha-Guzmán, N. E., Ochoa-Martínez, L.A., & Bernad-Bernad, M. J. (2015). Spray drying-microencapsulation of cinnamon infusions (Cinnamomum zeylanicum) with maltodextrin. LWT-Food Science and Technology, 64(2), 571-577. https://doi.org/10.1016/j.lwt.2015.06.020

Serafin, A., Culebras, M., & Collins, M. N. (2023). Synthesis and evaluation of alginate, gelatin, and hyaluronic acid hybrid hydrogels for tissue engineering applications. International journal of biological macromolecules, 233, 123438.

Souza, V. B., Thomazini, M., de Carvalho Balieiro, J. C., & Fávaro-Trindade, C. S. (2015). Effect of spray drying on the physicochemical properties and color stability of the powdered pigment obtained from vinification byproducts of the Bordo grape (Vitis labrusca). *Food and Bioproducts Processing*, *93*, 39-50. https://doi.org/10.1016/j.fbp.2013.11.001

Vidana Gamage, G. C., Lim, Y. Y., & Choo, W. S. (2022). Sources and relative stabilities of acylated and nonacylated anthocyanins in beverage systems. *Journal of Food Science and Technology*, *59*(3), 831-845. https://doi.org/10.1007/s13197-021-05054-z

Wang, J., Liu, Y., Zhang, X., Rahman, S. E., Su, S., Wei, J., Ning, F., Hu, Z., Martínez-Zaguilán, R., Sennoune, S., Cong, W., Christopher, G., Zhang, K., & Qiu, J. (2021). 3D printed agar/calcium alginate hydrogels with high shape fidelity and tailorable mechanical properties. Polymer, 214, 123238. https://doi.org/10.1016/j.polymer.2020.123238

Wei, Q., Zhou, J., An, Y., Li, M., Zhang, J., & Yang, S. (2023). Modification, 3D printing process and application of sodium alginate based hydrogels in soft tissue engineering: A review. *International Journal of Biological Macromolecules*, 123450. https://doi.org/10.1016/j.ijbiomac.2023.123450

Xing, Y. W., Lei, G. T., Wu, Q. H., Jiang, Y., & Huang, M. X. (2019). Procyanidin B2 protects against diet-induced obesity and non-alcoholic fatty liver disease via the modulation of the gut microbiota in rabbits. *World Journal of Gastroenterology*, *25*(8), 955. 10.3748/wjg.v25.i8.955

Yamashita, C., Moraes, I. C. F., Ferreira, A. G., Branco, C. C. Z., & Branco, I. G. (2021). Multi-response optimization of alginate bleaching technology extracted from brown seaweeds by an

eco-friendly agent. *Carbohydrate Polymers*, *251*, 116992. https://doi.org/10.1016/j.carbpol.2020.116992

Zeng, X., Li, T., Zhu, J., Chen, L., & Zheng, B. (2021). Printability improvement of rice starch gel via catechin and procyanidin in hot extrusion 3D printing. Food Hydrocolloids, 121, 106997. https://doi.org/10.1016/j.foodhyd.2021.106997

Zheng, Y., Li, X., Huang, Y., Li, H., Chen, L., & Liu, X. (2022). Two colorimetric films based on chitin whiskers and sodium alginate/gelatin incorporated with anthocyanins for monitoring food freshness. Food Hydrocolloids, 127, 107517. https://doi.org/10.1016/j.foodhyd.2022.107517

Zhuan, Q., Li, J., Du, X., Zhang, L., Meng, L., Luo, Y., Zhou, D., Liu, H., Wan, P., Hou, Y & Fu, X. (2022). Antioxidant procyanidin B2 protects oocytes against cryoinjuries via mitochondria regulated cortical tension. *Journal of Animal Science and Biotechnology*, *13*(1), 1-22. 10.1186/s40104-022-00742-y

Zou, C., Huang, L., Li, D., Ma, Y., Liu, Y., Wang, Y., Cao, M. G., Liu, G. M. & Sun, L. (2021). Assembling cyanidin-3-O-glucoside by using low-viscosity alginate to improve its in vitro bioaccessibility and in vivo bioavailability. *Food Chemistry*, *355*, 129681. https://doi.org/10.1016/j.foodchem.2021.129681

CHAPTER 3: DEVELOPMENT AND CHARACTERIZATION OF PRE-CROSSLINKED SODIUM ALGINATE/AGAR INK LOADED WITH ANTHOCYANIN-RICH EXTRACT FOR 3D PRINTING

Abstract

3D printing technology has gained significant attention for its versatility and the potential for personalized ink and design. Hydrogels, known for their biocompatibility and biodegradability, are extensively studied as inks with wide-ranging applications. This study explores the utilization of ozonized sodium alginate extracted from seaweeds as a base for the ink. However, recognizing the known rheological and mechanical limitations documented in the literature, the alginate was pre-crosslinked, combined with agar, and enriched with anthocyanin-rich extract. Oscillatory rheological investigations revealed suitable properties for 3D printing, while zeta potential, FTIR, and SEM analyses indicated interactions among the ink components. Optimized 3D printing parameters, including nozzle diameter, printing speed, filament length, and width, were determined through printability tests. Under these optimal conditions, 3D structures were successfully printed and remained stable for up to 24 h, exhibiting a texture profile comparable to the ink formulated with commercial sodium alginate. While adjustments for enhancing the mechanical properties of 3D constructs are considered, the study underscores the considerable potential of ozonized sodium alginate-based ink for diverse applications. The SA's low molecular viscosity and the pH-responsive nature of the anthocyanin-rich extract open avenues for exploration in various sectors, including its use in the food and medical industries.

Keywords: 3D printing; Anthocyanin; Hydrogel; Sodium Alginate; Depolymerization; Ozone

1. Introduction

Three-dimensional (3D) printing is an additive manufacturing technique employed for the fabrication of a wide spectrum of structures and geometries based on computer-aided design model data. The process involves the successive deposition of material layers stacked atop one another (Ngo et al., 2018). Among the current 3D printing methods, the extrusion-based printing process has gained greater popularity because of its capability to release a diverse range of materials, versatility and practicality (Sun et al., 2018).

Hydrogels are composed of three-dimensional network structure formed by cross-linking of polymers and are considered mainstream to prepare inks due to their ability to absorb and retain significant amounts of water within their hydrophilic structure (Ning et al., 2022). Additionally, their biomimetic qualities, biocompatibility, and biodegradability make them particularly appealing for different applications (Ahmed, 2015), thus making them an attractive option for the formulation of inks. Due to these features, they are commonly used to encapsulate bioactive compounds (Ahmadzadeh et al., 2023; Bider et al., 2024), such as anthocyanins, a subgroup of flavonoids, that the the benefits of anthocyanin supplementation on human health are extensive and increasingly evident in recent researches (Zhang et al., 2020; Mottaghipisheh et al., 2022).

Biopolymers such as alginate stands out as one of the most prevalent polysaccharides, widely employed in the formulation of hydrogel inks for extrusion-based 3D bioprinting processes (Lee & Mooney, 2012). Its adoption is attributed to its versatile attributes, including biocompatibility, biodegradability, hydrophilicity, and capacity for physical cross-linking (Axpe & Oyen, 2016).

Alginate oxidation is a strategy for increasing reactive groups and achieving faster polymer degradation, which is desirable for many industrial applications (Boontheekul et al., 2005). Oxidized alginate can be achieved by using ozone gas which is considered a green cutting-edge technology with a high oxidative potential (Pandiselvam et al., 2019; Yamashita et al., 2021). Partially oxidized alginate derivatives were found to be better metal ion chelators than their native compounds (Fernando et al., 2018; Fernando et al., 2019). The ability to chelate is essential for making sodium alginate more functionalized with desirable properties through chemical cross-linking. Because alginate is an anionic polymer, it can easily interact with cations via ionic bonding. Ions Ca^{+2} are the most studied cations for making cross-linked alginate, well known as “the egg box” model, which results in a gel (Cao et al., 2020).

However, given its inherent rheological limitations, it is common to combine it with other compounds such as proteins, or other polymers, commonly referred to as hybrids hydrogels. Agar

is a widely spread food material which contains two components named agarose and agaropectin (Saha & Bhattacharya, 2010). It can also be extracted from seaweeds and has demonstrated its ability to enhance the viscosity of hydrogels used in 3D printing (Wang et al., 2021b). Edible biomaterials have the potential to serve a valuable role not only in the food industry but also in the development of healthcare foods.

In order to achieve a suitable extrudability while ensuring accurate deposition and shape retention (Falcone et al., 2022), sodium alginate was pre-crosslinked with Ca^{+2} ions. The primary objective of this investigation was to develop a printable hydrogel formulation incorporating agar and pre-crosslinked ozonized sodium alginate (SA) sourced from seaweeds, with encapsulation of an anthocyanin-rich extract. This study aimed for a comprehensive examination and characterization of the formulations, including rheological and structural properties (zeta potential, particle size, Fourier infrared spectrum analysis (MIR) and scanning electron microscopy (SEM)). Furthermore, printability assessments were conducted to define the optimal printing parameters for the fabrication of 3D structures. Stability testing and mechanical properties (texture) were conducted in the 3D prints.

2. Materials and Methods

2.1 Materials

Alginate (A1112, alginic acid sodium salt, low viscosity, from brown algae) and agar (A1296 from algae *Rhodophyceae*) were obtained from Sigma-Aldrich (Cotia-SP, Brazil). Sodium carbonate anhydrous was acquired from Impex (Diadema-SP, Brazil), calcium chloride dihydrate ($CaCl_2$. $2H_2O$) from ACS Científica (Sumaré-SP, Brazil) and citric acid anhydrous from Synth (Diadema-SP, Brazil).

2.2. Extraction of sodium alginate (SA) from seaweeds

The brown seaweeds (*Sargassum* spp.) were harvested from Ubatuba-SP, Brazil, in October 2022. After collection, the seaweed samples were sanitized for 30 min in chlorinated water (25 ppm). Subsequently, the algal material was dried for 24 h at 45 °C in a convection oven (Model 420-1D, Ethik Technology, Vargem Grande Paulista, SP, Brazil), ground using a cutting mill and stored in airtight containers at room temperature. Extraction process was carried out twice on powder algae (7 g) pre-treated with 99% ethanol (EtOH 50 mL), under continuous agitation for 3

h. The sample was dried overnight in an air circulation oven at 40°C, supplemented with a 20% citric acid solution adjusted to a pH of 1.5. The algal suspension underwent ultrasonication at a power of 160 W for 9 min using a probe (12.7 mm diameter) by an ultrasonic horn (OR-T-500, OMNI International™, 20 kHz frequency, and 400 W full power). After ultrasonication, the samples were rinsed with distilled water and subsequently treated with 2% (m/v) sodium carbonate at a pH of 10, under magnetic stirring, for 90 min at 75.7 ºC (Nogueira et al., 2022). The extract was filtered, the supernatant precipitated using 99% ethanol (2v) and the extracted SA was then dried at 45 °C for 24 h in a convection oven.

2.3. Ozonation of sodium alginate (SA) extracted from *Sargassum* spp.

The 1% (w/v) SA aqueous solution was added in a 500 mL glass reactor, which was partially filled during the ozonation reaction. Ozone gas was generated by converting oxygen (O_2) to ozone (O_3) using an ozone generator (Model GOBSUS, OzonioBras, Araçatuba, SP, Brazil). The ozonation treatment involved exposing the SA solution to a controlled feed gas flow of 1 L/min for 10 min at 25 °C. The feed gas flow, comprised of oxygen (O_2), was regulated using a pressure regulator, while the solution temperature was maintained by a jacket connected to a thermostatic bath. To ensure uniform exposure of the sample to ozone, magnetic stirring was applied throughout the treatment duration. Following the ozone treatment, the samples were concentrated using a rotary evaporator at 60 °C, precipitated in 99% ethanol (2v), and subsequently dried at 45 °C for 24 h in a convection oven. Henceforth, this SA (viscosity-average molecular weight of 39.4 kDa) will be referred to as "ozonized," and, for comparative purposes, commercial-grade SA was also employed to assess and compare the outcomes.

2.4. Anthocyanin-rich extraction

Frozen blackberry (*Rubus* spp.) sourced from DeMarchi, Pelotas-RS, Brazil, was thawed in a refrigerator at 8 °C for 24 h. Extraction process was carried out by adding distilled water to the berries at a fruit-to-water ratio of 1:3 (w/v). This mixture was mechanically shaken at room temperature in the absence of light for 8 h. The resulting extract was filtered and concentrated using a rotary evaporator at 60 °C until volume reduces to one-third of the initial amount, according to Souza, Thomazini, Balieiro, and Fávaro-Trindade (2015). The concentrated extract was freeze-dried and stored in dark glass containers until further analysis.

The primary bioactive compounds in the extract were identified and quantified using high-performance liquid chromatography coupled with diode array detection (HPLC-DAD, Prominence Model, Shimadzu) employing a Hypersil BDS column (C18, 250 × 6 mm) at 35 °C. The identified compounds were Procyanidin B2 and Cyanidin-3-O-glucoside, present in concentrations of 3.4 and 0.8 mg/g of the extract, respectively.

2.5. Preparation of agar/SA hybrid hydrogel doped with anthocyanin-rich extract

Hydrogel formulations were prepared using agar and SA, either treated with ozone or sourced commercially. Initially, alginate powder (600 mg) was dissolved in distilled water (15 mL), and the pH adjusted to 5.0 ± 0.1 with 40 % citric acid solution. Following this adjustment, agar (600 mg) was introduced into the SA solution and allowed to hydrate overnight. To facilitate agar solubilization, the solution was heated to 95 °C in an air circulation oven for 20 min. Subsequently, 15 mL of 25 mM CaCl2 was added, the mixture homogenized using a vortex for 30 s with temperature reaching 50 °C. Anthocyanin-rich extract (750 mg) was introduced, and the components were homogenized using a Turrax homogenizer (NT 138, Nova Técnica, Piracicaba, SP, Brazil) for 30s at 10,600 rpm. The final composition of the formulations consisted of 2% (w/v) agar and 2% (w/v) SA, with the anthocyanin extract at a concentration of 25 mg/mL. The formulation was subjected to freeze drying to remove water content, which is essential for subsequent MIR-ATR and MEV analyses.

2.6. Rheological properties

Rheological behavior of the hydrogels formulations was analyzed by temperature sweep, stress sweep, strain sweep, frequency sweep and structure recovery tests using a rotational rheometer (Anton Paar MCR 92, Graz, Austria) immediately after its preparation.

Temperature sweep test was carried out to provide information regarding the gelation temperature of the hydrogel base (composed of agar, sodium alginate and $CaCl_2$, without the extract, as the biocompounds undergo degradation at high temperatures (Jiang & Zhang, 2023) anticipating its application in the 3D extrusion process. This test was conducted using cylinder concentric geometry at a cooling rate of 1.5 °C/min. From the obtained temperature of gelation (40 °C) of the two formulations (ozonized and commercial SA), all other measurements were analyzed using a parallel plate geometry (diameter of 25.0 mm) with a gap of 1.0 mm. All samples were equilibrated for 2 min at 40 °C to achieve a steady state before the following tests which were conducted at

the same temperature. An amplitude strain sweep test was accomplished to determine the linear viscoelasticity (LVE) range of the hydrogels. The frequency sweeps were performed in the linear viscoelasticity region. Stress amplitude test was performed to determine the yield stress of the hydrogels. Finally, structure recovery of hydrogels was tested in a viscosity recovery test where low and high shear strain cycles were combined over time and G′ and G″ changes were observed. The shear recoverability of hydrogels was determined by calculating the ratio of viscosity at 0.1 s-1 in the third stage to that in the first stage, representing the percentage of viscosity regained after shear stress (Lu, Rai & Nitin, 2023). The related process variables to each rheological test are listed in Table 1. All tests were conducted at least in duplicate and a solvent trap was used in the geometry to prevent the moisture evaporation and ensure stable temperature during the testing.

Table 1. An overview of all rheological tests

Rheological tests	Process variables	Fixed variables	Recorded outcome
Temperature sweep	Temperature (°C): 80-25	Frequency = 10Hz Strain = 1%	Storage modulus (G') and loss modulus (G")
Strain sweep	Strain (%): 0.01-200	Angular frequency = 10 Hz	Storage modulus (G') and loss modulus (G")
Stress sweep	Shear stress (Pa): 0-100	Frequency = 10 Hz	Storage modulus (G') and loss modulus (G")
Frequency Sweep	Angular frequency (rad/s): 100-0.1	Strain = 0.1 %	Storage modulus (G') and loss modulus (G")
3 interval thixotropy test (3iTT)	Time(s)/Shear rate (s^{-1}): 0–60 / 0.1, 61–70 / 100, 71–190 / 0.1	-	Recovery rate of the hydrogel

2.7. Zeta Potential (ZP) and Particle size (z-average)

The hydrogels were characterized through particle size (z-average) and ZP performed by dynamic light scattering (DLS) technique (Zetasizer Nano ZS90, Malvern) at 25 °C. The samples were diluted (1:10) with Milli-Q water and subjected to analysis.

2.8. Attenuated total reflectance–mid infrared (MIR-ATR) spectroscopy

The bonds of both formulations were characterized with MIR spectroscopy (Bruker, Hyperion 2000), equipped with Spectrum Universal Attenuated Total Reflectance (ATR) accessory. In order to investigate the functional groups of the hydrogels, the samples were freeze-dried and analysis

was carried out in the range of 4000 cm^{-1} to 400 cm^{-1} at a scan rate of 32 scans with a 4 cm^{-1} spectral resolution.

2.9. Scanning electron microscopy (SEM)

The morphological properties of both formulations were carried out using a scanning electron microscope (Zeiss, model EVO MA 15). The freeze-dried samples were coated with gold after attaching with the tape stubs. The samples were analyzed under 20 kV energy with 100, 1000 and 5000× magnification.

2.10. Printing process and printability assessment

A three-axis 3D bioprinter, the Educacional Starter (3DBS, Campinas-SP, Brazil), was employed for the extrusion of hydrogel and scaffold fabrication. Hydrogels (as detailed in Section 2.5) were loaded into 10.0 mL disposable syringes. Tinker-CAD (https://www.tinkercad.com/), a Computer-Aided Design software, was utilized to create the vectorized toolpath of the 3D construction, generating an STL file. The G-code was generated with Slicer software (https://slic3r.org/). Pronterface, an open-source software acting as a graphical user interface host for 3D printing, was employed for the actual printing process.

2.10.1. Evaluation of gel formation and stability

The establishment of a gel structure is crucial for 3D printing as it significantly impacts the material's extrusion capability and deposition. Following the hydrogel formulation process, they were placed in a 50 mL Falcon tube and stored at room temperature in a desiccator for 6h and 24 h. Employing the inverted-tube method, the flasks were gently shaken, and the hydrogels' appearance and stability with various formulations were examined to evaluate the stability of the gel structure (Fernandes et al., 2023).

2.10.2. Printability

The optimization of printing parameters for the formulated hydrogels (Table 1) was investigated by measuring strand thickness in a single-layer print, with continuous strands divided into nine

segments, as illustrated in Fig. 6. The first segment served as a brim and was consequently excluded from the measurements analysis. Image analysis was conducted using ImageJ software to measure the printed segments at three distinct points within each segment. The accuracy of the printing process was assessed through the following equations, where a ratio closer to 1 indicated a more precise printing outcome:

$$\text{Deposition accuracy (DA)} = \frac{\text{Printed strand length}}{\text{Designed length}} \quad (1)$$

$$\text{Spreading ratio (SR)} = \frac{\text{Printed strand width}}{\text{Needle inner width}} \quad (2)$$

2.11. 3D Printing and characterization

The hydrogels, previously incubated in an air circulation oven at 45 °C, were loaded into 10.0 mL disposable syringes. Three constructs of each hydrogel formulation in the form of 15-layer cuboids (1.5 × 1.5 × 1.5 cm^3) were printed with rectilinear infill, utilizing the optimal parameters determined in the printability tests: a nozzle diameter of 1.2 mm, print speed set at 5 mm/s, and layer height and width both configured to 1 mm. Additional printing parameters included a filling rate of 60%, a fill angle of 0°, and a printing temperature of 40 °C. Subsequent to the printing process, the dimensions (length, width, and height) of the printed samples were quantified utilizing image analysis performed with ImageJ software, facilitating the measurement of the printed segments. The dimensional printing deviation in each direction was assessed at intervals of 1 h, 6 h, and 24 h using the following equation:

$$\text{Printing deviation (PD) (\%)} = \frac{\text{Measured value} - \text{Target value}}{\text{Target value}} \times 100 \quad (3)$$

A higher positive value indicates a printed pattern that is thicker than that designed, whereas a lower negative value denotes a thinner pattern.

Texture properties of the 3D printed cuboids were determined using a texture analyzer (TA.XTplusC – Extralab) at ambient temperature equipped with a 50 Kg load cell and a 20 mm probe. The samples were tested at a pre-test, test, and post-test speeds of 1 mm/s, trigger force of 5g, and a compression distance of 3mm, ever two compression-decompression cycles The

texture analyzer software computed seven texture characteristics based on the average values of triplicate measurements: hardness, adhesiveness, springiness, cohesiveness, gumminess, and resilience. Five replicates were performed to each sample.

2.12. Statistical analysis

The format of mean ± standard deviation was used to represent data. All calculations were done with n = 3 unless otherwise stated. Significant differences were determined by one-way analysis of variance (ANOVA) followed by a post-hoc Tukey's test with a significance level of $p < 0.05$. Origin Pro 20218 (OriginLab Corporation, MA, USA) was used to perform quantitative and graphical analysis.

3. Results and Discussion

3.1. Rheological properties

The 3D printing process can be divided into three distinct stages: extrusion, recovery, and self-support. These stages are linked to the rheological properties of the hydrogels, including viscosity, yield stress, thixotropic characteristics, storage modulus (G′), and loss modulus (G″) (Liu et al., 2019a). To evaluate the printability of hydrogel compositions featuring pre-crosslinked SA (ozonized or commercial) and agar with encapsulated anthocyanin-rich extract, their rheological properties were examined. The following rheological measurements were employed to assess and analyze the rheological behavior of the two formulations.

3.1.1 Strain sweep

Dynamic strain sweep analysis was performed on the hydrogels to estimate the linear viscoelastic region (LVR), where the storage (G') and loss (G") moduli are independent from increasing stress conditions (Stojkov et al., 2021). The LVR serves as a critical parameter for assessing the viscoelastic properties of the material, indicating the range within the subsequent tests (such as frequency sweep) can be conducted without compromising the structural integrity of the sample (Rahman et al., 2020; Nelson et al., 2021). In Figure 1A, G' and G" of the hydrogel are depicted in response to the strain sweep, where the higher G' in comparison to G" throughout the LVR region signifies the dominance of solid-like (elastic) properties over the viscous. Furthermore, surpassing the shear strain intersection point, termed the flow point, results in the dominating liquid-like phase (G″) over the solid-like phase (G′), suggesting that the gel structures were sufficiently ruptured and the hydrogel started to flow (Guo, Zhang, & Devahastin, 2021).

The LVR is observed until 0.1% and 1% strain for hydrogels formulated with ozonized and commercial SA, respectively. In contrast to prior investigations employing SA in the formulation of 3D printing hydrogels (Karavasili et al., 2020; Mousavi, Rafe, & Yeganehzad, 2020; Nelson et al., 2021), the LVR length for the ozonized formulation is notably reduced. This phenomenon may be attributed to the low molecular weight SA, result from the ozonation process, as also observed by Smilek et al. (2019) who studied formulations with low and high molecular weight of hyaluronan. Furthermore, the hydrogel formulated with ozonized SA exhibited a lower critical shear strain, indicative of the initiation of hydrogel structural breakdown as evidenced by the decline in G'. These findings suggest a lower structural stability in the hydrogel containing ozonized SA, indicative of its decreased capacity to withstand substantial deformation before the predominance of viscous properties over elastic ones (Garcia-Hernandez et al., 2017). Nevertheless, while the LVR of commercial SA extended beyond that of ozonized SA, the hydrogel formulated with the latter exhibited the highest structural strength (G'). This outcome suggests that the formulation incorporating ozonized SA achieved a more rigid structure with strong mechanical strength (stiffness) (Rahman et al., 2020, Qiu et al., 2023a), which means that a greater force is required to induce deformation in the sample. Nevertheless, the decline in G' following the LVR was more rapid in the formulation with ozonized SA compared to the commercial sample, implying a quick breakdown of internal bonds (Nelson et al., 2021).

In alignment with the 3D printing process, the effective extrusion pressure must suppress the intersection point so the material can be extruded through the nozzle (Nelson et al., 2021). In

summary, a fixed deformation of 0.1% was maintained for both formulations to compare the data from the subsequent frequency sweep.

3.1.2. Frequency sweep

Angular frequency sweep measurements are performed to anticipate the structural integrity and mechanical strength of a material (Rahman et al., 2020). In the conducted tests within the LVR, both hydrogel samples demonstrated a higher storage modulus (G') compared to the loss modulus (G") (Figure 1B), indicative of the robust network integrity of molecules in SA-based hydrogels. The predominance of G' indicates a solid elastic behavior, providing superior resistance to deformations during handling and consequently enhancing the stability of the printed structures (Chung et al., 2013). The hydrogel formulated with ozonized SA exhibited a higher G' value, suggesting its suitability for extrusion printing. This result can be attributed to the lower M/G ratio of the ozonized SA (data not shown), where a higher content of G-monomers serves as crosslinking points in the hydrogel, exhibiting a higher G' due to a denser gel network (Zhong et al., 2024). The absence of a crossover point in the studied frequency region indicates a highly interconnected gel-like structure in the hydrogel formulations (Liu, Winter, & Perry, 2017). G' values align closely with those observed in hydrogels formulated with SA and gelatin (Kuo et al., 2021; Chung et al., 2013), hyaluronan and surfactants (Smilek et al., 2019). The rising trend in G' with increasing angular frequency, accompanied by a more pronounced increase in G", indicates a certain frequency dependence. This behavior, noted also by Mousavi, Rafe, & Yeganehzad (2020) in their study on gels formulated with alginate, $CaCl_2$, and guar gum, may be attributed to crosslinking kinetics where the experiments were conducted over a one-week period. Sardelli et al. (2021) observed a similar trend, reporting independent and maximum values of the viscoelastic moduli 24 h after sample preparation (alginate with $CaCO_3$ and D-(+)-gluconic acid d-lactone (GDL)). Consequently, it is concluded that biopolymers-hydrogels doped with anthocyanin-rich extract lack sufficient time to rearrange, resulting in enhanced elasticity characteristic of interacting biopolymers (Priftis, Laugel, & Tirrell, 2012).

3.1.3. Stress sweep

Rheological responses from stress sweep tests were assessed through yield stress, defined as the minimal force required to initiate hydrogel flow (Li, Liu, & Li, 2016). As depicted in Figure 1C, yield stress values were determined at the crossover point of the storage (G′) and loss (G″) moduli (Kiyotake et al., 2019). Both formulations exhibited low yield stress, measuring 36 and 21 Pa for commercial and ozonized SA, respectively. The yield stress can be also linked to the 3D printability of the material, serving as the pressure needed to initiate extrusion during 3D printing and ensuring the self-supporting capability of the printed object (Qiu et al., 2024). Given the complexities of 3D printing involving flow through narrow orifices and frequent starts and stops based on the printed shape, a low yield stress is desirable. Considering that optimal 3D printability necessitates a comprehensive assessment of various parameters involving not only rheology, but also printing parameters (Rastin et al., 2021; Qiu et al., 2024), both hydrogel formulations, from the perspective of yield stress, appear suitable for 3D printing.

3.1.4. 3 interval tixotropy test (3iTT)

During 3D printing, the hydrogels undergo alterations in shear force as they are extruded from the nozzle tip. Therefore, thixotropic, recovery, or creep tests can offer valuable insights into the hydrogel's ability to recover under shear conditions. To replicate shear conditions during extrusion printing, the hydrogels underwent an initial exposure to a low shear rate (0.1 s^{-1}), simulating the at-rest conditions before extrusion. Under these circumstances, the hydrogel formulated with commercial SA exhibited the highest viscosity. Subsequently, the shear rate was elevated (100 s^{-1}) to simulate the shear force encountered at the nozzle tip during extrusion, where both formulations exhibited similar viscosity values. Notably, the hydrogel formulated with commercial SA experienced a more pronounced decrease in viscosity. Finally, the shear rate was once again reduced (0.1 s^{-1}) to assess the hydrogel's recovery behavior, simulating post-printing conditions (Liu et al., 2019a).

In Fig. 1D, the shear recovery behavior of hydrogel viscosity is depicted under varying low and high shear rates. Both hydrogels exhibited a significant decrease in apparent viscosity at high shear rates, followed by low shear rates, reaching a stabilized state within 30 s, indicating partial

structural recovery. Samples formulated with commercial SA necessitated a slightly longer duration to reach viscosity stabilization, suggesting a reduced shape retention and fidelity (Paxton et al., 2017).

The hydrogel formulated with ozonized SA demonstrated a 48% recovery, while the formulation with commercial SA exhibited a higher recovery rate of 80.5%. This aligns with previous findings, where the formulation with ozonized SA displayed lower structural stability in strain sweep results, resulting in breakage without complete recovery of the internal network in this test. Failure to return to the original viscosity may indicate permanent material changes induced by the application of high shear rates (Paxton et al., 2017). The recovery of the commercial sample is deemed favorable, similar to results observed in hydrogels formulated with xanthan gum and kappa-carrageenan (Liu et al., 2019a) and alginate-carboxymethyl cellulose with calcium ions (Nelson et al., 2021). However, both hydrogels exhibited lower initial viscosity, suggesting potential challenges in achieving optimal shape fidelity compared to other considered compositions, where initial viscosities surpassed 200 Pa.s (Nelson et al., 2021).

Higher recovery rates were observed with 8% (w/v) SA, implying that the formulations studied may benefit from a higher concentration of biopolymer to achieve enhanced recovery rates. Based on the findings, both hydrogels, particularly the hydrogel formulated with ozonized SA, may encounter challenges in achieving optimal printability. Nevertheless, alternative parameters within the printing process could potentially mitigate this outcome.

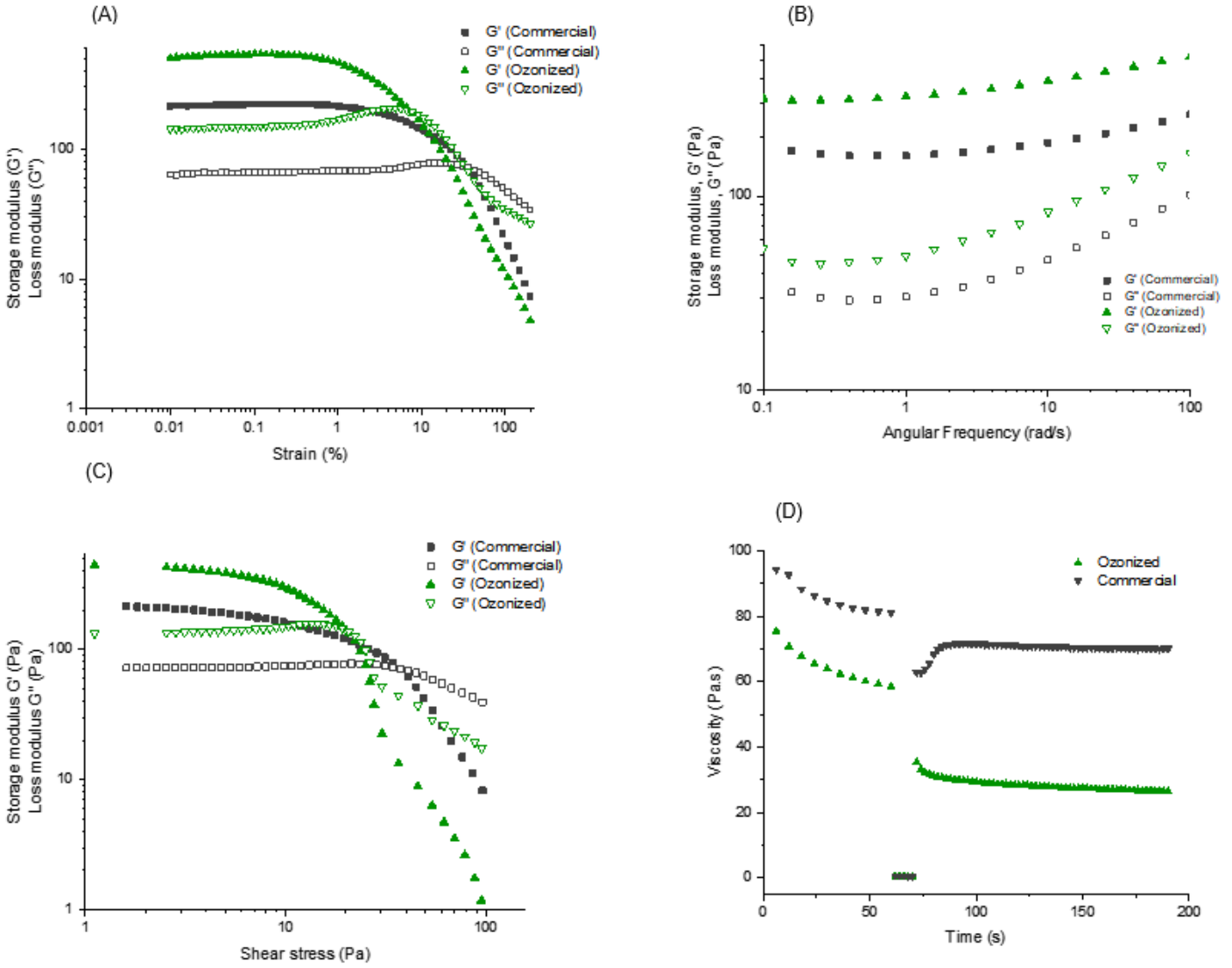

Fig. 1 - Rheological behavior of hydrogels formulated with sodium alginate (commercial or ozonized), agar and anthocyanin-rich extract. Storage G' and loss G'' moduli evaluated via (A) Oscillation strain profiles, (B) Oscillation frequency profiles, (C) Oscillation stress profiles and (D) Three-point thixotropic test

3.1.5. Temperature sweep

The rheological properties have an important role in processing edible hydrogels as well as in subsequent printing, which could bridge the gap between edible hydrogels and practical printing (Cheng et al., 2022). Temperature sweep analyses were conducted on hydrogels to assess their thermoresponsive properties, crucial for modulating viscoelastic properties during extrusion and subsequent solidification processes, ensuring the production of 3D constructs with shape fidelity (Suntornnond, An, & Chua, 2017). This property, characterized by temperature-dependent alterations, enables rapid solidification of the hydrogels during deposition, facilitating the creation of 3D structures after initial liquefaction for extrusion (Paxton et al., 2017).

Both formulations exhibited comparable behavior, with both storage (G') and loss (G”) moduli showing an increasing trend as the temperature decreased. Furthermore, a temperature-induced gelation was observed at 36.4 °C, characterized by the intersection of the loss modulus (G”) and the storage modulus (G’), signifying the phase transition from the elastic to the viscous region (Rahman et al., 2020). The only difference was the slightly higher value of the storage modulus (G') in the formulation with commercial SA which indicates a more solid-like behavior. Consequently, the printing temperature was set at 40 °C, wherein the prevalence of the loss modulus (G”) facilitates extrusion during the printing process, preventing nozzle clogging, while slightly higher than the gelation temperature (Tg) to ensure a gel-like behavior and the structural stability by forming gel rapidly after coming out of the nozzle (Liu et al., 2019b).

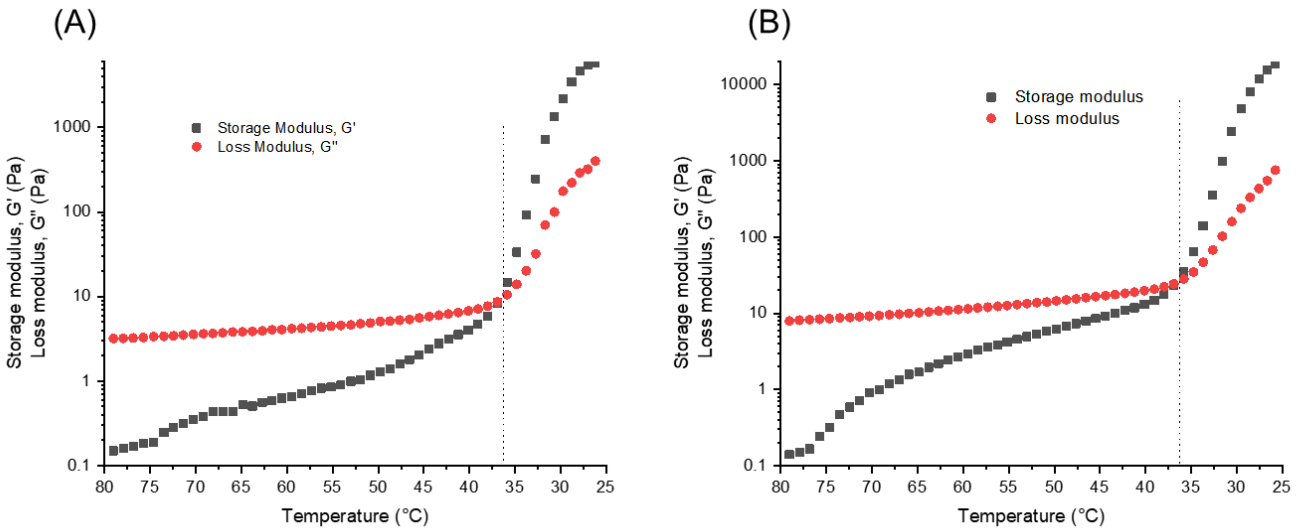

Fig. 2 - Temperature ramp tests conducted at a cooling rate of 1.5 °C/min for (A) Ozonized sodium alginate (SA)-based hydrogel formulation and (B) Commercial SA-based hydrogel formulation. The gelation temperature of the hydrogels was determined at the crossover point where the elastic modulus (G′) equals the viscous modulus (G″).

3.2. Zeta Potential (ZP) and Particle size (z-average)

The ZP of hydrogel based on ozonized and commercial SA was recorded as -15.72^{a} ± 1.82 mV and -27.13^{b} ± 3.97 mV, respectively. The negative zeta potential observed in all dispersions can be attributed to the negative charge of carboxyl groups in alginate and sulfate groups of agar (Kavoosi et al., 2018). Only ozonized and commercial SA (2% w/v) displayed more negative results, -33.2 mV and -32.5 mV, respectively. Upon incorporating hydrogel components ($CaCl_2$, agar, and anthocyanin-rich extract), the absolute value of the zeta potential decreased. This trend is attributed to the electrostatic interactions, specially Ca^{+2} ions and anthocyanin-rich extract, aligning with observations by Wu et al. (2018), where the negative charges in SA connected with the ions and are attracted by the positive charge of anthocyanins (De Oliveira et al., 2014; Kavoosi et al., 2018). Therefore, it is inferred that the incorporation of components into the SA solution resulted in significant changes in the ZP of both neat SA solutions, particularly for the ozonized variant, and hydrogels due to the effects of electrostatic interactions among them. The particle size of the hydrogels also reflects interactions among polymer chains, crosslinking agents, and the anthocyanin-rich extract, as evidenced by the larger mean particle size observed in the hydrogels. The averaged particle diameter (z-average) of ozonized and commercial SA solutions

(2%) were 1263 nm and 1943 nm, respectively, while the values of their respective hydrogels were 2738.25[a] nm ± 121.90 and 4103[b] nm ± 221.13 nm.

3.3. Attenuated total reflectance–mid infrared (MIR-ATR) spectroscopy

MIR spectroscopy characterized the molecular organization and composition of the hydrogels structures, confirming the presence of the components in the formulations and detecting potential interactions within the hydrogel systems. Fig. 3 shows the characteristic vibrational modes and wavenumbers of the ozonized SA based hydrogel (A) and commercial SA based hydrogel (B) and their components collected from the MIR experimental spectra.

The broad absorption band at 3300 cm^{-1} and 2930 cm^{-1} represents the stretching vibrations of O-H and aliphatic C-H, respectively, associated with the alginate structure (Tian et al., 2022). Peaks observed at 1610 cm^{-1} are attributed to carboxylic groups C–O–O, indicating asymmetric and symmetric stretching at 1419 cm^{-1} (Chidiebere et al., 2017), characteristic of SA. The absorption peak at 1029.83 cm^{-1} results from the asymmetric vibration stretching contributed by groups of C-O-C and C-O (Qiu et al., 2023b), present in the SA structure. The peak at 1650 cm^{-1} is assigned to the stretching vibration of the conjugated peptide bond formed by amine (NH) and acetone groups in agar (Kanmani & Rhim, 2014), as well as addressed to the aromatic ring stretching in anthocyanins (Qin et al., 2019), which intensifies with the combination of various components. The peak at 1372 cm^{-1} is attributed to an ester sulfate group related to the agar structure (Volery, Besson, & Schaffer-lequart, 2004). The representative band at 1240 cm^{-1} suggests the presence of CH2 and the vibration generated by benzopyran rings related to anthocyanin-rich extract (Zeng et al., 2018). Bands at 1025 cm^{-1}, with a shoulder at 1100 cm^{-1}, are related to C–C and C–O stretching and can be attributed to crosslinking (Serafin, Culebras, & Collins, 2023). These bands may also be associated with the C-H deformation of anthocyanins (Choi et al., 2017) and C=O stretching of 3,6-anhydrous-d-galactose in the agar component (Fernandes et al., 2023).

Notably, the formulation and combination of the four components (SA, agar, anthocyanin-rich extract and $CaCl_2$) did not significantly alter the band positions of the hydrogels. However, some band intensities around 1000 cm^{-1} notably increased due to the formation of intermolecular hydrogen bonds. Another indication of interactions among the components was some peak shifting caused by the combination of alginate with other hydrogel components not participating in the Ca^{+2} crosslinking regime (Serafin, Culebras, & Collins, 2023).

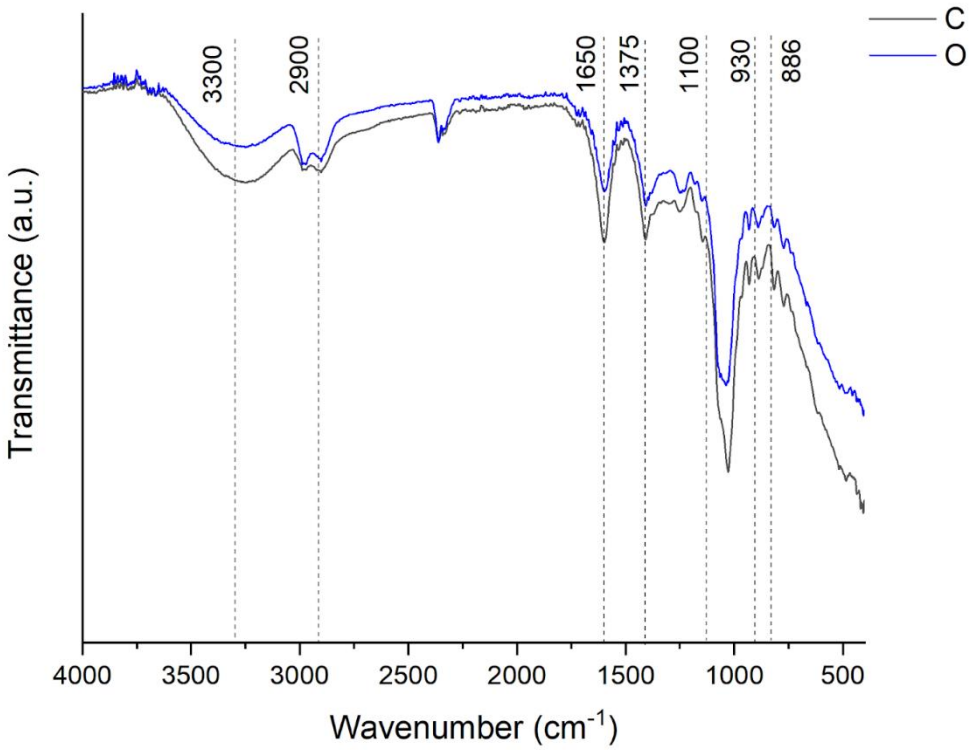

Fig. 3 - Attenuated total reflectance–mid infrared (ATR-MIR) spectra of commercial sodium alginate-based hydrogel and ozonized sodium alginate-based hydrogel with agar and anthocyanin-rich extract at room temperature.

3.4. Scanning electron microscopy (SEM)

Morphological analysis of the freeze-drying hydrogel was determined by SEM, as illustrated in Fig. 4. The SEM images reveal distinctive features between the commercial SA-based formulation and the ozonized-based hydrogel. The commercial-SA formulation exhibits a more fibrillated and fragmented structure, displaying a more dense and uniform interconnected network. This hierarchical structure indicates robust interactions among the compounds, contributing to the mechanical properties of the hydrogel (Wang et al., 2021a). Nevertheless, it is important to note that the excessive presence of pores observed in the commercial-SA variant increases the risk of bacterial contamination, particularly in medical applications (Siboro et al., 2021). Contrastingly, the SEM images of the ozonized-based hydrogel reveal a non-uniform pore distribution, with rough

microstructures with visible heterogeneous agglomerates on the surface. This observation may be attributed to the incomplete incorporation of the components in the hydrogel formulation (Fernandes et al., 2023). In addition to the pronounced shift in ZP values for neat ozonized-SA and its hydrogel formulation, indicating enhanced interactions among the components, SEM images reveal that these interactions were not as uniformly distributed as observed in the case of commercial SA. This difference in uniformity may be attributed to the more even distribution of carboxylate anions (COO−) within its structure, contributing to the expansion of the hydrogel network and an increase in pore quantity (Ma et al., 2008).

In general, SEM analysis revealed compatibility and a satisfactory intermolecular association among the hydrogel components, which includes SA, $CaCl_2$, agar loaded with anthocyanin-rich extract. Nevertheless, a notable difference in microstructure is observed when transitioning from ozonized SA to commercial SA in the hydrogel laden with anthocyanin-rich extract. The association of hydrogel components seems to be more uniform in the formulation with commercial SA.

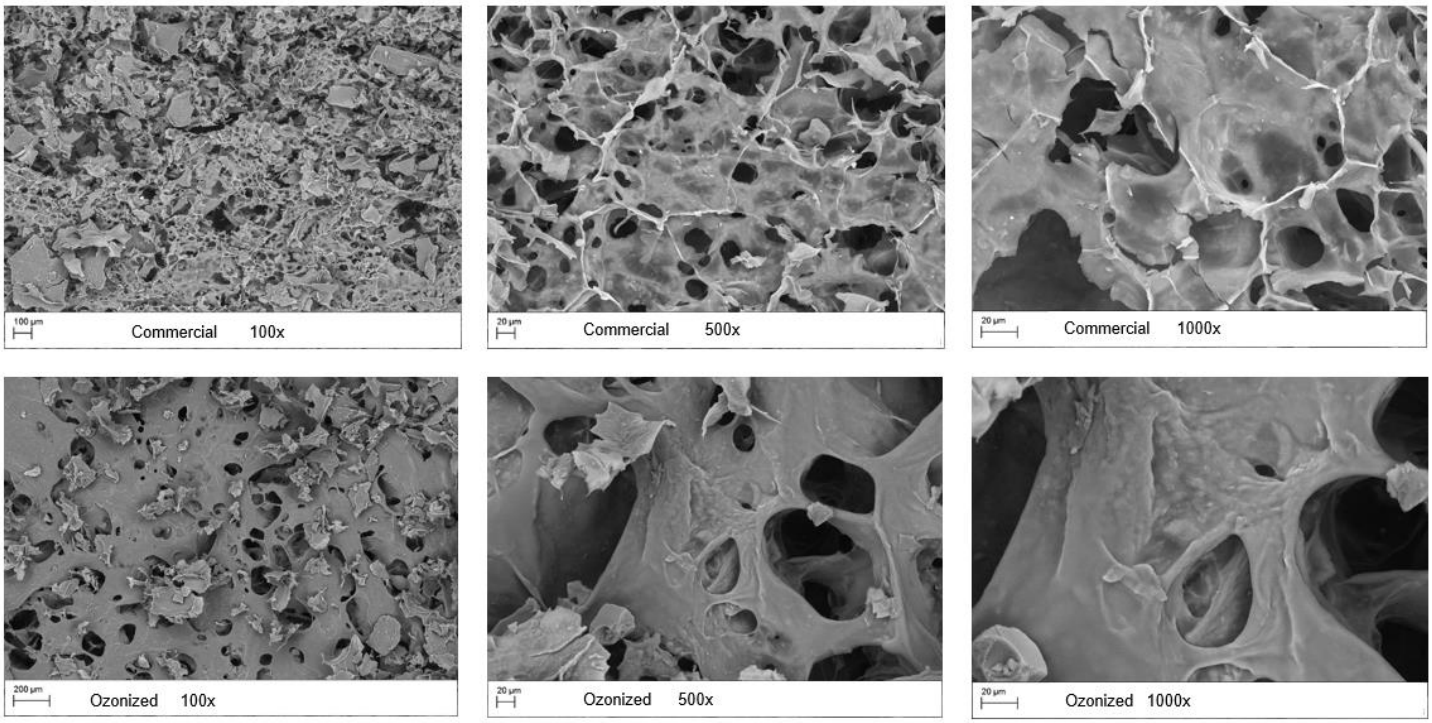

Fig. 4- SEM of hydrogels pre-crosslinked formulations with commercial or ozonized sodium alginate, agar, and anthocyanin-rich extract encapsulation

3.5. Gel formation and stability test

The bulk appearance of the hydrogels exhibits a deep red color attributed to the primary chemical form of the flavylium cation present in the pH 5 at which the hydrogels were formulated (Fig. 5). No discernible visual color difference was observed between the two formulations. Both hydrogel displayed a semisolid consistency, exhibiting no flow during the inversion experiment, indicative of a relatively stable gel structure immediately after preparation and even after 6 and 24 h. It is noteworthy that the use of Turrax homogenizer, a high-speed stirring method, was highly effective in homogenizing the hydrogel, ensuring uniform crosslinking and visually homogeneous and semisolid states. Furthermore, both hydrogel formulations exhibited homogeneous phases, good gel consistency, and a pleasant odor. Therefore, the development of hydrogel with SA and its components indicated robust crosslinking.

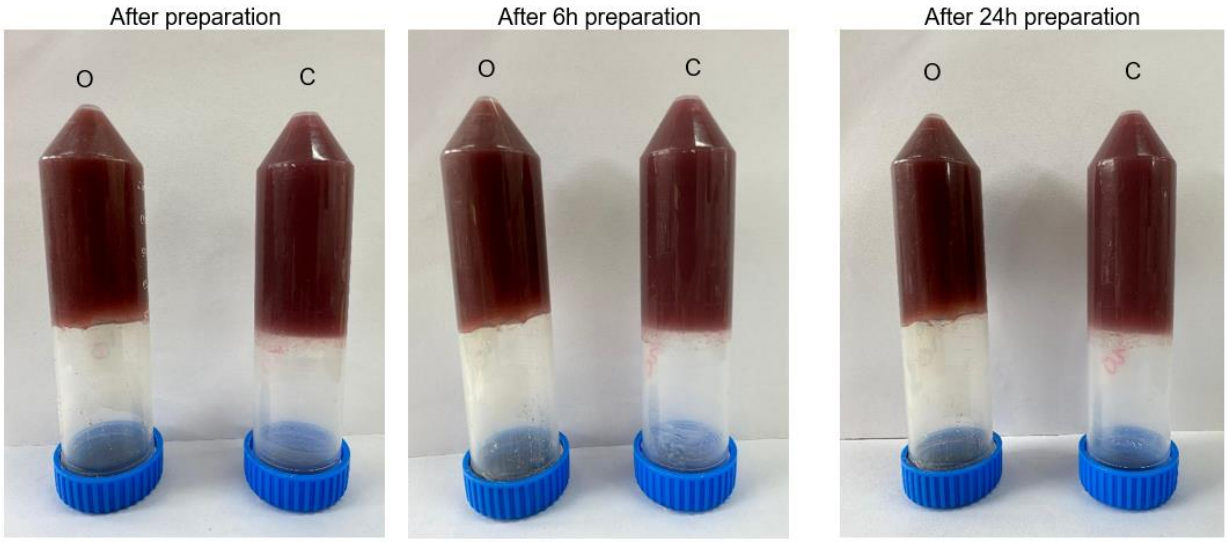

Fig. 5 - Visual characteristics and confirmation of gelling and stability through the inverted method of hydrogel at room temperature after preparation and 24 h of storage. O- Ozonized sodium alginate-based hydrogel with agar and anthocyanin-rich extract and C- commercial sodium alginate-based hydrogel with agar and anthocyanin-rich extract.

3.6. Printability

Printability assessment of the two hydrogel formulations involved varying needle diameter, printing speed, strand height and width, according to Table 1. A continuous strand was employed for the analysis of the printing filament, incorporating movements along both the x and y-axes. This approach facilitated a comprehensive examination of the filaments and hydrogel deposition. Both the ozonized SA-based hydrogel and the commercial hydrogel demonstrated deposition accuracy (DA) closer to 1, indicating more precise printing when employing an 18G needle (Table 1). Despite both needle (18G and 21G) types exhibiting a larger spreading ratio (SR) in the study—indicating that the printed filament had a width greater than designed—the greatest SR was observed using a 21G needle. In addition, the 0.8 mm needle experienced clogging issues and presented more gaps in strands prints for both formulations.

Comparing the two formulations, the ozonized SA-based hydrogel exhibited a higher SR than the commercial one. This was expected as the ozonized SA-based hydrogel displayed reduced viscosity recovery (3iTT test). After selecting the optimal needle gauge, a thorough analysis of DA and SR results was performed for both formulations (printing parameters 4 to 8). For the ozonized SA-based hydrogel, the optimal parameters were identified as number 6, whereas for the commercial hydrogel, it was number 7. Given that the results for number 7 in the commercial sample were not significantly different from those of number 6, the ozonized-based hydrogel results were prioritized in determining the optimal printing parameters.

Fig. 6 - Strand thickness analysis: Printed strands, designed with specific length and width parameters (on the top of the figure) and measured using ImageJ. The numerical annotations correspond to the associated printing parameters. "C" denotes the commercial sodium alginate-based ink, while "O" represents the ozonized sodium alginate hydrogel, both pre-crosslinked with $CaCl_2$ (25mM), incorporating agar and encapsulating an anthocyanin-rich extract

Table 1 - Effect of printing parameters on deposition accuracy (DA) and spreading ratio (SR) for strands printed with hydrogel formulated with pre-crosslinked ozonized sodium alginate-based hydrogel or commercial sodium alginate, with agar and anthocyanin-rich encapsulation

Printing Parameters	Layer height and width (mm)	Print speed (mm/s)	Needle Diameter (mm) / Gauge	Ozonized			Commercial		
				Length (40 mm)	Length (10 mm)	Width (1.2 mm)	Length (40 mm)	Length (10 mm)	Width (1.2 mm)
				DA	DA	SR	DA	DA	SR
1	0.8	10	0.8 / 18G	0.86	0.78	1.75	0.99	0.65	1.25
2	0.8	5		0.47	0.34	1.75	0.80	0.62	1.17
3	1	5		0.54	0.66	2.08	0.86	0.87	1.75
4	1	10		0.99	0.69	1.58	0.99	0.90	1.5
5	1	10	1.2 / 21G	0.99	0.87	1.92	0.99	0.87	1.33
6	1	5		0.99	0.91	1.66	0.99	0.88	1.5
7	1.2	5		0.99	1.04	2.08	0.99	1.08	1.33
8	1.2	10		0.97	1.04	2.08	0.97	1.08	1.5

3.7. 3D printing

3.7.1. Printing deviation

To assess dimensional printing accuracy, a cuboid shape (15 × 15 × 15 mm) was designed (Fig. 7), and the temporal evolution of dimensional printing deviation was carried out (Fig. 8), comparing the fidelity of the printed constructs with the dimensions of the projected geometric model. Measurements in three directions (length, width, and height) were taken immediately after printing, as well as after 1h, 6h, and 24h post-printing. Both hydrogel formulations exhibited easy extrusion from the nozzle tip due to their shear thinning behavior (data not shown), identified through rheological analyses (Cheng et al., 2022). The material composition significantly influences self-supporting properties, affecting the shape retention ability during 3D printing (Wilms et al., 2021). The ozonized SA-based hydrogel, despite showing low percentage of recovery in rheological tests (Fig. 1), achieved self-support after printing and maintained shape retention comparable to the commercial-SA formulation. 3D printing accuracy, assessed through printing deviation (PD) and surface structure appearance, demonstrated good printability, mechanical strength, and dimensional stability throughout the printing process (Kuo et al., 2021).

Both compositions exhibited the capability to maintain good inter-layer diffusion, ensuring accurate scaffold construction with traceable layer lines. The statistical analysis indicated that right after printing (T0), height and length were not significantly different, while width showed significance between the formulations. After 1h post-printing (T1), height became significantly different, width

showed no significant difference, and length remained insignificant. After 24h, the higher PD results for the commercial-SA formulation indicated a rough and dry surface structure resembling a shrinkage process. Conversely, the 3D structure printed with hydrogel based on ozonized SA exhibited a more rigid configuration compared to the structure formulated with commercial-grade SA, which demonstrated increased susceptibility to fracture within 24 hours. It appeared that the structure with ozonized-SA was fully gelled throughout the 3D construct, making it manageable by hand, while the structure printed with commercial SA remained soft. This phenomenon could possibly be explained by enhanced interconnection between the layers and more prominent crosslinking effects after printing, particularly noticeable in the hydrogel formulated with ozonized SA.

The rheological properties of the ozonized-SA based hydrogel may support these results, as materials with a proper G′ (Fig. 1) can adequately support and retain the deposited information, favoring low dimensional printing deviation (Yu et al., 2022). The temperature was also suitable for printing, as reported issues such as nozzle clogging or low shape fidelity were absent, considering the agar's gelation temperature is around 37°C (data not shown). Moreover, based on prior structural analysis (data not presented), ozonized SA showed a higher proportion of guluronic acid compared to mannuronic acid, whereas its commercial equivalent exhibits a greater concentration of mannuronic acid in its composition. Therefore, it is plausible that the polymeric matrix formulated with ozonized SA may exhibit elevated values of G' and G" attributable to its increased guluronic acid content (Mollah et al., 2023).

In conclusion, based on the printing results, the final product printed with ozonized-SA-based hydrogel exhibited promising results with good printing accuracy, maintaining stable shapes as per the design. However, as a study involving a unique material, we believe that the printability and textural properties of 3D printed hydrogel can be further improved by adjusting formulation proportions or implementing post-crosslinking, depending on the future application field.

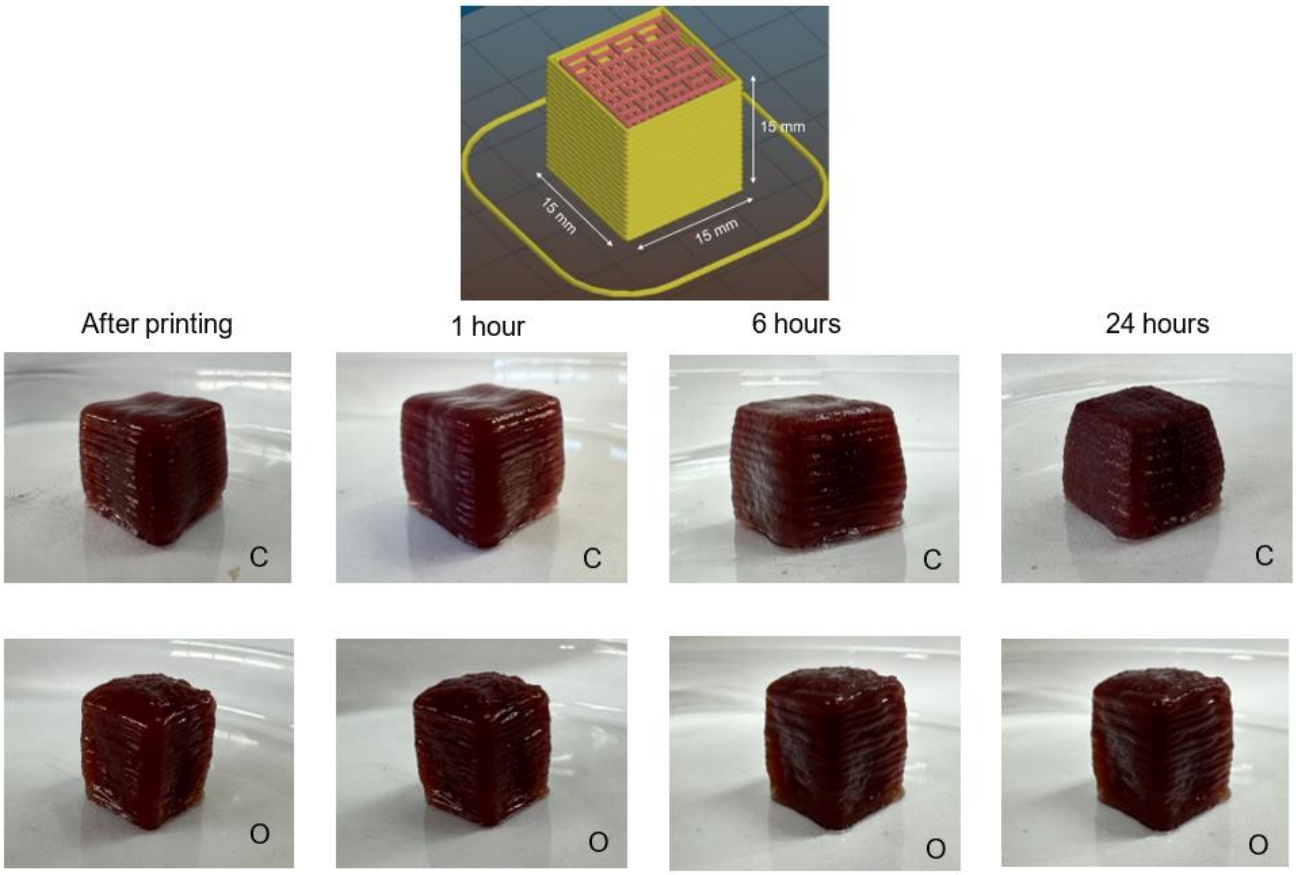

Figure 7 - 3D model and printed cubes: comparison of formulations with pre-crosslinked commercial sodium alginate-based hydrogel (C) and ozonized sodium alginate-based hydrogel (O) with agar and anthocyanin-rich extract at different time intervals

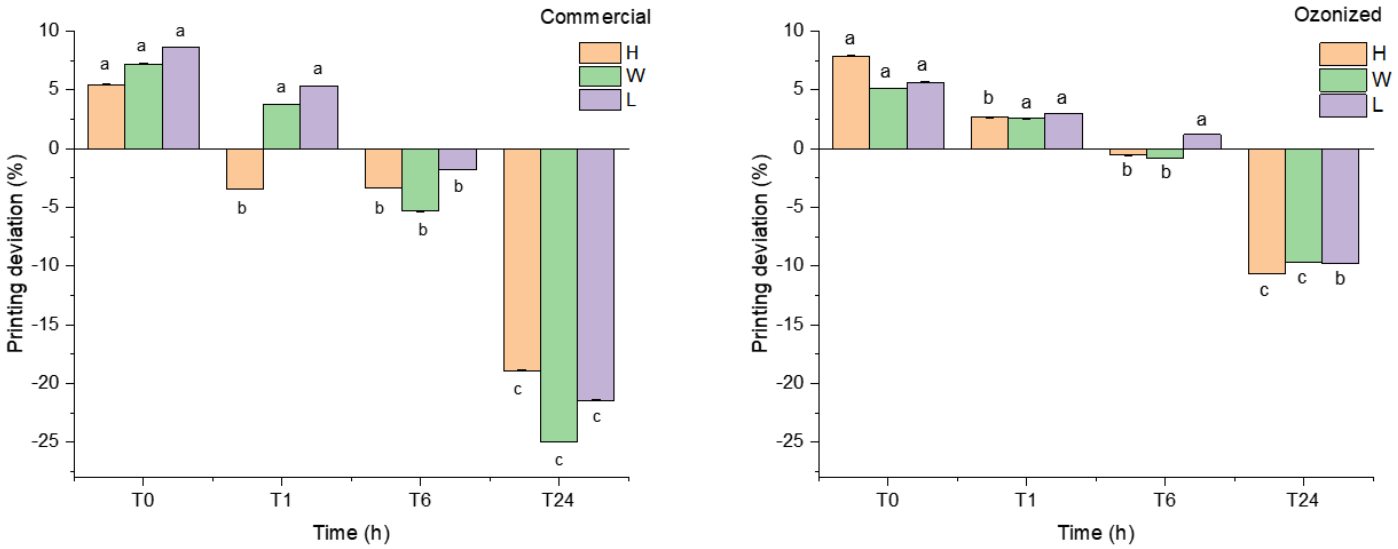

Figure 8 - 3D printed hydrogel dimensional analysis: height (H), width (W), and length (L) for commercial sodium alginate or ozonized sodium alginate formulation with agar and anthocyanin-rich extract encapsulation. Statistical analysis was conducted within the same dimension across the different time points of measurement where distinct letters denote significant differences ($p \leq 0.05$).

3.7.2. Texture profile analysis

The texture profile analysis attributes of the 3D constructs, printed with both hydrogels using the optimal parameters established in the printability test, are presented in Table 2. The parameters of hardness, springiness, gumminess, and chewiness did not exhibit a significant difference between the formulations. Hardness, which is indicative of the strength of the gel structure under compression (Lau, Tang & Paulson, 2000), displayed values in this study that were much lower compared to those reported in the literature. For instance, Kuo et al. (2021) observed a minimum hardness of 727 g in a study of gelatin/alginate hybrid hydrogel with a chocolate drop shape (height = 9.7 mm, diameter = 16 mm). Additionally, Fernandes et al. (2023) found a minimum hardness of 53 g in bigels agar-based formulations with a hexagonal model measuring 30 mm × 30 mm × 9.6 mm (length × width × height). It is evident that factors such as the composition of components, their proportions, the type of crosslinking, and filling density would influence this and other parameters (Suebsaen et al., 2019; Feng et al., 2024). Regardless of the application, there is a need to enhance the hardness of the 3D construct. Even for dietary considerations like

dysphagia, where lower hardness is preferred, the values typically range around 50 g (Qiu et al., 2023a) to improve the energy required to make food boluses suitable for swallowing, facilitating the swallow process of food bolus (Suebsaen et al., 2019). Springiness is the measure of the degree to which the sample returns to its original height after compression, representing how the initial compression impacts the breakdown of the gel structure (Sanderson, 1990). High springiness in a gel indicates that the structure breaks into a few large pieces during the initial compression, while low springiness results in the structure breaking into numerous small pieces (Lau, Tang, & Paulson, 2000). Our high observed values align closely with the findings of Ghazal et al. (2021), as well as the study of Fernandes et al. (2023) in agar-based bigels formulations.

Gumminess is utilized to describe the energy required for disintegrating semi-solid constructs (Szczesniak, 2002) and it is calculated by the product of cohesiveness times hardness, therefore it exhibited a similar trend from hardness. Our gumminess results closely align with the reported (range 9g to 26 g), in studies conducted by Fernandes et al. (2023) on agar-based bigels formulations, Xie et al. (2023) investigating bigels with gelatin, and Liu et al. (2021) exploring shiitake mushroom incorporation with gums. Hydrogels with lower gumminess may be considered more suitable for individuals with chewing difficulties (Szczesniak, 2002). Conversely, food materials characterized by high hardness and gumminess may exhibit increased resistance during extrusion through the 3D printing nozzle, potentially resulting in printing failures (Cai et al., 2022).

Adhesiveness is another parameter more commonly employed in the analysis of food printing, where high adhesiveness necessitates increased effort in the pharyngeal phase of swallowing, particularly for older adults and individuals with dysphagia (Keršienė et al., 2020). As observed in Table 2, it is evident that the commercial SA-based hydrogel would result in reduced swallowing effort, given its lower absolute value compared to the hydrogel formulated with ozonized SA. This can be attributed to the higher viscosity of the commercial-SA based hydrogel (Hurler et al., 2012), as adhesiveness is linked to the forces between the sample's surface and the surfaces of other materials it comes in contact with (Szczesniak, 2002). However, both values are considered low and closely resemble those found in fruit gel produced with agar (Suebsaen et al., 2019).

The cohesiveness parameter signifies the strength of internal bonds within a sample and the extent to which it can undergo deformation before rupturing (Civille & Szczesniak, 1973; Sanderson, 1990). In the realm of 3D printing, this parameter plays a crucial role in maintaining the integrity of the impression matrix, preventing it from breaking into fragments (Shahbazi et al., 2021). The ozonized-based hydrogel exhibited slightly higher cohesiveness compared to the commercial sample, indicating stronger internal bonds that hold the construct. In the context of

food engineering, the ozonized SA hydrogel would maintain the food bolus together, preventing its fragmentation into smaller particles during swallowing, ensuring safe swallowing (Cichero, 2016). The cohesiveness values obtained in this study closely resemble those reported by Fernandes et al. (2023), who studied gelatin-based bigels (0.93), as well as commercial gelatin-based gummies (0.89) in the work by Kuo et al. (2021).

Resilience is defined as the ability of a sample to recover from deformation in terms of both speed and force (Steffe, 1996). In this study, the resilience of the commercial SA-based hydrogel was slightly higher, closely aligning with the findings of Kuo et al. (2021), who investigated gelatin/alginate hybrid hydrogels. Conversely, the resilience of the ozonized hydrogel was comparable to the freeze-dried samples from the same study. As corroborated by the results of the 3iTT rheological test, the commercial SA-based hydrogel exhibited superior viscosity recovery. This characteristic, highlighted by the resilience test, underscores the hydrogel formulation's ability to resist compression and regain its original shape and size (Kuo et al., 2021).

The texture analysis indicates that the results obtained with the ozonized SA hydrogel are comparable to those of the commercially formulated hydrogel, with predominantly similar and mostly non-significant differences. On one hand, rheological results (Fig. 1) revealed a higher G' but with a low crossover % strain, for the ozonized-SA-based hydrogel, suggesting a more rigid yet fragile gel. On the other hand, SEM images displayed a more interconnected structure in the commercial-SA-based hydrogel, whereas the ozonized-SA-based hydrogel exhibited a denser formation. Thus, the observed differences cited were not substantial, resulting in similar textural profiles for both hydrogels. To enhance certain texture parameters, potential adjustments in the hydrogel formulation may be necessary, such as increasing the agar content to improve the mechanical properties of the 3D construct or modifying some ozonation parameters to prevent the polysaccharide from having its structure so extensively broken. Alternatively, a post-crosslinking method, as demonstrated by Nelson et al. (2021), could be explored as another viable option.

Table 2 - Texture profile analysis of 3D constructs printed with pre-crosslinked commercial sodium alginate or ozonized sodium alginate, agar, and anthocyanin-rich extract encapsulation

Hydrogel	Hardness (g)	Adhesiveness (g.s)	Springiness	Cohesiveness	Gumminess (g)	Resilience
Commercial	20.47^{a}± 2.96	-31.66^{a} ± 1.71	1.12^{a} ± 0.02	0.96^{a} ± 0.09	21.86^{a} ± 3.82	0.06^{a} ± 0.006
Ozonized	21.55^{a} ±2.42	-37.89^{b} ± 3.07	1.11^{a} ± 0.05	1.12^{b} ± 0.09	22.94^{a} ± 2.03	0.09^{b} ± 0.006

Statistical analysis was performed on each texture parameter and compared between the two formulations, where distinct letters indicate significant differences ($p \leq 0.05$). The data are presented as the mean ± standard deviation ($n = 3$)

4. Conclusion

In this study, we introduced a novel composite hydrogel based on extracted SA from seaweeds and modified through ozonation. The hydrogel formulation consisted of pre-crosslinked ozonized SA, agar, and encapsulated anthocyanin-rich extract designed for extrusion 3D printing applications, while commercial SA was also used to formulate a hydrogel for comparison. Oscillatory rheological analyses were performed to characterize the hydrogels formulations, revealing adequate properties for 3D printing. These studies also indicated temperature adjustments for printing and highlighted potential enhancements for the formulations. Successful 3D printing was achieved under optimized parameters derived from printability tests, resulting in structures with great shape fidelity. The 3D printed constructs exhibited a comparable texture profile to the commercial SA-based hydrogel. Overall, the ozonized SA-based hydrogel demonstrated promising features, aligning with its commercial counterpart and was suitable to incorporate anthocyanin-rich extract by using an integrated manufacturing processes of encapsulation and 3D printing. Further refinements may involve increasing SA molecular weight by reducing ozonation time, elevating agar content in the formulation, or exploring post-crosslinking strategies. Additionally, the pH-responsive nature of anthocyanin presents opportunities for applications in monitoring food freshness, cosmetics, or harnessing antioxidant properties. Consequently, this hydrogel formulation holds potential as a versatile delivery system for various bioactive components in bioengineering, pharmaceuticals, nutraceuticals, and the food industry.

5. References

Ahmadzadeh, S., Lenie, M. D. R., Mirmahdi, R. S., & Ubeyitogullari, A. (2023). Designing future foods: Harnessing 3D food printing technology to encapsulate bioactive compounds. Critical Reviews in Food Science and Nutrition, 1-17. https://doi.org/10.1080/10408398.2023.2273446

Ahmed, E. M. (2015). Hydrogel: Preparation, characterization, and applications: A review. Journal of advanced research, 6(2), 105-121. https://doi.org/10.1016/j.jare.2013.07.006

Axpe, E., & Oyen, M. L. (2016). Applications of alginate-based bioinks in 3D bioprinting. International journal of molecular sciences, 17(12), 1976. 10.3390/ijms17121976.

Bider, F., Miola, M., Clejanu, C. E., Götzelmann, J., Kuth, S., Vernè, E., Basu, B., & Boccaccini, A. R. (2024). 3D bioprinting of multifunctional alginate dialdehyde (ADA)–gelatin (GEL)(ADA-GEL) hydrogels incorporating ferulic acid. International Journal of Biological Macromolecules, 257, 128449. https://doi.org/10.1016/j.ijbiomac.2023.128449

Boontheekul, T., Kong, H. J., & Mooney, D. J. (2005). Controlling alginate gel degradation utilizing partial oxidation and bimodal molecular weight distribution. Biomaterials, 26(15), 2455-2465. https://doi.org/10.1016/j.biomaterials.2004.06.044

Cai, Q., Zhong, Y., Xu, M., Huang, Q., & Lu, X. (2022). 3D printed high oil custard cream: Effects of whey protein isolate, hydroxypropylated starch and carrageenan on physicochemical properties and printing performance. Lwt, 156, 113039. https://doi.org/10.1016/j.lwt.2021.113039

Cao, L., Lu, W., Mata, A., Nishinari, K., & Fang, Y. (2020). Egg-box model-based gelation of alginate and pectin: A review. Carbohydrate polymers, 242, 116389. https://doi.org/10.1016/j.carbpol.2020.116389

Cheng, Y., Fu, Y., Ma, L., Yap, P. L., Losic, D., Wang, H., & Zhang, Y. (2022). Rheology of edible food inks from 2D/3D/4D printing, and its role in future 5D/6D printing. Food Hydrocolloids, 132. https://doi.org/10.1016/j.foodhyd.2022.107855.

Chidiebere, M. A., Nwanonenyi, S., Njoku, D., Iroha, N. B., Oguzie, E. E., & Li, Y. (2017). Experimental study on the inhibitive effect of phytic acid as a corrosion inhibitor for Q235 mild steel in 1 M HCl environment. World News of Natural Sciences, (15), 1-19. https://doi.org/10.1016/j.fbp.2013.11.001

Choi, I., Lee, J. Y., Lacroix, M., & Han, J. (2017). Intelligent pH indicator film composed of agar/potato starch and anthocyanin extracts from purple sweet potato. Food chemistry, 218, 122-128. https://doi.org/10.1016/j.foodchem.2016.09.050

Chung, J. H., Naficy, S., Yue, Z., Kapsa, R., Quigley, A., Moulton, S. E., & Wallace, G. G. (2013). Bio-ink properties and printability for extrusion printing living cells. Biomaterials Science, 1(7), 763-773. DOI: 10.1039/C3BM00012E

Cichero, J. A. Y. (2016). Adjustment of food textural properties for elderly patients. Journal of Texture Studies, 47(4), 277-283. https://doi.org/10.1111/jtxs.12200

Civille, G. V., & Szczesniak, A. S. (1973). Guidelines to training a texture profile panel. Journal of texture studies, 4(2), 204-223.

de Oliveira, E. F., Paula, H. C., & de Paula, R. C. (2014). Alginate/cashew gum nanoparticles for essential oil encapsulation. Colloids and Surfaces B: Biointerfaces, 113, 146-151. https://doi.org/10.1016/j.colsurfb.2013.08.038

Falcone, G., Mazzei, P., Piccolo, A., Esposito, T., Mencherini, T., Aquino, R. P., Del Gaudio, P., & Russo, P. (2022). Advanced printable hydrogels from pre-crosslinked alginate as a new tool in semi solid extrusion 3D printing process. Carbohydrate Polymers, 276, 118746. https://doi.org/10.1016/j.carbpol.2021.118746

Feng, L., Qiu, X., Wu, J., Dai, Z., Xu, Y., Zhang, M., & Li, D. (2024). Design of geometric structures of hydrogel via 3D printing to regulate release kinetics and bioaccessibility of β-carotene. Additive Manufacturing, 79, 103927. https://doi.org/10.1016/j.addma.2023.103927

Fernandes, A. S., Neves, B. V., Mazzo, T. M., Longo, E., Jacob-Lopez, E., Zepka, L. Q., & de Rosso, V. V. (2023). Bigels as potential inks for extrusion-based 3d food printing: Effect of oleogel fraction on physical characterization and printability. Food Hydrocolloids, 108986. https://doi.org/10.1016/j.foodhyd.2023.108986

Fernando, I. S., Sanjeewa, K. A., Kim, S. Y., Lee, J. S., & Jeon, Y. J. (2018). Reduction of heavy metal (Pb2+) biosorption in zebrafish model using alginic acid purified from Ecklonia cava and two of its synthetic derivatives. International journal of biological macromolecules, 106, 330-337. https://doi.org/10.1016/j.ijbiomac.2017.08.027

Fernando, I. S., Kim, D., Nah, J. W., & Jeon, Y. J. (2019). Advances in functionalizing fucoidans and alginates (bio) polymers by structural modifications: A review. Chemical Engineering Journal, 355, 33-48. https://doi.org/10.1016/j.cej.2018.08.115

Garcia-Hernandez, A., Lobato-Calleros, C., Vernon-Carter, E. J., Sosa-Hernandez, E., & Alvarez-Ramirez, J. (2017). Effects of clay concentration on the morphology and rheological properties of xanthan gum-based hydrogels reinforced with montmorillonite particles. Journal of Applied Polymer Science, 134(8). https://doi.org/10.1002/app.44517

Ghazal, A. F., Zhang, M., Bhandari, B., & Chen, H. (2021). Investigation on spontaneous 4D changes in color and flavor of healthy 3D printed food materials over time in response to external or internal pH stimulus. Food Research International, 142, 110215. https://doi.org/10.1016/j.foodres.2021.110215

Guo, C., Zhang, M., & Devahastin, S. (2021). Improvement of 3D printability of buckwheat starch-pectin system via synergistic Ca2+-microwave pretreatment. Food Hydrocolloids, 113, 106483. https://doi.org/10.1016/j.foodhyd.2020.106483.

Hurler, J., Engesland, A., Poorahmary Kermany, B., & Škalko-Basnet, N. (2012). Improved texture analysis for hydrogel characterization: Gel cohesiveness, adhesiveness, and hardness. Journal of applied polymer science, 125(1), 180-188. https://doi.org/10.1002/app.35414

Jiang, M., & Zhang, Y. (2023). Biopolymer-based encapsulation of anthocyanins as reinforced natural colorants for food applications. Journal of Agriculture and Food Research, 100488. https://doi.org/10.1016/j.jafr.2022.100488

Kanmani, P., & Rhim, J. W. (2014). Antimicrobial and physical-mechanical properties of agar-based films incorporated with grapefruit seed extract. Carbohydrate polymers, 102, 708-716. https://doi.org/10.1016/j.carbpol.2013.10.099

Karavasili, C., Tsongas, K., Andreadis, I. I., Andriotis, E. G., Papachristou, E. T., Papi, R. M., Tzetzis, D., & Fatouros, D. G. (2020). Physico-mechanical and finite element analysis evaluation of 3D printable alginate-methylcellulose inks for wound healing applications. Carbohydrate polymers, 247, 116666. https://doi.org/10.1016/j.carbpol.2020.116666

Kavoosi, G., Derakhshan, M., Salehi, M., & Rahmati, L. (2018). Microencapsulation of zataria essential oil in agar, alginate and carrageenan. Innovative Food Science & Emerging Technologies, 45, 418-425. https://doi.org/10.1016/j.ifset.2017.12.010

Keršienė, M., Jasutienė, I., Eisinaitė, V., Pukalskienė, M., Venskutonis, P. R., Damulevičienė, G.,& Leskauskaitė, D. (2020). Development of a high-protein yoghurt-type product enriched with bioactive compounds for the elderly. Lwt, 131, 109820.https://doi.org/10.1016/j.lwt.2020.109820

Kiyotake, E. A., Douglas, A. W., Thomas, E. E., Nimmo, S. L., & Detamore, M. S. (2019). Development and quantitative characterization of the precursor rheology of hyaluronic acid hydrogels for bioprinting. Acta biomaterialia, 95, 176-187. https://doi.org/10.1016/j.actbio.2019.01.041

Kuo, C. C., Qin, H., Cheng, Y., Jiang, X., & Shi, X. (2021). An integrated manufacturing strategy to fabricate delivery system using gelatin/alginate hybrid hydrogels: 3D printing and freeze-drying. Food Hydrocolloids, 111, 106262. https://doi.org/10.1016/j.foodhyd.2020.106262

Lau, M. H., Tang, J., & Paulson, A. T. (2000). Texture profile and turbidity of gellan/gelatin mixed gels. Food Research International, 33(8), 665-671. https://doi.org/10.1016/S0963-9969(00)00111-3

Lee, K. Y., & Mooney, D. J. (2012). Alginate: properties and biomedical applications. Progress in polymer science, 37(1), 106-126. 10.1016/j.progpolymsci.2011.06.003

Li, H., Liu, S., & Li, L. (2016). Rheological study on 3D printability of alginate hydrogel and effect of graphene oxide. International Journal of Bioprinting, 2(2). http://dx.doi.org/10.18063/IJB.2016.02.007

Liu, Y., Winter, H. H., & Perry, S. L. (2017). Linear viscoelasticity of complex coacervates. Advances in colloid and interface science, 239, 46-60. https://doi.org/10.1016/j.cis.2016.08.010

Liu, Z., Bhandari, B., Prakash, S., Mantihal, S., & Zhang, M. (2019a). Linking rheology and printability of a multicomponent gel system of carrageenan-xanthan-starch in extrusion based additive manufacturing. Food Hydrocolloids, 87, 413-424. https://doi.org/10.1016/j.foodhyd.2018.08.026

Liu, Y., Zhang, W., Wang, K., Bao, Y., Regenstein, J. M., & Zhou, P. (2019b). Fabrication of gel-like emulsions with whey protein isolate using microfluidization: Rheological properties and 3D printing performance. Food and Bioprocess Technology, 12, 1967-1979. https://doi.org/10.1007/s11947-019-02344-5

Liu, Z., Bhandari, B., Guo, C., Zheng, W., Cao, S., Lu, H., Mo, H., & Li, H. (2021). 3D printing of shiitake mushroom incorporated with gums as dysphagia diet. Foods, 10(9), 2189. https://doi.org/10.3390/foods10092189

Lu, Y., Rai, R., & Nitin, N. (2023). Image-based assessment and machine learning-enabled prediction of printability of polysaccharides-based food ink for 3D printing. Food Research International, 173, 113384. https://doi.org/10.1016/j.foodres.2023.113384

Ma, J., Zhang, L., Fan, B., Xu, Y., & Liang, B. (2008). A novel sodium carboxymethylcellulose/poly (N-isopropylacrylamide)/Clay semi-IPN nanocomposite hydrogel with improved response rate and mechanical properties. Journal of Polymer Science Part B: Polymer Physics, 46(15), 1546-1555. https://doi.org/10.1002/polb.21490

Mottaghipisheh, J., Doustimotlagh, A. H., Irajie, C., Tanideh, N., Barzegar, A., & Iraji, A. (2022). The promising therapeutic and preventive properties of anthocyanidins/anthocyanins on prostate cancer. Cells, 11(7), 1070. https://doi.org/10.3390/cells11071070

Mousavi, S. M. R., Rafe, A., & Yeganehzad, S. (2020). Structure-rheology relationships of composite gels: Alginate and Basil seed gum/guar gum. Carbohydrate polymers, 232, 115809. https://doi.org/10.1016/j.carbpol.2019.115809

Nelson, C., Tuladhar, S., Launen, L., & Habib, A. (2021). 3D bio-printability of hybrid pre-crosslinked hydrogels. International Journal of Molecular Sciences, 22(24), 13481. https://doi.org/10.3390/ijms222413481

Ngo, T. D., Kashani, A., Imbalzano, G., Nguyen, K. T., & Hui, D. (2018). Additive manufacturing (3D printing): A review of materials, methods, applications and challenges. Composites Part B: Engineering, 143, 172-196. https://doi.org/10.1016/j.compositesb.2018.02.012

Ning, X., Huang, J., Yuan, N., Chen, C., & Lin, D. (2022). Research Advances in Mechanical Properties and Applications of Dual Network Hydrogels. International Journal of Molecular Sciences, 23(24), 15757. https://doi.org/10.3390/ijms232415757

Nogueira, M. T., Chica, L. R., Yamashita, C., Nunes, N. S. S., Moraes, I. C. F., Branco, C. C. Z., & Branco, I. G. (2022). Optimal conditions for alkaline treatment of alginate extraction from the brown seaweed Sargassum cymosum C. Agardh by response surface methodology. Applied Food Research, 2(2), 100141. https://doi.org/10.1016/j.afres.2022.100141

Pandiselvam, R., Manikantan, M. R., Divya, V., Ashokkumar, C., Kaavya, R., Kothakota, A., & Ramesh, S. V. (2019). Ozone: An advanced oxidation technology for starch modification. Ozone: Science & Engineering, 41(6), 491-507. https://doi.org/10.1080/01919512.2019.1577128

Paxton, N., Smolan, W., Böck, T., Melchels, F., Groll, J., & Jungst, T. (2017). Proposal to assess printability of bioinks for extrusion-based bioprinting and evaluation of rheological properties governing bioprintability. Biofabrication, 9(4), 044107. doi: 10.1088/1758-5090/aa8dd8

Priftis, D., Laugel, N., & Tirrell, M. (2012). Thermodynamic characterization of polypeptide complex coacervation. Langmuir, 28(45), 15947–15957. https://doi.org/10.1021/la302729r

Qin, Y., Liu, Y., Yong, H., Liu, J., Zhang, X., & Liu, J. (2019). Preparation and characterization of active and intelligent packaging films based on cassava starch and anthocyanins from Lycium ruthenicum Murr. International journal of biological macromolecules, 134, 80-90. https://doi.org/10.1016/j.ijbiomac.2019.05.029

Qiu, L., Zhang, M., Bhandari, B., Chitrakar, B., & Chang, L. (2023a). Investigation of 3D printing of apple and edible rose blends as a dysphagia food. Food Hydrocolloids, 135, 108184. https://doi.org/10.1016/j.foodhyd.2022.108184

Qiu, L., Zhang, M., Adhikari, B., & Chang, L. (2023b). Microencapsulation of rose essential oil using perilla protein isolate-sodium alginate complex coacervates and application of microcapsules to preserve ground beef. Food and Bioprocess Technology, 16(2), 368-381.

Qiu, L., Zhang, M., Adhikari, B., Lin, J., & Luo, Z. (2024). Preparation and characterization of 3D printed texture-modified food for the elderly using mung bean protein, rose powder, and flaxseed gum. Journal of Food Engineering, 361, 111750. https://doi.org/10.1016/j.jfoodeng.2023.111750

Rahman, J. M. H., Shiblee, M. N. I., Ahmed, K., Khosla, A., Kawakami, M., & Furukawa, H. (2020). Rheological and mechanical properties of edible gel materials for 3D food printing technology. Heliyon, 6(12). https://doi.org/10.1016/j.heliyon.2020.e05859

Rastin, H., Ramezanpour, M., Hassan, K., Mazinani, A., Tung, T. T., Vreugde, S., & Losic, D. (2021). 3D bioprinting of a cell-laden antibacterial polysaccharide hydrogel composite. Carbohydrate Polymers, 264, 117989.https://doi.org/10.1016/j.carbpol.2021.117989

Saha, D., & Bhattacharya, S. (2010). Hydrocolloids as thickening and gelling agents in food: a critical review. Journal of food science and technology, 47, 587-597. 10.1007/s13197-010-0162-6

Sanderson, G. R. (1990). Gellan gum. In Food gels (pp. 201-232). Dordrecht: Springer Netherlands.

Sardelli, L., Tunesi, M., Briatico-Vangosa, F., & Petrini, P. (2021). 3D-Reactive printing of engineered alginate inks. Soft Matter, 17(35), 8105-8117. DOI: 10.1039/D1SM00604E

Serafin, A., Culebras, M., & Collins, M. N. (2023). Synthesis and evaluation of alginate, gelatin, and hyaluronic acid hybrid hydrogels for tissue engineering applications. International journal of biological macromolecules, 233, 123438. https://doi.org/10.1016/j.ijbiomac.2023.123438

Shahbazi, M., Jäger, H., Chen, J., & Ettelaie, R. (2021). Construction of 3D printed reduced-fat meat analogue by emulsion gels. Part II: Printing performance, thermal, tribological, and dynamic sensory characterization of printed objects. Food Hydrocolloids, 121, 107054. https://doi.org/10.1016/j.foodhyd.2021.107054

Siboro, S. A., Anugrah, D. S., Ramesh, K., Park, S. H., Kim, H. R., & Lim, K. T. (2021). Tunable porosity of covalently crosslinked alginate-based hydrogels and its significance in drug release behavior. Carbohydrate Polymers, 260, 117779. https://doi.org/10.1016/j.carbpol.2021.117779

Smilek, J., Jarábková, S., Velcer, T., & Pekař, M. (2019). Compositional and temperature effects on the rheological properties of polyelectrolyte–surfactant hydrogels. Polymers, 11(5), 927. https://doi.org/10.3390/polym11050927

Souza, V. B., Thomazini, M., de Carvalho Balieiro, J. C., & Fávaro-Trindade, C. S. (2015). Effect of spray drying on the physicochemical properties and color stability of the powdered pigment obtained from vinification byproducts of the Bordo grape (Vitis labrusca). Food and Bioproducts Processing, 93, 39-50. https://doi.org/10.1016/j.fbp.2013.11.001

Steffe, J. (1996) C.5 Rheological methods. Polymer fractionation, Academic press, 317-339. https://doi.org/10.1016/B978-1-4832-3245-4.50016-9

Stojkov, G., Niyazov, Z., Picchioni, F., & Bose, R. K. (2021). Relationship between structure and rheology of hydrogels for various applications. Gels, 7(4), 255. https://doi.org/10.3390/gels7040255

Suebsaen, K., Suksatit, B., Kanha, N., & Laokuldilok, T. (2019). Instrumental characterization of banana dessert gels for the elderly with dysphagia. Food Bioscience, 32, 100477. https://doi.org/10.1016/j.fbio.2019.100477

Sun, J., Zhou, W., Yan, L., Huang, D., & Lin, L. Y. (2018). Extrusion-based food printing for digitalized food design and nutrition control. Journal of Food Engineering, 220, 1-11. https://doi.org/10.1016/j.jfoodeng.2017.02.028

Suntornnond, R., An, J., & Chua, C. K. (2017). Bioprinting of thermoresponsive hydrogels for next generation tissue engineering: a review. Macromolecular Materials and Engineering, 302(1), 1600266. https://doi.org/10.1002/mame.201600266

Szczesniak, A. S. (2002). Texture is a sensory property. Food quality and preference, 13(4), 215-225. https://doi.org/10.1016/S0950-3293(01)00039-8

Tian, S., Hu, Y., Chen, X., Liu, C., Xue, Y., & Han, B. (2022). Green synthesis of silver nanoparticles using sodium alginate and tannic acid: Characterization and anti-S. aureus activity. International Journal of Biological Macromolecules, 195, 515-522. https://doi.org/10.1016/j.ijbiomac.2021.12.031

Volery, P., Besson, R., & Schaffer-Lequart, C. (2004). Characterization of commercial carrageenans by Fourier transform infrared spectroscopy using single-reflection attenuated total reflection. Journal of agricultural and food chemistry, 52(25), 7457-7463. https://doi.org/10.1021/jf040229o

Wang, Z., Cheng, F., Cai, H., Li, X., Sun, J., Wu, Y., & Zhu, Y. (2021a). Robust versatile nanocellulose/polyvinyl alcohol/carbon dot hydrogels for biomechanical sensing. Carbohydrate polymers, 259, 117753.

Wang, J., Liu, Y., Zhang, X., Rahman, S. E., Su, S., Wei, J., Ning, F., Hu, Z., Martínez-Zaguilán, R., Sennoune, S. R., Cong, W., Christopher, G., Zhang, K. & Qiu, J. (2021b). 3D printed agar/calcium alginate hydrogels with high shape fidelity and tailorable mechanical properties. Polymer, 214, 123238. https://doi.org/10.1016/j.polymer.2020.123238

Wilms, P., Daffner, K., Kern, C., Gras, S. L., Schutyser, M. A. I., & Kohlus, R. (2021). Formulation engineering of food systems for 3D-printing applications–A review. Food Research International, 148, 110585.https://doi.org/10.1016/j.foodres.2021.110585

Wu, T., Huang, J., Jiang, Y., Hu, Y., Ye, X., Liu, D., & Chen, J. (2018). Formation of hydrogels based on chitosan/alginate for the delivery of lysozyme and their antibacterial activity. Food chemistry, 240, 361-369. https://doi.org/10.1016/j.foodchem.2017.07.052

Xie, D., Hu, H., Huang, Q., & Lu, X. (2023). Development and characterization of food-grade bigel system for 3D printing applications: Role of oleogel/hydrogel ratios and emulsifiers. Food Hydrocolloids, 139, 108565. https://doi.org/10.1016/j.foodhyd.2023.108565

Yamashita, C., Moraes, I. C. F., Ferreira, A. G., Branco, C. C. Z., & Branco, I. G. (2021). Multi-response optimization of alginate bleaching technology extracted from brown seaweeds by an eco-friendly agent. Carbohydrate Polymers, 251, 116992. https://doi.org/10.1016/j.carbpol.2020.116992

Yu, J., Wang, X. Y., Li, D., Wang, L. J., & Wang, Y. (2022). Development of soy protein isolate emulsion gels as extrusion-based 3D food printing inks: Effect of polysaccharides incorporation. Food Hydrocolloids, 131, 107824. https://doi.org/10.1016/j.foodhyd.2022.107824

Zeng, Y. J., Xu, P., Yang, H. R., Zong, M. H., & Lou, W. Y. (2018). Purification of anthocyanins from saskatoon berries and their microencapsulation in deep eutectic solvents. LWT, 95, 316-325. https://doi.org/10.1016/j.lwt.2018.04.087

Zhang, Y., Lin, Y., Huang, L., Tekliye, M., Rasheed, H. A., & Dong, M. (2020). Composition, antioxidant, and anti-biofilm activity of anthocyanin-rich aqueous extract from purple highland barley bran. LWT, 125, 109181. https://doi.org/10.1016/j.lwt.2020.109181

Zhong, Q., Chen, Y., Zhang, X., Yang, G., Jin, W., Peng, D., & Huang, Q. (2024). Correlation between 3D printability and rheological properties of biopolymer fluid: A case study of alginate-based hydrogels. Journal of Food Engineering, 111970

CONCLUSÃO GERAL

A modificação estrutural do alginato de sódio (AS), extraído de algas marinhas, através da técnica de ozonização revelou ser eficiente na despolimerização da cadeia polissacarídica, mantendo a integridade estrutural, pureza e estabilidade térmica do polissacarídeo. O alginato ozonizado apresentou potencial para diversas aplicações, destacando-se a encapsulação de compostos ativos e formulação de géis para impressão 3D. Antocianinas, provenientes de amoras, foram satisfatoriamente encapsuladas na solução de SA ozonizado, abrindo possibilidades para sua utilização como corante natural ou componente funcional em formulações alimentícias, cosméticas ou biomédicas. A interação entre esses compostos foi constatada através das análises físicas, químicas e estruturais. A aplicação do SA ozonizado na impressão 3D, em combinação com ágar e extrato rico em antocianinas, demonstrou resultados promissores. As condições de impressão otimizadas permitiram a produção de estruturas cúbicas 3D estáveis, indicando o potencial desse material modificado para aplicações em bioengenharia, farmacêutica, nutracêutica e indústria alimentícia. Apesar das potencialidades aqui encontradas, o SA ozonizado apresentou valores reduzidos de massa molecular viscosimétrica e viscosidade, quando comparados com a literatura, consequência da alta eficácia do tratamento aplicado. Assim, são recomendados ajustes nos parâmetros de ozonização para minimizar a quebra da cadeia polissacarídica, mesmo em aplicações que demandam polissacarídeo de baixo peso molecular. Para formulações de hidrogéis, pode-se considerar alterações na concentração dos componentes empregados ou estratégias de pós-reticulação, visando aprimorar o desempenho do hidrogel como tinta para impressão 3D. Em síntese, os resultados desta pesquisa ressaltam o potencial do SA ozonizado como uma solução versátil e sustentável, capaz de oferecer benefícios significativos em diversas áreas de aplicação, representando uma contribuição valiosa para o avanço da ciência e tecnologia de materiais biopoliméricos. Além disso, a complexação do SA com o extrato rico em antocianinas amplia suas possibilidades de aplicação, possibilitando seu uso em cosméticos sensíveis, curativos absorvíveis ou alimentos funcionais.

REFERÊNCIAS

ABASALIZADEH, F.; MOGHADDAM, S. V.; ALIZADEH, E.; AKBARI, E.; KASHANI, E.; FAZLJOU, S. M. B.; TORBATI, M.; AKBARZADEH, A. Alginate-based hydrogels as drug delivery vehicles in cancer treatment and their applications in wound dressing and 3D bioprinting. Journal of biological engineering, v. 14, p. 1-22, 2020. DOI: https://doi.org/10.1186/s13036-020-0227-7. Disponível em: https://link.springer.com/article/10.1186/s13036-020-0227-7. Acesso em: 03 abril 2023

ABBASIAN, M.; MASSOUMI, B.; MOHAMMAD-REZAEI, R.; SAMADIAN, H.; JAYMAND, M. Scaffolding polymeric biomaterials: Are naturally occurring biological macromolecules more appropriate for tissue engineering? International journal of biological macromolecules, v. 134, p. 673-694, 2019. DOI: https://doi.org/10.1016/j.ijbiomac.2019.04.197. Disponível em: https://www.sciencedirect.com/science/article/pii/S0141813019317969. Acesso em: 11 abril 2023.

AHMED, E. M. Hydrogel: Preparation, characterization, and applications: A review. Journal of advanced research, v. 6, n. 2, p. 105-121, 2015. DOI: https://doi.org/10.1016/j.jare.2013.07.006. Disponível em: https://www.sciencedirect.com/science/article/pii/S2090123213000969. Acesso em: 25 abril 2023.

ARROYO-MAYA, I. J.; MCCLEMENTS, D. J. Biopolymer nanoparticles as potential delivery systems for anthocyanins: Fabrication and properties. Food research international, v. 69, p. 1-8, 2015. https://doi.org/10.1016/j.foodres.2014.12.005. Disponível em: https://www.sciencedirect.com/science/article/pii/S0963996914007753. Acesso em: 11 janeiro 2024.

AZIMI, B.; MALEKI, H.; ZAVAGNA, L.; DE LA OSSA; J. G., LINARI; S., LAZZERI, A.; DANTI, S. Bio-based electrospun fibers for wound healing. Journal of Functional Biomaterials, v. 11, n. 3, p. 67, 2020. DOI: https://doi.org/10.3390/jfb11030067. Disponível em: https://www.mdpi.com/2079-4983/11/3/67. Acesso em: 09 abril 2023.

BANACH, M.; WILOCH, M.; ZAWADA, K.; CYPLIK, W.; KUJAWSKI, W. Evaluation of antioxidant and anti-inflammatory activity of anthocyanin-rich water-soluble aronia dry extracts. Molecules, v. 25, n. 18, p. 4055, 2020. DOI: https://doi.org/10.3390/molecules25184055. Disponível em: https://www.mdpi.com/1420-3049/25/18/4055. Acesso em: 20 abril 2023.

CHEN, J.; WU, A.; YANG, M.; GE, Y.; PRISTIJONO, P.; LI, J.; JIANRONG, L.; XU, B.; MI, H. Characterization of sodium alginate-based films incorporated with thymol for fresh-cut apple packaging. Food Control, v. 126, p. 108063, 2021. DOI: https://doi.org/10.1016/j.foodcont.2021.108063. Disponível em: https://www.sciencedirect.com/science/article/pii/S0956713521002012?casa_token=Tb5sOFuV1ZsAAAAA:SbXQ8Cmmata0OdbsZeWUpU1Ri39f1QYSiEaKelN0ZqwJER2zSf4nOnzNGHvhKyx4ZUPQiVQbvMA. Acesso em: 10 abril 2023

CHENG-RONG, T.; YUNG-KAI, L. Artificial steak: A 3D printable hydrogel composed of egg albumen, pea protein, gellan gum, sodium alginate and rice mill by-products. Future Foods, v. 5, p. 100121, 2022. DOI: https://doi.org/10.1016/j.fufo.2022.100121. Disponível em: https://www.sciencedirect.com/science/article/pii/S2666833522000090. Acesso em: 15 abril 2023

CORRALES-OROVIO, R.; CARVAJAL, F.; HOLMES, C.; MIRANDA, M.; GONZÁLEZ-ITIER, S.; CÁRDENAS, C.; VERA, C.; SCHENCK, T. L.; EGAÑA, J. T. Development of a photosynthetic hydrogel as potential wound dressing for the local delivery of oxygen and bioactive molecules. Acta Biomaterialia, v. 155, p. 154-166, 2023. DOI: https://doi.org/10.1016/j.actbio.2022.11.036. Disponível em: https://www.sciencedirect.com/science/article/pii/S1742706122007656?casa_token=dq_LI6ZojpEAAAAA:Ys6iiI2ihVfE94wT916c22cp0Z-TJgC86J6bywzw4_r9iz7AHhceEcQcowCEea5x2LelDVIKzeE. Acesso em: 10 abril 2023.

DIKMETAS, D. N.; UYSAL, E.; KARBANCIOGLU-GULER, F.; GURMEN, S. The production of pH indicator Ca and Cu alginate ((1, 4)-β-d-mannuronic acid and α-l-guluronic acid) cryogels containing anthocyanin obtained via red cabbage extraction for monitoring chicken fillet freshness. International Journal of Biological Macromolecules, v. 231, p. 123304, 2023. DOI: https://doi.org/10.1016/j.ijbiomac.2023.123304. Disponível em: https://www.sciencedirect.com/science/article/pii/S0141813023001861?casa_token=XfdhdqeVvcwAAAAA:0bbNJ2NZin8v3DiKe_Vg3JFOn0edmLaJMAQmme0lu7c5nOVsrjN74LHp3-YiG_qcZVgG5VPQdCc. Acesso em: 20 abril 2023.

FATIMI, A., OKORO, O. V., PODSTAWCZYK, D., SIMINSKA-STANNY, J., & SHAVANDI, A. Natural hydrogel-based bio-inks for 3D bioprinting in tissue engineering: A review. Gels, v. 8, n. 3, p. 179, 2022. DOI: https://doi.org/10.3390/gels8030179. Disponível em: https://www.mdpi.com/2310-2861/8/3/179. Acesso em: 29 setembro 2023.

FAWZY, M. A.; GOMAA, M. Low-cost biosorption of Methylene Blue and Congo Red from single and binary systems using Sargassum latifolium biorefinery waste/wastepaper xerogel: An optimization and modeling study. Journal of Applied Phycology, v. 33, p. 675-691, 2021. DOI: https://doi.org/10.1007/s10811-020-02290-2. Disponível em: https://link.springer.com/article/10.1007/s10811-020-02290-2. Acesso em: 12 abril 2023.

GRANT, G. T.; MORRIS, E. R.; REES, D. A.; SMITH, P. J.; THOM, D. Biological interactions between polysaccharides and divalent cations: the egg-box model. FEBS letters, v. 32, n. 1, p. 195-198, 1973. DOI: https://doi.org/10.1016/0014-5793(73)80770-7. Disponível em: https://www.sciencedirect.com/science/article/pii/0014579373807707. Acesso em: 05 abril 2023.

HU, C.; LU, W.; MATA, A.; NISHINARI, K.; FANG, Y. Ions-induced gelation of alginate: Mechanisms and applications. International Journal of Biological Macromolecules, v. 177, p. 578-588, 2021. DOI: https://doi.org/10.1016/j.ijbiomac.2021.02.086. Disponível em: https://www.sciencedirect.com/science/article/pii/S0141813021003652?casa_token=9eeQuSvA5L4AAAAA:ieSZRZgGvDLmhVz_zzxEGPTh2Fe8oPl4oFIvIydX7Q-cd32PZ3Bei7l8tu1ryrAZeFWwdx29Y5M. Acesso em: 20 março 2023.

IM, S.; CHOE, G.; SEOK, J. M.; YEO, S. J.; LEE, J. H.; KIM, W. D.; LEE, J. Y.; PARK, S. A. An osteogenic bioink composed of alginate, cellulose nanofibrils, and polydopamine nanoparticles for 3D bioprinting and bone tissue engineering. International Journal of Biological Macromolecules, v. 205, p. 520-529, 2022. DOI: https://doi.org/10.1016/j.ijbiomac.2022.02.012. Disponível em: https://www.sciencedirect.com/science/article/pii/S0141813022002483. Acesso em: 22 abril 2023

KHATTAB, T. A.; KAMEL, S. Advances in polysaccharide-based hydrogels: Self-healing and electrical conductivity. Journal of Molecular Liquids, p. 118712, 2022. DOI: https://doi.org/10.1016/j.molliq.2022.118712. Disponível em: https://www.sciencedirect.com/science/article/pii/S0167732222002495?casa_token=E4nX8sDl0

-
oAAAAA:d7nxb9l21xWg2P9f1WjKN0dVu3UzCNwbOEWvvXgLLIzoqjG9SS6ccpdv4W0lbvUtMw7HOgIaKUE. Acesso em: 29 abril 2023.

LEE, K. Y.; MOONEY, D. J. Alginate: properties and biomedical applications. Progress in polymer science, v. 37, n. 1, p. 106-126, 2012. DOI: https://doi.org/10.1016/j.progpolymsci.2011.06.003. Disponível em: https://www.sciencedirect.com/science/article/pii/S0079670011000918?casa_token=TTjKoQJo-I0AAAAA:AUu9rQSWCBQkA98D1iSMHRKdYfVK628TkUSi1NQMYIslz7cm1lNnShLQeN0Wn8R5QNx3jU66xGE. Acesso em: 1 abril 2023

LEITE, F. P.; BOTTCHER, C.; LEWINSOHN, I. D.; SIQUEIRA, S. G.; MANSUR, K. F.; LONGO, P. A.; VIEIRA, E. A. Asymmetric effects of changes in the habitat-forming algae Sargassum on different associated mobile faunas along São Paulo coast, Brazil. Marine Ecology, v. 42, n. 3, p. e12649, 2021. DOI: https://doi.org/10.1111/maec.12649. Disponível em: https://onlinelibrary.wiley.com/doi/full/10.1111/maec.12649?casa_token=mb9fY7794GcAAAAA%3A96gx70Jo3oMCe3vHrBpaLs2Z1NSKRRq3LGlm6x13dyuHjLYF6sd6EhS_dnX-tdskxhqbPOgLrHSnMdTY. Acesso em: 02 abril 2023.

LIU, Y.; TANG, T.; DUAN, S.; QIN, Z.; LI, C.; ZHANG, Z.; LIU, A.; WU, D.; CHEN, H.; HAN, G.; LIN, B.; HE, J.; WU, W. Effects of sodium alginate and rice variety on the physicochemical characteristics and 3D printing feasibility of rice paste. LWT, v. 127, p. 109360, 2020. DOI: https://doi.org/10.1016/j.lwt.2020.109360. Disponível em: https://www.sciencedirect.com/science/article/pii/S0023643820303492?casa_token=HpCIHpNW4QkAAAAA:2j6eRaKHyGhR2BCIpDrzsPmWDv86r0JE3HG4hIE5Wgf7pSwY_kyJTkTj7mhNB-ShkLBbphswcsU. Acesso em: 18 abril 2023.

LIUDVINAVICIUTE, D.; RUTKAITE, R.; BENDORAITIENE, J.; KLIMAVICIUTE, R.; DAGYS, L. Formation and characteristics of alginate and anthocyanin complexes. International Journal of Biological Macromolecules, v. 164, p. 726-734, 2020. DOI: https://doi.org/10.1016/j.ijbiomac.2020.07.157. Disponível em: https://www.sciencedirect.com/science/article/pii/S0141813020339180?casa_token=H5aFe_8TJ9QAAAAA:lDvEsKYzBSJz1jodNabQq6fVoYQZ5P5Td_Wx1zwvoKyhMhiCU5RqjPUDUiZ7hcMIEOuIOz13bCM. Acesso em: 13 abril 2023.

LOTFINIA, F.; NOROUZI, M. R.; GHASEMI-MOBARAKEH, L.; NAEIMIRAD, M. Anthocyanin/Honey-Incorporated Alginate Hydrogel as a Bio-Based pH-Responsive/Antibacterial/Antioxidant Wound Dressing. Journal of Functional Biomaterials, v. 14, n. 2, p. 72, 2023. DOI: https://doi.org/10.3390/jfb14020072. Disponível em: https://www.mdpi.com/2079-4983/14/2/72. Acesso em: 10 abril 2023.

MA, H.; ZHAO, J.; LIU, Y.; LIU, L.; YU, J.; FAN, Y. Controlled delivery of aspirin from nanocellulose-sodium alginate interpenetrating network hydrogels. Industrial Crops and Products, v. 192, p. 116081, 2023. DOI: https://doi.org/10.1016/j.indcrop.2022.116081. Disponível em: https://www.sciencedirect.com/science/article/pii/S0926669022015643?casa_token=OekVwno7XHkAAAAA:DCHa4LWF8TknEb-GyLTfTi2eldJ_vjOKh-KQjNkS9noAkc4dyBkRlsOnI7DbKrkIrCvsJmDpwrg. Acesso em: 14 abril 2023.

MOHAMMED, C.; LALGEE, L.; KISTOW, M.; JALSA, N.; WARD, K. On the binding affinity and thermodynamics of sodium alginate-heavy metal ion interactions for efficient adsorption. Carbohydrate Polymer Technologies and Applications, v. 3, p. 100203, 2022. DOI:

https://doi.org/10.1016/j.carpta.2022.100203. Disponível em: https://www.sciencedirect.com/science/article/pii/S2666893922000214. Acesso em: 25 abril 2023

PANDISELVAM, R.; MANIKANTAN, M. R.; DIVYA, V.; ASHOKKUMAR, C.; KAAVYA, R.; KOTHAKOTA, A.; RAMESH, S. V. Ozone: An advanced oxidation technology for starch modification. Ozone: Science & Engineering, v. 41, n. 6, p. 491-507, 2019. DOI: https://doi.org/10.1080/01919512.2019.1577128. Disponível em: https://www.tandfonline.com/doi/full/10.1080/01919512.2019.1577128?casa_token=5mfy-9hVzpAAAAAA%3AimU9gPd0Q9kNNLC_UaOEsw-F1IKyKr4VMZ0KxuYPCBSE8Fd0GVrObz9ECIKxlqLbNi9A8gwNp-kczQ. Acesso em: 20 abril 2023.

PRABHU, M. S.; ISRAEL, A.; PALATNIK, R. R.; ZILBERMAN, D.; GOLBERG, A. Integrated biorefinery process for sustainable fractionation of Ulva ohnoi (Chlorophyta): process optimization and revenue analysis. Journal of Applied Phycology, v. 32, p. 2271-2282, 2020. DOI: https://doi.org/10.1007/s10811-020-02044-0. Disponível em: https://link.springer.com/article/10.1007/s10811-020-02044-0. Acesso em: 11 abril 2023

RUSSO, R.; MALINCONICO, M.; SANTAGATA, G. Effect of cross-linking with calcium ions on the physical properties of alginate films. Biomacromolecules, v. 8, n. 10, p. 3193-3197, 2007. DOI: https://doi.org/10.1021/bm700565h. Disponível em: https://pubs.acs.org/doi/full/10.1021/bm700565h?casa_token=9noILSqYxjAAAAAA%3Aw5kK4QPUUEP0ldnz_tHCscsfX_t9ETwfHmjvKT6Ux0NXJWkBO5f4QFg-DP_HZFDmr_x8MzV6umtcdhb4. Acesso em: 15 abril 2023.

SAHA, D.; BHATTACHARYA, S. Hydrocolloids as thickening and gelling agents in food: a critical review. Journal of food science and technology, v. 47, p. 587-597, 2010. DOI: https://doi.org/10.1007/s13197-010-0162-6. Disponível em: https://link.springer.com/article/10.1007/s13197-010-0162-6. Acesso em: 20 outubro 2023.

SAHOO, D. R.; BISWAL, T. Alginate and its application to tissue engineering. SN Applied Sciences, v. 3, n. 1, p. 30, 2021. DOI: https://doi.org/10.1007/s42452-020-04096-w. Disponível em: https://link.springer.com/article/10.1007/s42452-020-04096-w. Acesso em: 29 setembro 2023.

SALEHI, B.; SHARIFI-RAD, J.; SECA, A. M.; PINTO, D. C.; MICHALAK, I.; TRINCONE, A.; MISHRA, A. P.; NIGAM, M.; ZAM, W.; MARTINS, N. Current trends on seaweeds: Looking at chemical composition, phytopharmacology, and cosmetic applications. Molecules, v. 24, n. 22, p. 4182, 2019. DOI: https://doi.org/10.3390/molecules24224182. Disponível em: https://www.mdpi.com/1420-3049/24/22/4182. Acesso em: 15 abril 2023.

SARAVANOU, S. F.; IOANNIDIS, K.; DIMOPOULOS, A.; PAXINOU, A.; KOUNELAKI, F.; VARSAMI, S. M.; TSITSILIANIS, C.; PAPANTONIOU, I; PASPARAKIS, G. Dually crosslinked injectable alginate-based graft copolymer thermoresponsive hydrogels as 3D printing bioinks for cell spheroid growth and release. Carbohydrate Polymers, p. 120790, 2023. DOI: https://doi.org/10.1016/j.carbpol.2023.120790. Disponível em: https://www.sciencedirect.com/science/article/pii/S0144861723002552. Acesso em: 03 maio 2023

SHARIF, N.; KHOSHNOUDI-NIA, S.; JAFARI, S. M. Nano/microencapsulation of anthocyanins; a systematic review and meta-analysis. Food Research International, v. 132, p. 109077, 2020.

https://doi.org/10.1016/j.foodres.2020.109077. Disponível em: https://www.sciencedirect.com/science/article/pii/S0963996920301022. Acesso em: 11 janeiro 2024.

SHARMA, R., NATH, P. C., HAZARIKA, T. K., OJHA, A., NAYAK, P. K., & SRIDHAR, K. Recent advances in 3-D printing properties of natural food gels: Application of innovative food additives. Food Chemistry, p. 137196, 2023. DOI: 10.1016/j.foodchem.2023.137196 Disponível em: https://www.sciencedirect.com/science/article/pii/S0308814623018149?casa_token=jw5fImlWMOQAAAAA:vd0J8F7t1QRc-0o7Uv77y4tLkE1Jao_tGRqs0NRTGC3hPk7Id2Bv1R9VyJLK7T5MRdyiFmBiYLc. Acesso em: 29 setembro 2023

SHI, T.; XIE, Z.; ZHU, Z.; SHI, W.; LIU, Y.; LIU, M. Highly efficient and selective adsorption of heavy metal ions by hydrazide-modified sodium alginate. Carbohydrate Polymers, v. 276, p. 118797, 2022. DOI: https://doi.org/10.1016/j.carbpol.2021.118797. Disponível em: https://www.sciencedirect.com/science/article/pii/S014486172101184X?casa_token=4xJu85-C3ycAAAAA:yXxcR3L-aGCKZkewRNXBapUm7emHAScBgs6ELhvm8OLH4Ux63heV9OS_BOaj1W1HUuLaFzhLDXE. Acesso em: 26 abril 2023

SONG, B.; LIANG, H.; SUN, R.; PENG, P.; JIANG, Y.; SHE, D. Hydrogel synthesis based on lignin/sodium alginate and application in agriculture. International Journal of Biological Macromolecules, v. 144, p. 219-230, 2020. DOI: https://doi.org/10.1016/j.ijbiomac.2019.12.082. Disponível em: https://www.sciencedirect.com/science/article/pii/S0141813019383448?casa_token=KMyh7WlvD2wAAAAA:S79H2xW3_3-7IctCMYUkOrCjwHcNOJ1PQKnkwUc1Kg4l_6nVeUu5PdfZN5SPrzxDEOJMNK-zSkE. Acesso em: 20 abril 2023

VU, B. T., HUA, V. M., TANG, T. N., DANG, N. N. T., CAO, H. T. T., PHAN, T. B., TA, H. T. K.; PHAM, V. H.; TRAN, Q. N.; LE, T. D.; VO, T. V.; NGUYEN, H. T. Fabrication of in situ crosslinking hydrogels based on oxidized alginate/N, O-carboxymethyl chitosan/β-tricalcium phosphate for bone regeneration. Journal of Science: Advanced Materials and Devices, v. 7, n. 4, p. 100503, 2022. DOI: https://doi.org/10.1016/j.jsamd.2022.100503. Disponível em: https://www.sciencedirect.com/science/article/pii/S2468217922000879. Acesso em: 18 abril 2023

WANG, S., JU, J., WU, S., LIN, M., SUI, K., XIA, Y., & TAN, Y. Electrospinning of biocompatible alginate-based nanofiber membranes via tailoring chain flexibility. Carbohydrate polymers, v. 230, p. 115665, 2020. DOI: https://doi.org/10.1016/j.carbpol.2019.115665. Disponível em: https://www.sciencedirect.com/science/article/pii/S0144861719313335?casa_token=q6xRy-kHU0wAAAAA:sbw1TzLxZVvPNgLVYjWQ5ocjZc6Lv67Yl9ZlCkdcCM8AdDe13jas1DJFA5FZ9YW8ld2M7xK8c9Q. Acesso em: 22 abril 2023

WANG, J., LIU, Y., ZHANG, X., RAHMAN, S. E., SU, S., WEI, J., NING, F., HU, Z., MARTÍNEZ-ZAGUILÁN, R., SENNOUNE, S. R., CONG, W., CHRISTOPHER, G., ZHANG, K.; QIU, J. 3D printed agar/calcium alginate hydrogels with high shape fidelity and tailorable mechanical properties. Polymer, v. 214, p. 123238, 2021. DOI: https://doi.org/10.1016/j.polymer.2020.123238. Disponível em: 3D https://www.sciencedirect.com/science/article/pii/S0032386120310636 printed agar/ calcium alginate hydrogels with high shape fidelity and tailorable mechanical properties - ScienceDirect. Acesso em: 20 outubro 2023.

WANG, W.; LIU, M.; SHAFIQ, M.; LI, H.; HASHIM, R.; MOHAMED, E. N.; HANY, E.H.; MORSI, Y.; MO, X. Synthesis of oxidized sodium alginate and its electrospun bio-hybrids with zinc oxide nanoparticles to promote wound healing. International Journal of Biological Macromolecules, v. 232, p. 123480, 2023. DOI: https://doi.org/10.1016/j.ijbiomac.2023.123480. Disponível em: https://www.sciencedirect.com/science/article/pii/S0141813023003720?casa_token=K_WCYNQuh1gAAAAA:mCvfaOuxRs3zNKOI51LJEaZFFdbf7N5XmXtyVKaDuZb6sNZgaYVuTM4WCp0mWpmiQmMBkVWOtyM. Acesso em: 19 abril 2023.

YAMASHITA, C.; MORAES, I. C. F.; FERREIRA, A. G.; BRANCO, C. C. Z.; BRANCO, I. G. Multi-response optimization of alginate bleaching technology extracted from brown seaweeds by an eco-friendly agent. Carbohydrate Polymers, v. 251, p. 116992, 2021. DOI: https://doi.org/10.1016/j.carbpol.2020.116992. Disponível em: https://www.sciencedirect.com/science/article/pii/S0144861720311656. Acesso em: 30 março 2023

YANG, W., GUO, Y., LIU, M., CHEN, X., XIAO, X., WANG, S., GONG, P., MA, Y., & CHEN, F. Structure and function of blueberry anthocyanins: A review of recent advances. Journal of Functional Foods, v. 88, p. 104864, 2022. https://doi.org/10.1016/j.jff.2021.104864. Disponível em: https://www.sciencedirect.com/science/article/pii/S1756464621005132. Acesso em: 11 janeiro 2024.

ZHANG, H.; BIAN, X.; LUO, S.; LIU, C.; HU, X. Effect of sodium alginate on the yogurt stability was dependent on the thickening effect and interaction between casein micelles and sodium alginate. International Journal of Biological Macromolecules, p. 123887, 2023. DOI: https://doi.org/10.1016/j.ijbiomac.2023.123887. Disponível em: https://www.sciencedirect.com/science/article/pii/S014181302300781X?casa_token=1S3yYwcT51UAAAAA:mO3kzpqMiAlsVQehWDcVH5AukZSlfwWq0jpI0RkhYEX7u9OTvDbu4M640pcB4UnvmFzqVgzLLX8. Acesso em: 18 abril 2023

ZHAO, Q.; JIANG, Y.; DUAN, Z.; YUAN, Z.; ZHA, J.; WU, Z.; HUANG, Q.; ZHOU, Z.; LI, H.; HE, F.; SU, Y.; TAN, C.; TAI, H. A Nb2CTx/sodium alginate-based composite film with neuron-like network for self-powered humidity sensing. Chemical Engineering Journal, v. 438, p. 135588, 2022. DOI: https://doi.org/10.1016/j.cej.2022.135588. Disponível em: https://www.sciencedirect.com/science/article/pii/S1385894722010907?casa_token=t1iPwq1VrWAAAAAA:pgwyYsVaWhFvIt1OijD1jVrSK53Y3ocYmlM0KFj0W_FaYNhFlKO3niGhvh-WJvqcuxG29Tr9x1c. Acesso em: 29 abril 2023